Experimental and molecular dynamics study of the interactions of lipid membranes and the pulmonary surfactant-associated protein B in model pulmonary surfactant systems

by

Min Wu

A thesis submitted in partial fulfillment of the requirements for the degree of

Doctor of Philosophy

in

Materials Engineering

Department of Chemical and Materials Engineering
University of Alberta

**Abstract**

The pulmonary surfactant exists as an active film, easing the work of lung by fast absorption and desorption during respiratory cycles, which the principle function of both the lipid and protein components is to reduce the surface tension of the air-liquid interface. The pulmonary surfactant is not simply a mixture of lipids and proteins, but a high ordered architecture, where the pulmonary proteins play crucial roles in structure establishment. Of all the pulmonary surfactant proteins, SP-A, SP-B, SP-C and SP-D, the pulmonary surfactant associated-protein B (SP-B) is critically required for the respiratory process. The mechanisms of the SP-B interaction with lipids involved in the lipid layers of surfactant film remains unsettled, from details about the effects of protein in lipid monolayer to protein-mediated membrane fusion when the multilayer structure of stored surfactant sites, e.g. lamellar bodies, were unpacked into the active film. One of the difficulties in understanding the protein-lipid interactions lies in the complexity of the structural conversion of SP-B and lipid membranes. Molecular dynamics simulation is a powerful tool for probing the free energy profiles between membranes as well as structure and dynamics variations of biological molecules in the membrane system, and surface force apparatus provides a high-resolution way to directly measure the molecular interactions.

We experimentally prepared Langmuir Blodgett monolayers after different compression-expansion cycles and simulated the lipid monolayer in the presence of SP-B to study the role of protein in the interfacial properties of the dipalmitoylphosphatidylcholine (DPPC) monolayer. Using atomic force microscopy and transmission electronic microscopy imaging, we found that SP-B containing DPPC monolayers generated a network with a highly detailed structure, accompanying an enhanced re-spreading efficiency characterized by fewer aggregates observed following the monolayer expansion from high surface pressure. Molecular dynamics studies

indicated that SP-B induced a local groom by disordering the packing of lipid chains upon monolayer compression. SP-B might provide nucleation sites during monolayer compression, which possibly explained how the network of nano-domains was developed and agreed the morphological observation from the experiment. The interactions between lipid layers determined the initialization of transformation from intermediate multilayered state of pulmonary surfactant to the final active film. For probing the model lipid bilayer-bilayer interactions, we used umbrella sampling molecular dynamics simulations to characterize the energy minimum for the opposing DPPC bilayers. The simulated energy minimum between lipid bilayers was highly matched with the experimental results. When the two bilayers were compressed together, the lipid chains were found interdigitated due to the high pressure and dehydration of lipid head groups. The structure and dynamics of water molecules showed the confinement of water molecules with the average separation of bilayers reduced to ~ 0.6 nm. The release of lamellar bodies initiates with the fusing of their limiting membrane with the type II pneumocytes membrane. To further investigate the function of SP-B involved in membrane fusing, we directly measured molecular forces between model bilayers. As confirmed by the thickness variation measured from surface force apparatus, fusing was observed for proteins containing DPPC bilayers. Large adhesive energy was obtained and expected to mainly originate from hydrophobic interactions between α-helix and lipid chains. For palmitoyloleoylphosphoglycerol (POPG) involved interactions between membranes, SP-B modified the fusing process of bilayers with obvious hysteresis for the approach and separation pathways, indicating the protein-mediated lipid bilayer reconstruction. These results shed light on the information about the structural conversion of SP-B and membranes (monolayer and bilayer) involved in surfactant film systems and illustrate a general method of combined experiments and simulations for

studying the lipid-protein and lipid-lipid interactions at a molecular level, with applications in seeking a plausible surfactant candidate for surfactant replacement therapy.

## Preface

Chapter 3 of this thesis will be submitted for publication as Wu, M.; Zeng, H.; Zhang, H., "Probing DPPC phospholipid bilayer interactions through surface force measurements and molecular dynamics simulations." I contributed to atomic force microscopy imaging, surface force measurement, simulation, data analysis and writing the manuscript. Dr. Zeng, H and Dr. Zhang, H. are supervisory authors and contribute to assistance in the design of work, paper composition and editing.

Chapter 4 of this thesis has been submitted to Scientific Reports for publication as Wu, M.; Zeng, H.; Zhang, H., "The effects of pulmonary surfactant-associated protein B on the interfacial properties of phospholipid monolayer." I contributed to cyclic isotherm tests, atomic force microscopy imaging, simulation, data analysis and writing the manuscript. Dr. Zeng, H. designed the experiments and Dr. Zhang, H. designed the simulations. All the authors edited the manuscript.

Chapter 5 of this thesis will be submitted for publication as Wu, M.; Zeng, H.; Zhang, H., "Fusing and adhesion mediated by pulmonary surfactant-associated protein B in model lipid bilayers." I contributed to atomic force microscopy imaging, surface force measurement and circular dichroism experiment. Dr. Zeng, H. designed the experiments, contributed to manuscript composition and editing. Dr. Zhang, H. was involved in manuscript editing.

Min Wu originally write chapter 1, 2 and 7, and they have never been published before.

**Dedication**


In memory of my grandfather,


Liangyun Wu


1935-2017

# Acknowledgement

First of all, I would like to express my deepest gratitude to my supervisors, Dr. Hongbo Zeng and Dr. Hao Zhang. Dr. Zeng introduced me to the beautiful world of colloids and surface sciences. He taught me to measure the forces between surfaces in a fully water-filled surface force apparatus (SFA) chamber, from the overall design of the experiments to steps like gluing mica surfaces and transferring the bilayer-covered disks under water. Dr. Zhang brought me to the amazing field of molecular dynamics of simulations. With his great guidance, I carried out the simulations and learned to analyze the results with computer languages. The great talent of Dr. Zhang in molecular dynamics simulation and the professionality of Dr. Zeng in probing surface force guided my research. The discussions with them would be priceless treasures that will inspire my future work.

I would also like to thank all the members of Dr. Zeng's and Dr. Zhang's group. Dr. Qingye Lu and Dr. Jingyi Wang taught me how to use surface force apparatus and atomic force microscopy. Dr. Jun Huang and Dr. Lei Xie contributed a lot in designing and discussing the experiments of force measurement. Dr. Ling Zhang guided me with peering those thin mica films for silver depositions. My first installation of Ubuntu for molecular dynamics simulation was finished with the help of Dr. Mohammad Khalkhali. I want to give my thanks to Xuhang Tong and Dr. Xiao Xing for their help with data analysis from simulation results.

Thanks to Dr. Wang Zheng from the Department of Physiology for suggestions on conducting experiments about biological materials. Thanks to Dr. Xuejun Sun from the Department of Oncology for training and discussions on all the fluorescent experiments. Thanks to Dr. Xinzheng Chen for guiding experiments about extracting surfactant from the porcine lung in his lab.

I thank my husband, Zhihui, my parents and my parents-in law. Thank you for taking care of my two kids and taking them out for fun. And to my grandparents, thank you for your spiritual support on my way to the Ph.D. degree. To my dear kids, Yifeng and Jasmine, thank you for coming to my life and teaching me to be a responsible person. Thank you to all of my friends for the great time living with you.

**Table of Contents**

# List of Tables

## List of Figures

# Symbols and Nomenclature

NRDS        neonatal respiratory distress syndrome

ARDS        adult respiratory distress syndrome

DPPC        dipalmitoylphosphatidylcholine

POPG        palmitoyloleolphosphoglycerol

PI        phosphatidylinositol

PS        phosphatidylserine

PE        phosphatidylethanolamine

PG        phosphatidylglycerol

SP-A, B, C, D    pulmonary surfactant-associated protein A, B, C, D

SFA        surface forces apparatus

$A$        Hamaker constant

AFM        atomic force microscope

LB        Langmuir Blodgett

BLES        bovine lung extract surfactant

DOPC        dioleoylphosphatidylcholine

DOPG        dioleoylphosphatidylglycerol

TOF-SIMS        time-of-flight secondary ion mass spectrometry

LE        liquid-expanded phase

LC        liquid condensed phase

μ        refractive index

| | |
|---|---|
| $\lambda$ | wave length |
| $V$ | force potential |
| $k_{ts}$ | tip-sample spring constant |
| $F_{ts}$ | tip-sample force |
| Y | Young's modulus |
| $f_0$ | eigenfrequency |
| GCMC | Grand-Canonical Monte Carlo |
| TEM | transmission electronic microscopy |
| LBs | lamellar bodies |
| MD | molecular dynamics |
| PMF | potential of mean force |
| $\xi$ | coordinate |
| $U$ | total energy of the system |
| WHAM | weighted histogram analysis method |
| COM | center of mass |
| PME | particle mesh ewald |
| $D_w$ | thickness of water |
| $D_{p-p}$ | distance between phosphate atoms in lipid bilayer |
| $D_{com}$ | distance of COMs |
| RDFs | radial distribution functions |
| $N_m$ | number of atoms |

| | |
|---|---|
| ϭ | delta function |
| $r_{ij}$ | distance between atom $i$ and $j$ |
| $N_c$ | coordination number |
| MSD | mean squared displacement |
| t.r. | transfer ratio |
| $A$ | area |
| g (OH) | radius distribution function between oxygen and hydrogen in water |
| g (OO) | radius distribution function between oxygen atoms in water |
| g (HH) | radius distribution function between hydrogen atoms in water |
| $S_{cd}$ | order parameter |
| Ɵ | angle between carbon-deuterium (C-D) hydrogen bond to the normal of the monolayer surface |
| ARG | arginine |
| FECO | fringes of equal chromatic order |
| CD | circular dichroism |
| $\gamma_{water}$ | surface tension of water |
| FTIR | Fourier-transform infrared spectroscopy |
| $P_n$ | normal pressure |
| $P_t(z)$ | tangential pressure |

# Chapter 1. Introduction

## 1.1 Pulmonary surfactant

### 1.1.1 Diseases and pulmonary surfactant replacement therapy

The pulmonary surfactant stabilizes the alveoli and reduces the work of lung during the respiratory cycles. Either A deficiency or an absence of the normal surfactant leads to severe diseases. One of the diseases, the neonatal respiratory distress syndrome (NRDS) due to shortage of mature pulmonary surfactant can cause high lethality in preterm neonates. A recent study found that babies born at term after assisted conception were at an even higher risk of NRDS.[1] The surfactant replacement therapy was developed and has largely reduced risks of the mortality for new born babies since 1980s.[2, 3] Adult respiratory distress syndrome (ARDS) can be resulted from various factors, such as damages to lung tissue due to diseases, smoking and so on. ARDS can induce leaking problems of the lung,[4] during which proteins leaked to the alveolar surface could inhibit the functions of pulmonary surfactant. Even with increased self-production of surfactant, the functional molecules can't balance with those inhibitors. A better way to reversing the effects of the leaked proteins is to supplement large quantities of artificial surfactant. However, surfactant extracted from animals was unsatisfactory since it can cause immunological responses and has significant associated reutilization costs. Hence, attention is turning to synthetic lipids and genetically engineered proteins as possible resources of exogenous surfactant products. Furthermore, the surfactant replacement therapy was not as efficient for adults as the babies. Although the ARDS patients got improvement on surfactant treatment, the newly supplemented surfactant could not be evenly distributed in the whole lung tissue due to the effects of gravity.[5] Understanding the roles of each component of surfactant is quite necessary for exploring the surfactant substitute and efficiently delivering of surfactant.

### 1.1.2 Functions and composition of pulmonary surfactant

The research about pulmonary surfactant dates back to 1929, with a publication by Von Neergaard.[6] According to the results from pressure-volume tests for exercised lung, it was found that higher pressure was required for inflating air-filled lung than a liquid-filled lung, where the liquid was to decrease the surface tension at the air-liquid interface. However, the significance of his work was not noticed until Clement demonstrated that a surface active

substance was present at the surface of alveoli by using Langmuir trough equipped with a Wilhelmy dipping plate and plastic barriers.[7] The functions of the extract from the lung (mostly pulmonary surfactant), were to reduce the surface tension, inhibit the collapse of alveoli and ease breathing cycles. In addition, the pulmonary surfactant also behaves as the first barrier to bacterium, viruses and other tiny inhaled particles by interacting with alveolar macrophages and lymphocyte.[8, 9]

The composition of pulmonary surfactant is mainly lipids, ~ 90% and proteins ~ 10%.[10, 11] The categories and weight percent of lipids vary depending on types of animals. Generally, the majority of the lipids are phospholipids. Of all the lipids, dipalmitoylphosphatidylcholine (DPPC) makes up ~ 50%, which bears the main function of reducing the surface tension of water to a near zero upon compression. The second most common lipids in pulmonary surfactant are phsphatidylglycerol (PG), about ~ 10%. The PG regulated the surface activity by promoting the re-spreading of lipid molecules upon monolayer expansion and affected the binding ability of DPPC with surfactant protein.[12] The major neutral lipid of surfactant, i.e., cholesterol, may affect surfactant fluidity.[13] The remaining minor parts are phsphatidylserine (PS), phsphatidylethanolamine (PE) and phosphatidylinositol (PI). In animals including turtles [14] and chicken,[15] a higher proportion of acidic phospholipid, PI, was found than PG. PI also exists in higher level in young mammalian species than adults counterpart. Numerous proteins were detected from the lung lavage. SP-A, a glycoprotein, which plays a role in aspects of surfactant function and metabolism, like binding carbohydrates [16] and phospholipids,[17] activating phagocytosis and bacterial killing,[18, 19] and enhancing the biophysical activity of surfactant.[20] Like SP-A, SP-D is glycosylated and mainly involved in activities related to the defense mechanism of pulmonary surfactant.[9] Hydrophobic proteins, SP-B and SP-C, enhanced the absorption of surfactant and promoted surface tension-lowering properties of phospholipids.[21, 22] SP-B can change the physical structure of the vesicles,[23] which suggests a role for this protein in the recycling of surfactant. SP-G and SP-H are two newly identified pulmonary surfactant proteins. Their functions and structures are not clear.[24, 25]

### 1.1.3 Synthesis and metabolism of pulmonary surfactant

The pulmonary proteins and bulk of surfactant lipids are first synthesized in the endoplasmic reticulum of type II pneumocytes before they are transferred to the Golgi apparatus.[26] It is in

the Golgi apparatus that the routes of proteins and lipids diverge. The lipids are carried by so-called "small lamellar bodies" to larger lamellar bodies. The autoradiography studies have shown that multi-vesicular bodies take the pulmonary surfactant proteins to lamellar bodies, where the proteins and lipids reassemble to the final storage form of the surfactant. Studies have found that content-labelled lipids appear in lamellar bodies as well as the extract of lung from lavage.[27-29] Hence, the lamellar body is expected as the intracellular storage sites of surfactant. During breathing cycles, a surfactant film quickly forms at the surface of alveoli. The secretion of surfactant is critically controlled through autonomous nervous system [30, 31] and mechanical factors.[32] Most surfactant lipids are taken up and reutilized by pneumocyte type II cells,[33, 34] where pulmonary proteins were supposed to play a role in this surfactant recycling process.

### 1.2 Pulmonary surfactant-associated protein B

### 1.2.1 Structure and key features

The pulmonary surfactant-associated protein B (SP-B), similar to pulmonary surfactant protein C (SP-C), is hydrophobic protein and mostly related with the structure and mechanical properties of surfactant film. However, SP-B is vital as the absence of gene expression of SP-B results in the respiratory failure.[35, 36] Gene sequencing shows that SP-B belongs to the Saposin-like family.[37] The full length of active SP-B monomer is composed of 79 amino acids with a dimer molecular weight of 19 kDa.[38] SP-B has two intra di-sulfide bonds and one inter di-sulfide bond when dimers are formed. Though the structure of the whole protein has not been obtained, the N- terminal and C-terminal of SP-B are found with mainly α-helixes. The structures of both N- and C- terminals are shown in Fig. 1.1.
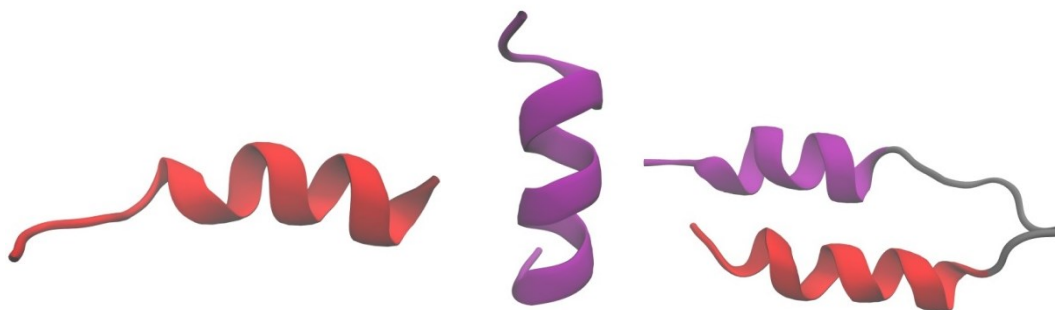
**Figure 1.1** Structure of N- terminal of C- terminal of SP-B from World Protein Data Bank. Helixes were shown (a) in the C terminal with PDB entry 1RG4,[39] (b) in the N terminal with PDB entry 1KMR,[40] and (c) in the mini-SP-B (2DWF) used in the simulation for this thesis.

### 1.2.2 Protein-lipid interactions of SP-B and related lipid-lipid interaction

Understanding the protein-lipid interactions of SP-B is important, as they provide fundamental information for all the processes including production, functioning and recycling of pulmonary surfactant. Through fluorescent microscopy and Brewster angle microscopy studies, the synthesized peptides of SP-B$_{1-25}$ and SP-B$_{1-78}$ could have similar effects on the PA monolayer: they promoted the formation of a network of liquid expanded (LE) phase with separated solid phases and facilitated the fast expansion of a monolayer.[41, 42] The peptides could also induce a reversible buckling for mixed composition of lipid monolayers (DPPC/POPG/PA) during film collapse.[43] Multi-layer protrusions were found for SP-B$_{1-25}$ containing monolayers of DPPC mixed with POPG [44] and BLES (a commercial clinical preparation with both lipids and SP-B and SP-C).[45] An X-ray experiment showed that the protein SP-B$_{1-25}$ is orientated ~ 56 degrees relative to the normal interface and fluidized a portion of the PA monolayer.[46]

In addition to experimental studies, simulations have been employed to investigate the protein-lipid interactions. From the atomistic molecular dynamics simulations, the SP-B$_{1-25}$ was found inserted in the PA monolayer up to a specific area per lipid. The stability of monolayer system was determined by the electrostatic interactions involving the polar residues of the peptide and negatively charged lipid head-groups. Forces originated from the hydrophobic match of aromatic residues with the lipid chains might also played a role in stabilizing the monolayers. [47] All-atom molecular dynamics simulations showed that the predicted structure of the full-length protein SP-B could explain the mechanisms related to lipid reorganization in the lipid bilayers.[48] SP-B was also reported to promote the formation of bilayer reservoirs from monolayers and lipid transportation.[49] From a coarse-grained model simulation, the SP-B$_{1-25}$ was observed to reside in the LE phase, perturb the packing of lipid chains and possibly provide nucleation sites for disordered phase.[50] In addition, the SP-B could mediate the fusing of two vesicles through stalk---hemi-fusion diaphragm---pore-opening pathway.[51]

**1.3 The molecular mechanisms of interactions**

**1.3.1 Models of pulmonary surfactant**

The "squeeze out" model of pulmonary surfactant requires that the composition of the monolayer at the air/water interface should contain DPPC with saturated chains as well as lipid species with disordered chains at low pressure. The model can be described as follows: as the monolayer is compressed to high surface pressure (low surface tension), the unsaturated or more mobile lipids are squeezed out of the monolayer, leading to an enrichment of DPPC remaining in the monolayer. A representative isotherm of squeeze-out showed that the monolayer entered a high compressibility region near equilibrium surface tension followed by a low compressibility phase and finally collapsed.[52-54] The extent of removing of those unsaturated lipids was dependent on the rate of film compression.[55] Non-selectivity was observed for dioleoylphosphatidylcholine (DOPC) and dioleoylphosphatidylglycerol (DOPG) when they formed a binary mixed monolayer with DPPC.[56] When present in the monolayer, SP-B was possibly reported to facilitate the squeeze-out of unsaturated lipids.[57]

The updated squeeze-out model has been shown that to reach a low surface tension there is no need for DPPC enrichment for surfactant monolayers. A test of extract from calf lung found that expanded phases could coexist with the condensed phases at surface pressures as high as ~ 70 mN/m.[58] Furthermore, the onset of main phase (LE)-liquid condensed (LC) transition for mixed monolayers of DPPC combination with palmitoyl and/or myristoyl acyl residues happened up to high surface pressure, ~ 65 mN/m.[59] The low surface tension could also be achieved without the refinement of the lipid composition through a rapid compression of monolayer.[60] The observation of multilayer structure called reservoirs attached to monolayer provided further modification to the classical model. Through a filter paper-supported wet bridge technique, the absorbed surfactant monolayers and their reservoirs showed no difference in their lipid composition.[61] Results from Atomic force microscopy and TOF-SIMs studies revealed that hydrophobic proteins formed multilayered structure with unsaturated lipids rich phase functionally attached with the di-saturated lipid rich phase.[62] Similarly, nano-aggregates also called nanosilo were found trapped with peptide of SP-B and POPG at high surface pressures. [63]

**1.3.2 Lipid-lipid interactions, water molecules at membrane surface and protein-mediated membrane interaction**

At the air-water interface, when dipping the droplets of liquid solution dissolved with lipids, a monolayer was assembled characterized with lipid head-groups toward the water phase and hydrophobic chains toward the air side. When compressing this monolayer, different phases evolve sequentially, e.g. the gas phase, the LE phase, the liquid condensed phase (LC), and the solid phase. The co-existence of LE and solid phases are general for even a single lipid component PA monolayer and a DPPC monolayer. Electrostatic forces elongated the solid phases to stripe-like domains while surface tension probably makes the solid phases with round shapes.[64] Upon increasing the compression speed, the bean-like structures were transformed to multilobed domains, which were not stable and returned backed to bean-like shapes with time.[65] More detailed research showed that an equilibrium state was the competing consequence of line tension and dipole density differences by analyzing size distribution of the round domains.[66]

While the lateral lipid-lipid interactions are responsible for the varied morphology of monolayers, the interactions between lipid membranes determine the stability of stacked multilayers. The lipid reservoirs with multilayered structures were reported to facilitate the re-spreading of surfactant film after low surface tension was reached. Attractive forces, like van der Waals forces tend to bring the bilayers towards a relative close distance while repulsive forces (e.g. steric repulsive forces and hydration forces) prevent the bilayers from attaching each other.[67-69]

The van der Waals forces was determined by the properties of membranes themselves, e.g. the Hamaker constant, the hydration forces were more correlated with lipid head-groups and those water molecules at the lipid-water interface. Hydrogen bond analysis of the lipid head-groups gave a conclusion that the hydration repulsion was a result of the removal of one or two layers of solvating water and the steric interactions of the head groups.[70] The structure parameters of membranes, including the thickness of bilayer, area per lipid, order parameters are in turn affected by these attractive or repulsive forces.[71, 72] Similarly, the structure and order of water molecules changed correspondingly to the deformation of hydrated membranes.[73, 74]

Water molecules were confined at the membrane-water interface and showed slowed dynamics depending on the location of water molecules near the lipid head groups.[73, 75, 76]

In vitro, membrane fusing and adhesion were observed when measuring the bilayer-bilayer interactions through surface force apparatus. The fusing was mainly due to the internal hydrocarbon chains-mediated hydrophobic forces. Adhesion probably originates from the exterior surface of membranes.[77] For pulmonary surfactant systems, proteins are usually involved in the fusing process. In vivo, multi-vesicular bodies were found to be fusing with lamellar bodies in wild-type mice, where the mice without of SP-B failed to pack the surfactant phospholipids to concentric lamellae.[78] Coarse-grained molecular simulations showed that SP-B could mediate the vesicle fusing through bending and anchoring to both vesicles.[51]

### 1.4 Objectives and outline of the thesis

Though models for functional pulmonary surfactant have been modified continually, there are still unresolved issues. Some studies have found that the composition of the reservoirs attached to monolayer was the same as the monolayer while other studies proposed the multilayered structure was composed mainly by proteins and unsaturated lipids. While the protein SP-B is hydrophobic and positively charged, what is not clear is whether and how it interacts with the most majority lipid species (e.g. DPPC with hydrophobic chains) and negatively charged PG? The direct experimental evidence for SP-B-mediated membrane fusion in vitro is still lacking, while the molecular forces involved in protein-lipid interactions remains unsettled. So in this thesis, I focus on model surfactant film systems to study the DPPC bilayer-bilayer interactions and effects of recombined and synthesized SP-B in lipid monolayer and bilayer environments. Detailed objectives are listed as follows:

(1) Investigate the behaviors of both membranes and water molecules by using umbrella sampling molecular dynamics simulations in DPPC bilayer-bilayer interactions and compare the simulated energy minimum with surface force experimental results.

(2) Illustrate the evolution of the DPPC monolayer in the presence of recombinant protein SP-B after multiple compression–expansion cycles and demonstrate the structure conversion of SP-B in the monolayer on monolayer compression. Elucidate the possible interacting mechanism of SP-B with the DPPC monolayer.

(3) Prepare SP-B-conjugated DPPC bilayers and DPPC/DPPC:POPG (7:3) bilayers using Langmuir Blodgett deposition methods. Characterize the morphology change of DPPC bilayers under the effects of SP-B and POPG using AFM. The molecular forces between these model bilayers were investigated through experimental surface force measurement.

The expectations of the proposed research are to enhance the fundamental understanding of the mechanisms of lipid-lipid and SP-B mediated protein-lipid interactions, to contribute the key structural components of both SP-B and membranes related with monolayer spreading and membrane fusing, and finally to provide new clues to seek successful substitute for pulmonary surfactant.

The outline of the thesis is provided as follows:

1)      In Chapter 1, firstly, the diseases resulting from deficiency or abnormality of surfactant and the basic information such as composition, synthesis and metabolism of pulmonary surfactant were reviewed. Then the key features of pulmonary surfactant protein SP-B and the SP-B mediated protein-lipid interactions were discussed. Finally, several models related to the pulmonary surfactant were compared and explained.

2)      In Chapter 2, the experimental techniques including the Langmuir Blodgett trough for isotherm test and membrane preparation, AFM for sample imaging and SFA for force measurement were introduced. In addition, the methods of molecular dynamics simulation were briefly described.

3)      In Chapter 3, the experimentally measuring the DPPC bilayer-bilayer interactions and characterizing the energy minimum through umbrella sampling molecular dynamics simulations were mainly discussed.

4)      In Chapter 4, the protein's effects on the model DPPC monolayer were demonstrated, showing a network with nano-domains was induced after cyclic compression-expansion of the monolayer. The structural conversion of SP-B on monolayer compression was illustrated through simulation results.

5)      In Chapter 5, the SP-B-mediated adhesion and fusing of membranes between model lipid bilayers was studied. Fusion and large

adhesion was observed for DPPC bilayers in the presence of SP-B and the fusion process was modified by SP-B for DPPC/POPG bilayers.

6)    Finally, in Chapter 6, the outlook of molecular force measurement and molecular dynamics simulation approaches to research pulmonary surfactant and the future directions were provided.

**Reference**

[1] V. Condo, S. Cipriani, M. Colnaghi, R. Bellu, R. Zanini, C. Bulfoni, F. Parazzini, F. Mosca, Neonatal respiratory distress syndrome: are risk factors the same in preterm and term infants?, J Matern-Fetal Neo M, 30 (2017) 1267-1272.

[2] R.H. Notter, D.L. Shapiro, Lung Surfactant in an Era of Replacement Therapy, Pediatrics, 68 (1981) 781-789.

[3] B. Robertson, Lung Surfactant for Replacement Therapy, Clin Physiol, 3 (1983) 97-110.

[4] W. Seeger, A. Gunther, H.D. Walmrath, F. Griminger, H.G. Lasch, Alveolar Surfactant and Adult Respiratory-Distress Syndrome - Pathogenetic Role and Therapeutic Prospects, Clin Investigator, 71 (1993) 177-190.

[5] M. Filoche, C.F. Tai, J.B. Grotberg, Three-dimensional model of surfactant replacement therapy, P Natl Acad Sci USA, 112 (2015) 9287-9292.

[6] K. von neergaard, Neue Auffassungen uber einen Grundbegriff der Atemmechanik. Die Retraktionskraft der Lunge, abhangig von der Ober-flachenspannung in den Alveolen, Z.Gesamte. Exp. Med., 66 (1929) 373-394.

[7] J.A. Clements, Surface Tension of Lung Extracts, P Soc Exp Biol Med, 95 (1957) 170-172.

[8] K.L. Hartshorn, E.C. Crouch, M.R. White, P. Eggleton, A.I. Tauber, D. Chang, K. Sastry, Evidence for a Protective Role of Pulmonary Surfactant Protein-D (Sp-D) against Influenza-a Viruses, J Clin Invest, 94 (1994) 311-319.

[9] A.M. LeVine, J.A. Whitsett, J.A. Gwozdz, T.R. Richardson, J.H. Fisher, M.S. Burhans, T.R. Korfhagen, Distinct effects of surfactant protein A or D deficiency during bacterial infection on the lung, J Immunol, 165 (2000) 3934-3940.

[10] R.J. King, Pulmonary Surfactant, J Appl Physiol, 53 (1982) 1-8.

[11] S.A. Rooney, The Surfactant System and Lung Phospholipid Biochemistry, Am Rev Respir Dis, 131 (1985) 439-460.

[12] R.J.a.M. King, M.C., Interactions of lthe lipid and protein components of pulmonary surfactant: role of phophatidylglycerol and calcium, Biochim Biophys Acta, 647 (1981) 159-168.

[13] M.W. Hawco, Davis, P. J., and Keough, K. M. W., Lipid fluidity in lung surfactant: monolayers of saturated and unsaturated lections, J Appl Physiol, (1981) 509.

[14] M.J. Lau, K.M.W. Keough, Lipid-Composition of Lung and Lung Lavage Fluid from Map Turtles (Malaclemys-Geographica) Maintained at Different Environmental Temperatures, Canadian Journal of Biochemistry, 59 (1981) 208-219.

[15] M. Hallman, L. Gluck, Phosphatidylglycerol in Lung Surfactant .3. Possible Modifier of Surfactant Function, J Lipid Res, 17 (1976) 257-262.

[16] H.P. Haagsman, S. Hawgood, T. Sargeant, D. Buckley, R.T. White, K. Drickamer, B.J. Benson, The major lung surfactant protein, SP 28-36, is a calcium-dependent, carbohydrate-binding protein, J Biol Chem, 262 (1987) 13877.

[17] B.J. Benson, S. Hawgood, Structural and functional aspects of protein: phospholipid interactions in surfactant, European Journal of Respiratory Diseases Supplement, 142 (1985) 29-36.

[18] A.J. Tenner, S.L. Robinson, J. Borchelt, J.R. Wright, Human pulmonary surfactant protein (SP-A), a protein structurally homologous to C1q, can enhance FcR- and CR1-mediated phagocytosis, J Biol Chem, 264 (1989) 13923-13928.

[19] E. Wintergerst, H. Manzkeinke, H. Plattner, J. Schlepperschäfer, The interaction of a lung surfactant protein (SP-A) with macrophages is mannose dependent, European Journal of Cell Biology, 50 (1989) 291.

[20] S. Hawgood, ., B.J. Benson, J. Schilling, ., D. Damm, ., J.A. Clements, R.T. White, Nucleotide and amino acid sequences of pulmonary surfactant protein SP 18 and evidence for cooperation between SP 18 and SP 28-36 in surfactant lipid adsorption, P Natl Acad Sci USA, 84 (1987) 66.

[21] J. PerezGil, A. Cruz, I. Plasencia, C. Casals, Interaction of pulmonary surfactant proteins SP-B and SP-C with bilayers of DPPC, studied by fluorescence spectroscopy, Biophys J, 70 (1996).

[22] A. Takahashi, A.J. Waring, J. Amirkhanian, B. Fan, H.W. Taeusch, Structure-Function-Relationships of Bovine Pulmonary Surfactant Proteins - Sp-B and Sp-C, Biochim Biophys Acta, 1044 (1990) 43-49.

[23] W.R. Rice, V.K. Sarin, J.L. Fox, J. Baatz, S. Wert, J.A. Whitsett, Surfactant peptides stimulate uptake of phosphatidylcholine by isolated cells, Biochim Biophys Acta, 1006 (1989) 237.

[24] F. Rausch, M. Schicht, F. Paulsen, I. Ngueya, L. Brauer, W. Brandt, "SP-G", a Putative New Surfactant Protein - Tissue Localization and 3D Structure, Plos One, 7 (2012) e47789.

[25] M. Schicht, F. Rausch, S. Finotto, M. Mathews, A. Mattil, M. Schubert, B. Koch, M. Traxdorf, C. Bohr, D. Worlitzsch, W. Brandt, F. Garreis, S. Sel, F. Paulsen, L. Brauer, SFTA3, a novel protein of the lung: three-dimensional structure, characterisation and immune activation, Eur Respir J, 44 (2014) 447-456.

[26] G. Chevalier, A.J. Collet, In-Vivo Incorporation of Choline-H-3, Leucine-H-3 and Galactose-H-3 in Alveolar Type-Ii Pneumocytes in Relation to Surfactant Synthesis - Quantitative Autoradiographic Study in Mouse by Electron-Microscopy, Anat Rec, 174 (1972) 289.

[27] M. Hallman, B.L. Epstein, L. Gluck, Analysis of Labeling and Clearance of Lung Surfactant Phospholipids in Rabbit - Evidence of Bidirectional Surfactant Flux between Lamellar Bodies and Alveolar-Lavage, J Clin Invest, 68 (1981) 742-751.

[28] H. Jacobs, A. Jobe, M. Ikegami, S. Jones, Surfactant Phosphatidylcholine Source, Fluxes, and Turnover Times in 3-Day-Old, 10-Day-Old, and Adult-Rabbits, J Biol Chem, 257 (1982) 1805-1810.

[29] S.L. Young, S.A. Kremers, J.S. Apple, J.D. Crapo, G.W. Brumley, Rat Lung Surfactant Kinetics - Biochemical and Morphometric Correlation, J Appl Physiol, 51 (1981) 248-253.

[30] G. Enhorning, D. Chamberlain, C. Contreras, R. Burgoyne, B. Robertson, Isoxsuprine-induced release of pulmonary surfactant in the rabbit fetus, American Journal of Obstetrics & Gynecology, 129 (1977) 197-202.

[31] J.P. Fabisiak, E.S. Vesell, D.E. Rannels, Interactions of beta adrenergic antagonists with isolated rat alveolar type II pneumocytes. I. Analysis, characterization and regulation of specific beta adrenergic receptors, Journal of Pharmacology & Experimental Therapeutics, 241 (1987) 722-727.

[32] E.E. Lawson, R.L. Birdwell, P.S. Huang, T.H. Jr, Augmentation of pulmonary surfactant secretion by lung expansion at birth, Pediatr Res, 13 (1979) 611-614.

[33] A.B. Fisher, A. Chander, J. Reicherter, Uptake and degradation of natural surfactant by isolated rat granular pneumocytes, Am J Physiol, 253 (1987) 792-796.

[34] K. Oguchi, M. Ikegami, H. Jacobs, A. Jobe, Clearance of Large Amounts of Natural Surfactants and Liposomes of Dipalmitoylphosphatidylcholine from the Lungs of Rabbits, Exp Lung Res, 9 (1985) 221.

[35] L.M. Nogee, D.E. Demello, L.P. Dehner, H.R. Colten, Brief Report - Deficiency of Pulmonary Surfactant Protein-B in Congenital Alveolar Proteinosis, New Engl J Med, 328 (1993) 406-410.

[36] L.M. Nogee, G. Garnier, H.C. Dietz, L. Singer, A.M. Murphy, D.E. Demello, H.R. Colten, A Mutation in the Surfactant Protein-B Gene Responsible for Fatal Neonatal Respiratory-Disease in Multiple Kindreds, J Clin Invest, 93 (1994) 1860-1863.

[37] R.S. Munford, P.O. Sheppard, P.J. Ohara, Saposin-Like Proteins (Saplip) Carry out Diverse Functions on a Common Backbone Structure, J Lipid Res, 36 (1995) 1653-1663.

[38] S. Hawgood, M. Derrick, F. Poulain, Structure and properties of surfactant protein B, Bba-Mol Basis Dis, 1408 (1998) 150-160.

[39] V. Booth, A.J. Waring, F.J. Walther, K.M.W. Keough, NMR structures of the C-terminal segment of surfactant protein B in detergent micelles and hexafluoro-2-propanol, Biochemistry, 43 (2004) 15187-15194.

[40] J.W. Kurutz, K.Y.C. Lee, NMR structure of lung surfactant peptide SP-B11-25, Biochemistry, 41 (2002) 9627-9636.

[41] M.M. Lipp, K.Y.C. Lee, A. Waring, J.A. Zasadzinski, Fluorescence, polarized fluorescence, and Brewster angle microscopy of palmitic acid and lung surfactant protein B monolayers, Biophys J, 72 (1997) 2783-2804.

[42] M.M. Lipp, K.Y.C. Lee, J.A. Zasadzinski, A.J. Waring, Phase and morphology changes in lipid monolayers induced by SP-B protein and its amino-terminal peptide, Science, 273 (1996) 1196-1199.

[43] J.Q. Ding, D.Y. Takamoto, A. von Nahmen, M.M. Lipp, K.Y.C. Lee, A.J. Waring, J.A. Zasadzinski, Effects of lung surfactant proteins, SP-B and SP-C, and palmitic acid on monolayer stability, Biophys J, 80 (2001) 2262-2272.

[44] R.V. Diemel, M.M.E. Snel, A.J. Waring, F.J. Walther, L.M.G. van Golde, G. Putz, H.P. Haagsman, J.J. Batenburg, Multilayer formation upon compression of surfactant monolayers depends on protein concentration as well as lipid composition - An atomic force microscopy study, J Biol Chem, 277 (2002) 21179-21188.

[45] Y.Y. Zuo, E. Keating, L. Zhao, S.M. Tadayyon, R.A.W. Veldhuizen, N.O. Petersen, F. Possmayer, Atomic force microscopy studies of functional and dysfunctional pulmonary surfactant films. I. Micro- and nanostructures of functional pulmonary surfactant films and the effect of SP-A, Biophys J, 94 (2008) 3549-3564.

[46] K.Y.C. Lee, J. Majewski, T.L. Kuhl, P.B. Howes, K. Kjaer, M.M. Lipp, A.J. Waring, J.A. Zasadzinski, G.S. Smith, Synchrotron X-ray study of lung surfactant-specific protein SP-B in lipid monolayers, Biophys J, 81 (2001) 572-585.

[47] J.A. Freites, Y. Choi, D.J. Tobias, Molecular dynamics simulations of a pulmonary surfactant protein B peptide in a lipid monolayer, Biophys J, 84 (2003) 2169-2180.

[48] M.H. Khatami, I. Saika-Voivod, V. Booth, All-atom molecular dynamics simulations of lung surfactant protein B: Structural features of SP-B promote lipid reorganization, Bba-Biomembranes, 1858 (2016) 3082-3092.

[49] S. Baoukina, D.P. Tieleman, Lung Surfactant Protein SP-B Promotes Formation of Bilayer Reservoirs from Monolayer and Lipid Transfer between the Interface and Subphase, Biophys J, 100 (2011) 1678-1687.

[50] S.L. Duncan, I.S. Dalal, R.G. Larson, Molecular dynamics simulation of phase transitions in model lung surfactant monolayers, Bba-Biomembranes, 1808 (2011) 2450-2465.

[51] S. Baoukina, D.P. Tieleman, Direct Simulation of Protein-Mediated Vesicle Fusion: Lung Surfactant Protein B, Biophys J, 99 (2010) 2134-2142.

[52] J. Egberts, H. Sloot, A. Mazure, Minimal Surface-Tension, Squeeze-out and Transition-Temperatures of Binary-Mixtures of Dipalmitoylphosphatidylcholine and Unsaturated Phospholipids, Biochim Biophys Acta, 1002 (1989) 109-113.

[53] J.N. Hildebran, J. Goerke, J.A. Clements, Pulmonary Surface-Film Stability and Composition, J Appl Physiol, 47 (1979) 604-611.

[54] K.M.W. Keough, E. Farrell, M. Cox, G. Harrell, H.W. Taeusch, Physical, Chemical, and Physiological-Characteristics of Isolates of Pulmonary Surfactant from Adult-Rabbits, Can J Physiol Pharm, 63 (1985) 1043-1051.

[55] B. Pastranarios, C.R. Flach, J.W. Brauner, A.J. Mautone, R. Mendelsohn, A Direct Test of the Squeeze-out Hypothesis of Lung Surfactant Function - External Reflection Ft-Ir at the Air/Water Interface, Biochemistry-Us, 33 (1994) 5121-5127.

[56] J.P.J.G. Vanliempd, A.A.H. Boonman, R.A. Demel, P.M.C. Gieles, T.C.M. Gorree, Nonselective Squeeze-out of Dioleoylphosphatidylcholine and Dioleoylphosphatidylglycerol from Binary Mixed Monolayers with Dipalmitoylphosphatidylcholine, Biochim Biophys Acta, 897 (1987) 495-501.

[57] N. Mathialagan, F. Possmayer, Low-Molecular-Weight Hydrophobic Proteins from Bovine Pulmonary Surfactant, Biochim Biophys Acta, 1045 (1990) 121-127.

[58] B. Piknova, W.R. Schief, V. Vogel, B.M. Discher, S.B. Hall, Discrepancy between phase behavior of lung surfactant phospholipids and the classical model of surfactant function, Biophys J, 81 (2001) 2172-2180.

[59] J.M. Crane, G. Putz, S.B. Hall, Persistence of phase coexistence in disaturated phosphatidylcholine monolayers at high surface pressures, Biophys J, 77 (1999) 3134-3143.

[60] J.M. Crane, S.B. Hall, Rapid compression transforms interfacial monolayers of pulmonary surfactant, Biophys J, 80 (2001) 1863-1872.

[61] S.H. Yu, F. Possmayer, Lipid compositional analysis of pulmonary surfactant monolayers and monolayer-associated reservoirs, J Lipid Res, 44 (2003) 621-629.

[62] E. Keating, Y.Y. Zuo, S.M. Tadayyon, N.O. Petersen, F. Possmayer, R.A.W. Veldhuizen, A modified squeeze-out mechanism for generating high surface pressures with pulmonary surfactant, Bba-Biomembranes, 1818 (2012) 1225-1234.

[63] J.Q. Ding, I. Doudevski, H.E. Warriner, T. Alig, J.A. Zasadzinski, Nanostructure changes in lung surfactant monolayers induced by interactions between palmitoyloleoylphosphatidylglycerol and surfactant protein B, Langmuir, 19 (2003) 1539-1550.

[64] D.J. Keller, H.M. Mcconnell, V.T. Moy, Theory of Superstructures in Lipid Monolayer Phase-Transitions, J Phys Chem-Us, 90 (1986) 2311-2315.

[65] C.W. McConlogue, T.K. Vanderlick, A close look at domain formation in DPPC monolayers, Langmuir, 13 (1997) 7158-7164.

[66] D.W. Lee, Y.J. Min, P. Dhar, A. Ramachandran, J.N. Israelachvili, J.A. Zasadzinski, Relating domain size distribution to line tension and molecular dipole density in model cytoplasmic myelin lipid monolayers, P Natl Acad Sci USA, 108 (2011) 9425-9430.

[67] L.J. Lis, M. Mcalister, N. Fuller, R.P. Rand, V.A. Parsegian, Interactions between Neutral Phospholipid-Bilayer Membranes, Biophys J, 37 (1982) 657-665.

[68] J. Marra, Direct Measurements of Attractive Vanderwaals and Adhesion Forces between Uncharged Lipid Bilayers in Aqueous-Solutions, J Colloid Interf Sci, 109 (1986) 11-20.

[69] J. Marra, J. Israelachvili, Direct Measurements of Forces between Phosphatidylcholine and Phosphatidylethanolamine Bilayers in Aqueous-Electrolyte Solutions, Biochemistry, 24 (1985) 4608-4618.

[70] L. Perera, U. Essmann, M.L. Berkowitz, Role of water in the hydration force acting between lipid bilayers, Langmuir, 12 (1996) 2625-2629.

[71] K. Hristova, S.H. White, Determination of the hydrocarbon core structure of fluid dioleoylphosphocholine (DOPC) bilayers by x-ray diffraction using specific bromination of the double-bonds: Effect of hydration, Biophys J, 74 (1998) 2419-2433.

[72] F. Volke, A. Pampel, Membrane Hydration and Structure on a Subnanometer Scale as Seen by High-Resolution Solid-State Nuclear-Magnetic-Resonance - Popc and Popc/C(12)Eo(4) Model Membranes, Biophys J, 68 (1995) 1960-1965.

[73] E.A. Disalvo, F. Lairion, F. Martini, E. Tymczyszyn, M. Frias, H. Almaleck, G.J. Gordillo, Structural and functional properties of hydration and confined water in membrane interfaces, Bba-Biomembranes, 1778 (2008) 2655-2670.

[74] R.J. Mashl, H.L. Scott, S. Subramaniam, E. Jakobsson, Molecular simulation of dioleoylphosphatidylcholine lipid bilayers at differing levels of hydration, Biophys J, 81 (2001) 3005-3015.

[75] S.Y. Bhide, M.L. Berkowitz, Structure and dynamics of water at the interface with phospholipid bilayers, J Chem Phys, 123 (2005) 224702-1-16.

[76] Z.C. Zhang, M.L. Berkowitz, Orientational Dynamics of Water in Phospholipid Bilayers with Different Hydration Levels, J Phys Chem B, 113 (2009) 7676-7680.

[77] C.A. Helm, J.N. Israelachvili, P.M. Mcguiggan, Molecular Mechanisms and Forces Involved in the Adhesion and Fusion of Amphiphilic Bilayers, Science, 246 (1989) 919-922.

[78] M.T. Stahlman, M.P. Gray, M.W. Falconieri, J.A. Whitsett, T.E. Weaver, Lamellar body formation in normal and surfactant protein B-deficient fetal mice, Lab Invest, 80 (2000) 395-403.

# Chapter 2. Experimental and simulation methods

## 2.1 Langmuir Blodgett trough for isotherm tests and surfactant film preparation

The Langmuir Blodgett trough combined the techniques of apparatus for transferring a monomolecular film from a water surface to a solid surface [1] and surface pressure apparatus.[2] A standard Langmuir Blodgett trough contains following parts: frame, two barriers, trough top, surface pressure sensor, dipping mechanism and interface unit seen in Fig. 2.1.
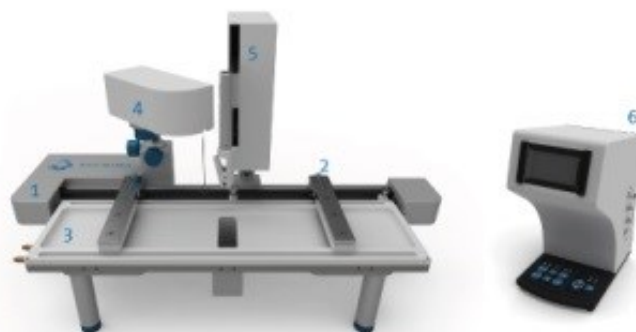


**Figure 2.1** Outlook of Langmuir Blodgett trough: 1: frame, 2: two barriers, 3: trough top, 4: surface pressure sensor, 5: dipping mechanism, 6: interface unit. Figures were retrieved from http://www.biolinscientific.com/ksvnima/technologies/.

The application of the Langmuir trough in the study of surfactant could be mainly divided into two parts: one is the surface tension isotherm test of surfactant absorption [3-5] and the other is the film assembling.[6, 7] For the isotherm test of pulmonary surfactant, the compression of two barriers is similar to the deflating process of the lung, when expansion corresponds to the inflating process. Parameters like spreading rate, equilibrium surface tension, film compressibility and minimum surface tension are useful to measure the activity of surfactant. Monolayers, bilayers and multilayers of surfactant can be assembled by dipping different substrates outwards or inwards the subphase.

## 2.2 Surface force apparatus for the study of interactions between surfactant films

The surface force apparatus was invented in the 1960's [8, 9] and has been utilized for decades to measure the physical forces such as van der Waals force, hydration force, double-

layer electrostatic force, and adhesion. Three features are essential for the apparatus: separation measurement, separation control and force measurement. A schematic drawing of the apparatus was shown in Fig. 2.2.
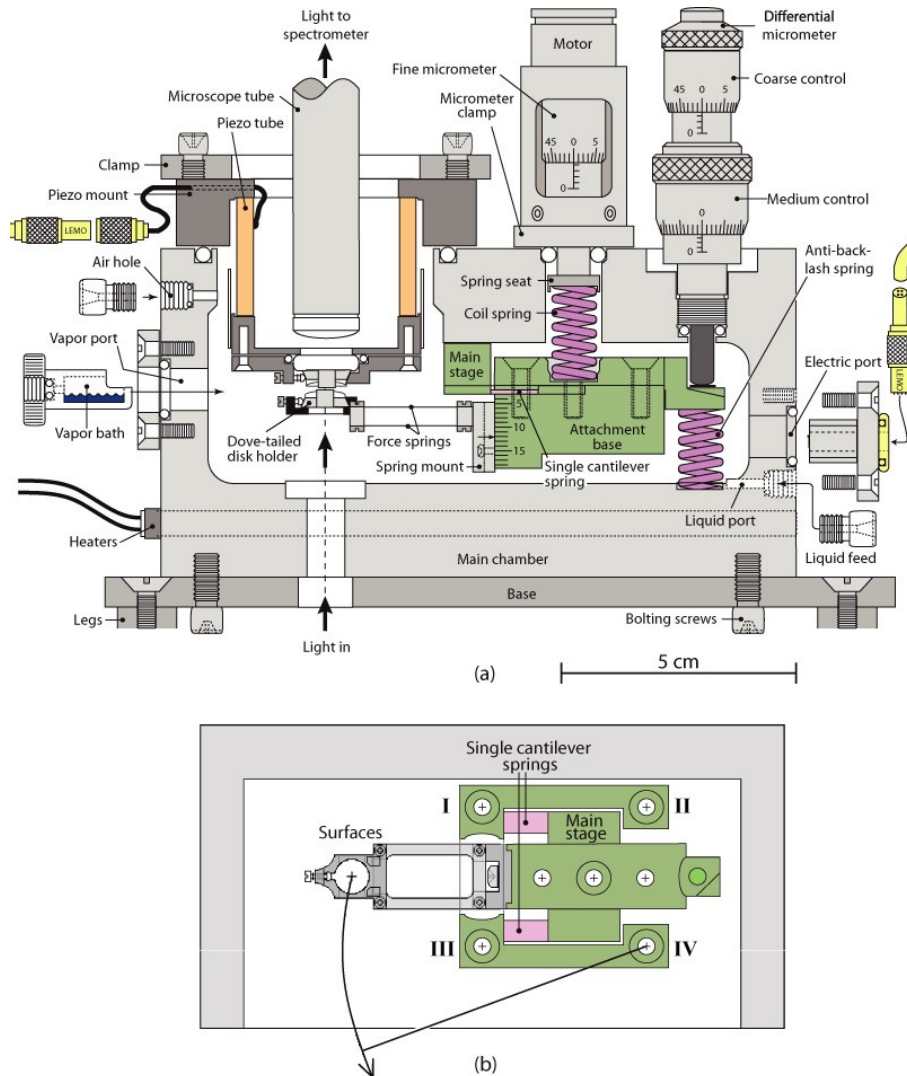


**Figure 2.2** (a) SFA 2000 for force measurement. (b) top view of the main stage and bottom disk holder.[10]

The separation between the surface, D, can be measured thorough a technique called multiple beam interference fringes. The surfaces are usually back silver-coated mica glued on cylindrical glass disks. The finite and uneven thickness of glue between the mica and disk correlate with the curvature of the mica surfaces. When monochromatic light passes through the crossed cylinders, an interference pattern similar as the classical Newton's ring is obtained with a

distance resolution in the order of several nm. When white light is utilized, each wavelength creates its own set of Newton's rings with a common center. The various wavelengths are deviated and linked up to parabolic-shaped curves when the diametric portion of the interference system passes through a vertical slit and then is dispersed in a horizontal plane through a prism. The relationship of components in the interference system of silver-mica-air-mica-silver was derived by Bailey and Kay (1965), which is

$$\tan kb = \frac{(1 - r^2)\sin 2\mu ka}{2r - (1 + r^2)\cos 2\mu ka},\tag{2.1}$$

where k = $2\pi$ / $\lambda$, b is the thickness of the air gap, r = ($\mu$-1) / ($\mu$+1) corresponds to the reflection coefficient at the mica/air interface, $\mu$ is the refractive index, and a is the equal thickness of two mica sheet. The value of $\mu a$ can be calculated based on the positions of the fringes when the two mica surfaces contact. From the Eq. 2.1, the value b can be obtained from wavelengths at which the fringes of equal chromatic order occur. The accuracy for measurement of b or D is about 0.1 nm in the range of 0-200 nm.

Generations of surface force apparatus have been developed and continually improved since the apparatus was invented. This is especially the case for apparent improvement in its accuracy to control the distances between the surfaces. For SFA 2000, the separation between the surfaces is controlled by a four-stage mechanism of increasing sensitivity from micrometer to ångstroms. The differential micrometer includes both the coarse and medium controls which are mounted against an anti-back-lash spring. Another fine micrometer is connected to the attachment base through a coil spring and driven by a motor.

**2.3 Atomic force microscopy imaging of the surfactant monolayer and bilayers**

Atomic force microscopy (AFM) is employed for imaging the surfactant monolayer in the air and surfactant bilayers in aqueous solutions. The force potential between the sharp tip of AFM and the sample $V_{ts}$ creates a z component of the tip-sample force, $F_{ts} = -\partial V_{ts} / \partial z$, and a tip-sample spring constant, $k_{ts} = -\partial F_{ts} / \partial z$. The deflection of the force sensor, called a cantilever (with sharp tip at the end), is mostly measured by bouncing a light beam off the cantilever. The quality of AFM imaging is dependent on the properties of the cantilever and the tip. For a cantilever with dimensions *w, t*, and *L,* the spring constant is given by

$$k = \frac{Ywt^3}{4L^3} \ , \tag{2.2}$$

where Y is the Young's modulus. The fundamental eigenfrequency $f_0$ is given as

$$f_0 = 0.162 \frac{t}{L^2} \sqrt{\frac{Y}{\rho}} \ , \tag{2.3}$$

where $\rho$ is the mass density of the cantilever. Other properties affecting the quality of the AFM imaging are the quality factor Q, the variation of the eigenfrequency with temperature and the structure and chemical composition of the tip.

## 2.4 Molecular dynamics simulation

### 2.4.1 The basic principles of molecular dynamics simulation

Through the surface force apparatus, the forces between surfactant films of several nano meter thick can be accurately measured. The molecular details involved can't be fully understood. On the other hands, the methods of molecular dynamics simulations are introduced for providing quite complemental information about the structure and dynamics of the lipids, protein and water molecules in the surfactant systems.

The molecular dynamics simulation is based on the classical mechanics, where the interaction forces of many particles' system (interacting through potential $V$, force field) could be calculated by solving Newton's equation:

$$F = -\frac{\partial V}{\partial r} = ma \qquad (2.4)$$

where $F$ is the forces acting on the particle, $m$ is the mass and $a$ is the acceleration.

Once the initial velocity $v_0$ and position $r_0$ were provided, a series of coordinates and velocities are updated step-by-step using the equations of motion:

$$v = v_0 + a\Delta t \qquad (2.5)$$

$$r = r_0 + v_0\Delta t + \frac{1}{2}a\Delta t^2 \qquad (2.6)$$

where $v$ is the velocity, $r$ is the position vector and $\Delta t$ is the time. Trajectories of all the particles (or atoms) are updated continually with the simulation time. Based on the ergodicity hypothesis of statistical mechanics, the time averages of the interest along this trajectory are expected to be equivalent to the ensemble averages of the appropriate microcanonical (N V E) ensemble.

The temperatures and pressures of the system display fluctuations and can be inferred indirectly. By coupling the system to the appropriate external bath, simulations can also be conducted at a constant temperature (N V T) ensemble [11, 12] or a constant pressure (N p T) ensemble.[11]

**2.4.2 Application of molecular dynamics simulations in the lipid membrane systems**

Molecular dynamics simulations could be applied to investigate the pressure-area isotherms of the lipid monolayers.[13, 14] The surface pressure $\Pi$ is defined by the equation, $\Pi = \gamma_0 - \gamma_m$, where $\gamma_0$ is the surface tension of water, $\gamma_m$ means the surface tension when the water subphase is covered by the monolayer. In the simulation,

$$\gamma = \int_{-\infty}^{+\infty} dz [P_n - P_t(z)] \tag{2.7}$$

where $P_n$ is the normal pressure, $P_t(z)$ is the tangential pressure and equals $(P_{xx}+P_{yy}) / 2$. While the isotherm simulation can be finished with both atomistic and coarse-grained (CG) model, the phase coexistence of the lipid monolayer was usually studied using a CG model.[15] When considering the large structural transformation of membrane, the CG model simulation was also used to investigate the formation of pores and domains in lipid films.[16]

For lipid bilayers, the molecular dynamics simulation could provide the structural details about the hydrated lipid head-groups, order parameter of lipid chain, phase transition etc.[17-20] Known as the storage form of pulmonary surfactant, the lamellar bodies were constructed with a multilayered structure. A simplicity of the inter-membrane interaction involved in lamellar bodies and the bilayer-bilayer interaction was mainly discussed and correlated with the interfacial water properties through the molecular dynamics simulations.[21-23]

**Reference**

[1] K.B. Blodgett, Films built by depositing successive monomolecular layers on a solid surface, J Am Chem Soc, 57 (1935) 1007-1022.

[2] F.A. Askew, J.F. Danielli, Measurements of the pressures due to monolayers at oil-water interfaces., T Faraday Soc, 36 (1940) 0785-0793.

[3] F. Bringezu, J.Q. Ding, G. Brezesinski, J.A. Zasadzinski, Changes in model lung surfactant monolayers induced by palmitic acid, Langmuir, 17 (2001) 4641-4648.

[4] B.M. Discher, K.M. Maloney, D.W. Grainger, C.A. Sousa, S.B. Hall, Neutral lipids induce critical behavior in interfacial monolayers of pulmonary surfactant, Am J Resp Crit Care, 159 (1999) A896-A896.

[5] S.Y. Park, R.E. Hannemann, E.I. Franses, Dynamic tension and adsorption behavior of aqueous lung surfactants, Colloid Surface B, 15 (1999) 325-338.

[6] M. Amrein, A. vonNahmen, M. Sieber, A scanning force and fluorescence light microscopy study of the structure and function of a model pulmonary surfactant, Eur Biophys J Biophy, 26 (1997) 349-357.

[7] M. Fujihira, K. Nishiyama, H. Yamada, Photoelectrochemical Responses of Optically Transparent Electrodes Modified with Langmuir-Blodgett-Films Consisting of Surfactant Derivatives of Electron-Donor, Acceptor and Sensitizer Molecules, Thin Solid Films, 132 (1985) 77-82.

[8] J.N. Israelachvili, D. Tabor, Measurement of Van-Der-Waals Dispersion Forces in Range 1.4 to 130 Nm, Nature-Phys Sci, 236 (1972) 106.

[9] D. Tabor, Winterto.Rh, Direct Measurement of Normal and Retarded Van Der Waals Forces, Proc R Soc Lon Ser-A, 312 (1969) 435.

[10] J. Israelachvili, Y. Min, M. Akbulut, A. Alig, G. Carver, W. Greene, K. Kristiansen, E. Meyer, N. Pesika, K. Rosenberg, H. Zeng, Recent advances in the surface forces apparatus (SFA) technique, Rep Prog Phys, 73 (2010) 036601.

[11] H.J.C. Berendsen, J.P.M. Postma, W.F. Vangunsteren, A. Dinola, J.R. Haak, Molecular-Dynamics with Coupling to an External Bath, J Chem Phys, 81 (1984) 3684-3690.

[12] S. Nose, A Molecular-Dynamics Method for Simulations in the Canonical Ensemble, Mol Phys, 52 (1984) 255-268.

[13] S. Baoukina, L. Monticelli, S.J. Marrink, D.P. Tieleman, Pressure-area isotherm of a lipid monolayer from molecular dynamics simulations, Langmuir, 23 (2007) 12617-12623.

[14] A.J. Kox, J.P.J. Michels, F.W. Wiegel, Simulation of a Lipid Monolayer Using Molecular-Dynamics, Nature, 287 (1980) 317-319.

[15] S. Baoukina, E. Mendez-Villuendas, D.P. Tieleman, Molecular View of Phase Coexistence in Lipid Monolayers, J Am Chem Soc, 134 (2012) 17543-17553.

[16] V. Knecht, M. Muller, M. Bonn, S.J. Marrink, A.E. Mark, Simulation studies of pore and domain formation in a phospholipid monolayer, J Chem Phys, 122 (2005) 024704-1-9.

[17] O. Berger, O. Edholm, F. Jahnig, Molecular dynamics simulations of a fluid bilayer of dipalmitoylphosphatidylcholine at full hydration, constant pressure, and constant temperature, Biophys J, 72 (1997) 2002-2013.

[18] P.B. Moore, C.F. Lopez, M.L. Klein, Dynamical properties of a hydrated lipid bilayer from a multinanosecond molecular dynamics simulation, Biophys J, 81 (2001) 2484-2494.

[19] D.P. Tieleman, H. Leontiadou, A.E. Mark, S.J. Marrink, Simulation of pore formation in lipid bilayers by mechanical stress and electric fields, J Am Chem Soc, 125 (2003) 6382-6383.

[20] S. Leekumjorn, A.K. Sum, Molecular studies of the gel to liquid-crystalline phase transition for fully hydrated DPPC and DPPE bilayers, Bba-Biomembranes, 1768 (2007) 354-365.

[21] S.J. Marrink, M. Berkowitz, H.J.C. Berendsen, Molecular-Dynamics Simulation of a Membrane Water Interface - the Ordering of Water and Its Relation to the Hydration Force, Langmuir, 9 (1993) 3122-3131.

[22] L. Perera, U. Essmann, M.L. Berkowitz, Role of water in the hydration force acting between lipid bilayers, Langmuir, 12 (1996) 2625-2629.

[23] S. Tristram-Nagle, H.I. Petrache, J.F. Nagle, Structure and interactions of fully hydrated dioleoylphosphatidylcholine bilayers, Biophys J, 75 (1998) 917-925.

# Chapter 3. Probing DPPC phospholipid bilayer interactions through surface force measurements and molecular dynamics simulations*

## 3.1 Introduction

The pulmonary surfactant is synthesized and secreted by pneumocyte type II cells. Before the molecules of surfactant enter the air-water interface, they exist as the storage form of pulmonary surfactant, named lamellar bodies (LBs). Evidences from electron microscopy [1, 2] and neutron reflection [3] show that part of the surfactant film together with LBs was a multilayered system. Therefore understanding both intra- and inter-membrane interactions is critical for unravelling the mechanisms for membrane stacking and unfolding which may provide essential information for production optimization and drug delivery of artificial surfactant.

Numerous techniques have been used to measure the forces between lipid membranes. The hydration repulsive pressure on egg phosphatidylcholine/water multilayers was investigated by utilizing osmotic, hydrostatic and vapor pressures, in which the deformation and space change of lipid bilayers during the pressure measurement was tracked by X-ray diffraction.[4, 5] For the interactions between charged lipid membranes, micropipette aspiration technique has been used to determine the mechanical properties of lipid vesicles by varying surface charge [6] and it was found that the stability of vesicles was closely related with intramembrane electrostatic forces. SFA has been widely used for measuring physical forces (e.g. van der Waals interaction, electric double layer interaction, hydration interaction, hydrophobic interaction) in both biological and non-biological systems in vapors and complex fluids over the past 4 decades.[7-9] The interactions between lipid bilayers, not only repulsive forces, but also adhesive forces could be accurately determined by applying SFA force measurement. However, it has been hardly discussed how the interactions affect the lipid conformations. That is, the structural details about the bilayer-water interface are obscured especially when the lipid bilayers are dehydrated.

Different computer simulation techniques, Monte Carlo and molecular dynamics methods have been performed to investigate the interaction mechanisms of lipid bilayers in water. To investigate the hydration repulsion, Grand-Canonical Monte Carlo (GCMC) methods were applied between oriented and non- oriented structureless walls,[10] between phospholipid bilayers on substrates.[11, 12] Thermodynamic extrapolation method was capable to extract the

interaction pressures between bilayers by determining the variations of water chemical potential during lipid bilayer dehydration.[13, 14] Umbrella sampling method could also be utilized to investigate the hydration repulsion involved between lipid bilayers.[15] While the mechanisms involved in hydration force were discussed mainly in these simulations, the attractive part of interactions reported in the DPPC bilayers surface force measurement,[16] was not well characterized by simulations. The attractive force could bring out the "jump in" of the two surfaces during surface force measurement. An energy minimum was shown when the attractive force was balanced with repulsive part.  Locating this energy minimum is important for tracking the equilibrium distance of interacting lipid bilayers and explaining the stability of lamella bodies during pulmonary surfactant secretory. However, simulation about the energy minimum between phospholipid bilayers has not been available.

In this work, DPPC was chosen to build the model lipid bilayer. It accounts for 55% of the lipid component of pulmonary surfactant,[17] and it is an essential component for surface tension reduction of current clinical surfactant for replacement therapy.[18] The interactions of DPPC bilayers were investigated through both SFA experiments and umbrella sampling molecular dynamics (MD) simulations. Compared to ref. 15, instead of coarse grained model, we employed atomistic model for both the lipid and water molecules. The interactions between two bilayers were measured using a SFA. MD simulations were conducted for bilayers in water and correlated to the interaction forces measured experimentally, which showed good agreement. In addition, the static and dynamic properties of water molecules trapped between two closely approached lipid bilayers were investigated to further explore the lipid bilayer interactions.

### 3.2 Materials and experimental methods

1, 2 Dipalmitoyl-sn-glycero-3-phosphocholine (DPPC) (melting point 41 °C) was purchased from Avanti Polar Lipids, Inc. (Alabaster, AL). DPPC was dissolved in chloroform at a concentration of 1 mg/mL. Mill-Q water with a resistivity of 18 MΩ·cm was used for preparing all the aqueous solutions in this work.

A MFP-3D AFM (Santa Barbara, CA) and silica nitride cantilevers were used to characterize DPPC bilayer in water. Mica-supported lipid bilayers were prepared by Langmuir Blodgett (LB) deposition using a temperature-controlled trough through a procedure described

elsewhere.[19] First, the DPPC was spread on the air-water interface of the trough and compressed to a surface density with area per lipid head group was ~ 52 Å². Then by raising the mica substrates vertically through the DPPC monolayer covered air/water interface the inner layer was prepared and finally by lowering down the substrate the outer layer was deposited.

The force measurements were performed in a SFA 2000. The distance between surfaces (mounted on two cylinder disks) was determined by introducing an optical technique using multi-beam interference fringe called "fringes of equal chromatic order" (FECO), which could be achieved by coating the mica sheets with a semi-reflective silver layer. The forces, attractive or repulsive, could be evaluated through the deformation of the spring attached to the lower disk. In particular, the SFA chamber was first filled with Milli-Q water saturated with DPPC molecules to prevent lipid desorption from mica-supported bilayer during the measurement process. Then the cylindrical disks (glued with mica) with DPPC bilayer deposited from LB method were carefully transferred and mounted into SFA under water. The experimental devices were placed in a temperature-controlled room at 25 °C. An automated data collection system was introduced as described previously.[20]

## 3.3 Simulation methods

### 3.3.1 Potential of mean force (PMF) and umbrella sampling

The PMF ($W(\xi)$) along with coordinate $\xi$, is defined by

$$W(\xi) = W(\xi') - k_B T \ln[\frac{<\rho(\xi)>}{<\rho(\xi')>}],$$  (3.1)

where $<\rho(\xi)>$ is average distribution function, $W(\xi)$ and $W(\xi')$ are arbitrary constants. The average distribution function along with some coordinate $\xi$ is deduced from a Boltzmann weighted average,

$$<\rho(\xi)> = \frac{\int dR \sigma(\xi'[R] - \xi)e^{-U(R)/k_B T}}{\int d\,\mathrm{Re}^{-U(R)/k_B T}},$$  (3.2)

where $U$ (R) means the total energy of the system as a function of coordinate R and $\xi'$ (R) is a function correlated with the several freedoms of the system.

Although $W(\xi)$ was useful for the dynamical information of macromolecular systems, it was not practical to get $<\rho(\xi)>$. Umbrella sampling method is introduced to enhance the sampling of whole system while a biased potential (also called windows potential) usually a harmonic function was applied,

$$w_i(\xi) = \frac{1}{2}K(\xi - \xi_i)^2 \tag{3.3}$$

Then the new energy of the system equals $U(R) + w(\xi)$. The biased potential is responsible for confining the sampling of the system in small regions of $\xi$. After a series of biased window simulations, the results of each window were unbiased and recombined to obtain the PMF. From Eq. 3.2, the biased distribution function from the $i^{th}$ window is,

$$< \rho(\xi) >_i = e^{-w_i(\xi)/k_B T} < \rho(\xi) >< e^{-w_i(\xi)/k_B T} >^{-1} \tag{3.4}$$

The expression for unbiased PMF from the $i^{th}$ window is,

$$W_i(\xi) = W(\xi') - k_B T \ln[\frac{< \rho(\xi) >}{\rho(\xi')}] - w_i(\xi) + F_i \tag{3.5}$$

And the constant $F_i$ is correlating with the free energy change resulted from introduction of the biased potential,

$$e^{-F_i/k_B T} = < e^{-w_i(\xi)/k_B T} > \tag{3.6}$$

To estimate the constant $F_i$, weighted histogram analysis method (WHAM) [21] was applied.

### 3.3.2 Simulation box, force fields and models

The simulation box contained two hydrated planner all-atom DPPC bilayer systems, which was built from CHARMM-GUI *membrane builder*,[22] with dimensions Lx, Ly and Lz [6.74 nm，6.74 nm，and 22.60 nm]. The initial thickness of water between the bilayers was ~ 3 nm and the remaining water thickness is ~ 10 nm to avoid the interactions between bilayers due to periodic boundary condition. Both lipid bilayers were arranged parallel with the x-y plane of the simulation box with initial area per lipid molecule of 50.5 Å$^2$. The box size was allowed to change during simulation. Each bilayer was composed of $N_{lip}$ = 180 DPPC molecules (90 for one

leaflet), varying thickness of water between bilayer $D_w = D_{com} - D_{p-p}$ from $\sim$ 27 Å to 6 Å, where $D_{com}$ and $D_{p-p}$ stand for the distance between center of mass and between phosphate atoms of the bilayers respectively. An atomistic configuration of the two bilayers in water was shown in Fig. 3.1. At a periodic boundary condition, the MD simulations were carried out with a GROMACS package of 4.6.1 with CHARMM36 force field and CHARMM TIP3P water model. The simulations were performed in following steps: firstly, the all atom bilayer systems were equilibrated for 5 steps and 1 step of energy minimization. Then the center of mass for bottom bilayer was pulled towards the upper bilayer just as the process of experiment done in surface force measurement in SFA. The pulling was accomplished in three stages through the pull code from GROMACS package. The time and spring constant for pulling for each stage was shown in Table 3.1. After generating series of configurations with varied distances between bilayers, all the water molecules with higher or lower density were removed and the simulation box was filled with constant total water molecules but varied number of water between bilayers due to varied $D_{com}$. Umbrella sampling was done for 20 ns simulation for PMF calculation. Finally, each of the configurations with a COM difference of $\sim$ 0.2 nm was chosen to conduct an equilibrium production run of 20 ns for further structure and dynamics analysis. Nose-Hoover thermostat [23] was used to maintain a constant temperature at 298K and Parrinello-Rahman method [24] was used to control the pressure at 1 bar. Both the short-range cut-off distance for van der Waal and Coulombic energy calculation was 1.2 nm. For long-range electrostatic force, Particle Mesh Ewald (PME) was employed.

The radius distribution function (RDF), mean square displacement (MSD) and self-intermediate scattering function (SISF) were calculated at different thicknesses of water from 23.8 Å to 6.1 Å.

**Table 3.1** The spring constant and time used when pulling the bottom bilayer towards the upper bilayer during the three stages.

| Stages | Time | Spring constant (kJ mol$^{-1}$nm$^{-1}$) | Water thickness $D_w$ between bilayers |
|--------|------|------------------------------------------|----------------------------------------|
| 1 | 1.5 ns | 2000 | ~ 2.5 nm to 1.8 nm |
| 2 | 0.5 ns | 3000 | 1.8 nm to 1.0 nm |

| 3 | 1 ns | 4000 | 1.0 nm to 0.6 nm |
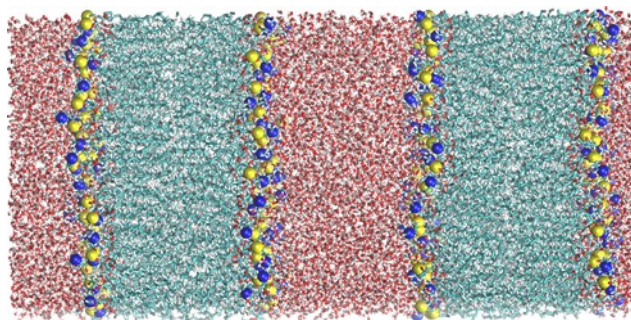


**Figure 3.1** Atomic configuration of DPPC lipid bilayers in water. Green lines stand for the lipid chains, blue and yellow solid circles stand for nitrogen and phosphate atoms in the head groups. For water molecules, red dot stands for oxygen and white dot stands for hydrogen.

### 3.4 Results and discussion

#### 3.4.1 Atomic force microscopy of DPPC bilayer covered Mica

DPPC Lipid Bilayers were prepared on mica through the LB methods described above. The structure of the lipid membrane in water was shown in Fig. 3.2A. Large areas of mica were covered with lipid bilayer exhibiting clearly defined edges. As described previously, the film deposited at a surface pressure of 15 mN/m contains irregular defects with the appearances of furrows represented by green arrows, which are ~ 2.6 nm lower than the surrounding bilayer. The size of the defects was reported to correlate with the different surface pressures and the speed of raising and dipping the substrate.[25] Holes were also formed on the membrane as reported before [26] using the same preparation method. The desorption of the lipid molecules of inner leaflet during bilayer deposition processes was responsible for the formation of these holes.[27] The vertical height profile of DPPC bilayer was shown in Fig. 3.2B.
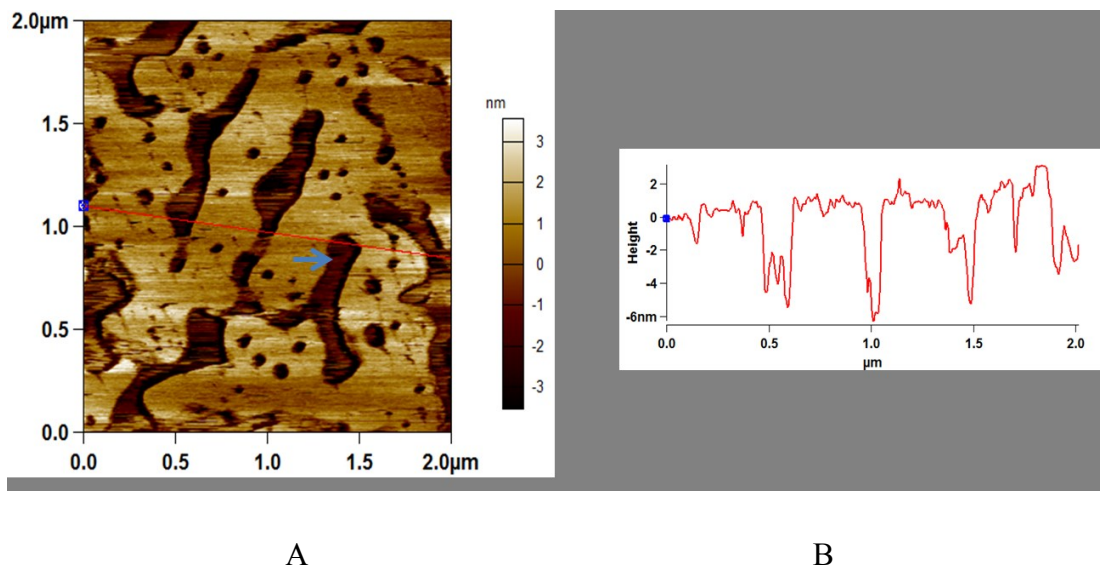
**Figure 3.2** AFM images of DPPC bilayer prepared on mica substrate from LB trough. A: a DPPC bilayer, the blue arrow indicates defects. B: Z-direction profile indicates the depth of defects and thickness of the deposit film.

### 3.4.2 Surface force measurements between two DPPC bilayers
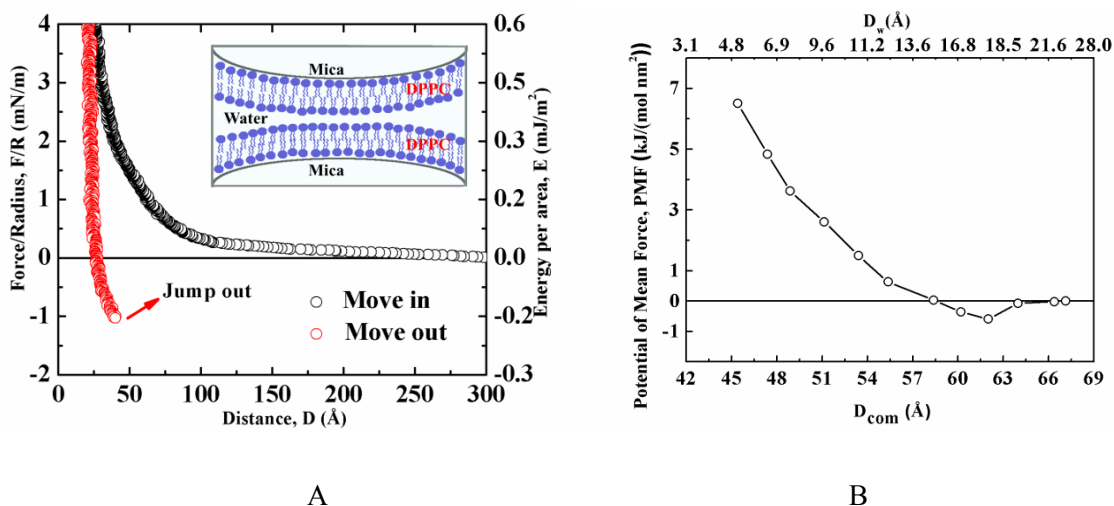




**Figure 3.3** A: Measured forces between DPPC bilayers in water. The surfaces were brought together (red open circles) into contact and then separated (black open circles), where D = 0 is defined as lipid-lipid contact.  Note: A jump out indicated adhesion happened. The inset shows schematic of the supported bilayers and surface geometry in the SFA experiment. B: Simulated

energy-distance profiles of DPPC bilayers in water, where $D_w = 0$ is defined as the phosphate-phosphate contact of opposing lipid bilayer.

The measured force profile of two DPPC bilayers deposited on mica in water at room temperature was represented in Fig. 3.3A. The thickness of hydrated DPPC bilayer was determined to be 5.98±0.04 nm by measuring the mica-mica contact before bilayer deposition and measuring bilayer-bilayer contact after the bilayers were prepared with the LB methods. The thickness measured through SFA was agreed with the AFM test as mentioned before. For the approaching process, a weak repulsion started at a distance of around 250 Å, which was a shorter range compared to the results measured in electrolyte solution.[16]  However, this repulsion begun with a longer range than normal results supposed to obtain in water, which was ascribed to a fact that DPPC bilayer bears a small but significant charge in even pure water. The process of bring the two surfaces together was a difficult "dehydration" process [28] in which the initial water-water and lipid-water structure should be broken and reorganized continuously as the limited space remained for the system. For the separating process, a jump out occurred, suggesting adhesion was measured with a value of $\sim 1$ mN/m with area per lipid 52 Å$^2$. The reported adhesion between DPPC in water ranged from $\sim 0.3$-0.5 mN/m [20]  with area per lipid 48 Å$^2$ to $\sim 0.8$ mN/m [16] with the same area per lipid as our case. For adhesion between lipid membranes, one origin is from the van der Waals force [20] and the other contribution is from the hydrophobic force due to the defects.[29, 30] Therefore, we propose that the hydrophobic force due to increased probability of exposing the hydrophobic chains at larger area per lipid is accounted for the adhesion measured.

### 3.4.3 Potential of mean force (PMF)

There was no unique way to define the distance between lipid bilayers due to the thermal fluctuation and surface roughness of lipid bilayer in simulation. Here the separation $D_w$ was obtained as the average distance of COMs ($D_{com}$) of the two bilayers deducted by the average distance between phosphate atoms in lipid bilayer ($D_{p-p}$).  All the distances were calculated based on configurations of the last 2 ns of the total 20 ns production simulation.

Fig. 3.3B displays the PMF for the two DPPC bilayers as a function of intermembrane distance. It can be seen that the PMF exhibited an energy minimum as the water thickness $D_w$

was ~ 18 Å, consistent with the place of the energy minimum between vesicles [31] and equilibrium separation measured for DPPC bilayers.[16] The PMF changed from negative to positive when the water thickness was ~ 13 Å. When $D_w$ ranges from ~ 10 Å to ~ 6 Å, the energy calculated was from ~ 2 to ~ 6 kJ/(mol nm$^2$), which was generally matched with the results of PMF method for DPPC bilayer interaction in coarse grained water model.[15]

The agreement between MD simulation and SFA experiments suggests the current molecular model can reasonably describe the physical experimental system composed of the lipids bilayers in water. There has been lasting debates for the resources of the short range repulsive force between neutral lipid bilayers in water: osmotic pressure, "double layer" force, undulation force, head-group overlapping force and hydration force, et al. The first four models based on the lipid membrane itself while hydration force is ascribed to the solvent effect. Obviously, water molecules play a critical role in this complex system and mediate interactions between the lipid films. Therefore, it is necessary to perform more quantitatively analysis on the model system to investigate the origin of the molecular interaction between lipid layers.

### 3.4.4 Water molecules between lipid bilayers

The water structure was first characterized by radial distribution functions (RDFs) noted as g (r), by the following equation,[32]

$$g(r) = \frac{2V}{N^2_m} \left\langle \sum_{i<j} \delta(r - r_{ij}) \right\rangle \tag{3.7}$$

where $V$ and $N_m$ stand for the volume and number of atom in the sample and σ is the delta function of relative separation between radius $r$ and atoms pair separation $r_{ij}$. In molecular dynamics, the RDF can be calculated using a histogram of discretized separations. Then

$$g(r_n) = \frac{Vh_n}{2\pi N_m^2 r_n^2 \Delta r} \tag{3.8}$$

where $h_n$ is the number of atom pairs (i, j) for which $(n-1)\Delta r \le r_{ij} < n\Delta r$, assuming $\Delta r$ is sufficiently small, and

$$r_n = (n - \frac{1}{2})\Delta r \tag{3.9}$$

The intensity of the RDF at distance $r$ is proportional to the probability of finding an atom at $r$. At larger distances, g (r) of bulk water tends to unity and at small intermolecular distances it tends to zero due to repulsive forces forbidding interpenetration. The coordination number $N_c$ changes with the sharpness and height of first peak of RDF [33] and could be defined as:

$$N_c = 4\pi\rho \int_0^{r_{min}} r^2 drg(r) \tag{3.10}$$

In the coordination number calculation, $\rho$ is the number density of water, $r_{min}$ is the location of first minimum of $g$ (r). As shown in Fig. 3.4A, positions of the first peak (2.75) were nearly same for all the three separations, suggesting the nearest neighbor distance between water molecules was insensitive to the separation distance. According to Eq. 3.10, the calculated $N_c$ was 4.2 for $D_w$ = 23.8 Å, 4.0 for $D_w$ = 10.8 Å and 3.7 for $D_w$ = 6.1 Å. The coordinate number for bulk water here was 4.9 consistent with the experimental value, which was reported to 5.0.[22] $N_c$ has shown to be reduced when water molecules were confined between lipid bilayers compared to their bulk counterparts, suggesting the water structure changed as separation distance reduced to 6.1 Å. The $g$ (OO) could not tell us more about structural information beyond the first peak. In Fig. 3.4B, the two peaks of $g$ (OH) happen at ~ 1.85 Å and 3.25 Å, where the second peak is higher than the first. The number of hydrogen bond number is estimated by integration under the first peak of $g$ (OH).[33, 34] The integral of the first peak in g (OH) declines from 1.74 (bulk water) to 1.20 ($D_w$ = 6.1 Å). In this way, the average number of hydrogen bond reduces from 3.48 to 2.40 when water is gradually reduced between the bilayers. The HH partial structure functions, exhibiting the characteristic tetrahedral ordering of water-water hydrogen bonds [35] are shown in Fig. 3.4C. Similarly, two peaks were observed and locate at 2.45 Å and 3.95 Å, respectively. Overall, with reduced number of the water molecules, the peak value decreased correspondingly. The peaks of g (OH) and g (HH) shift a little bit inwards, which is a sign for narrower geometric range for hydrogen bonding with shorting the distance between the opposing bilayers.
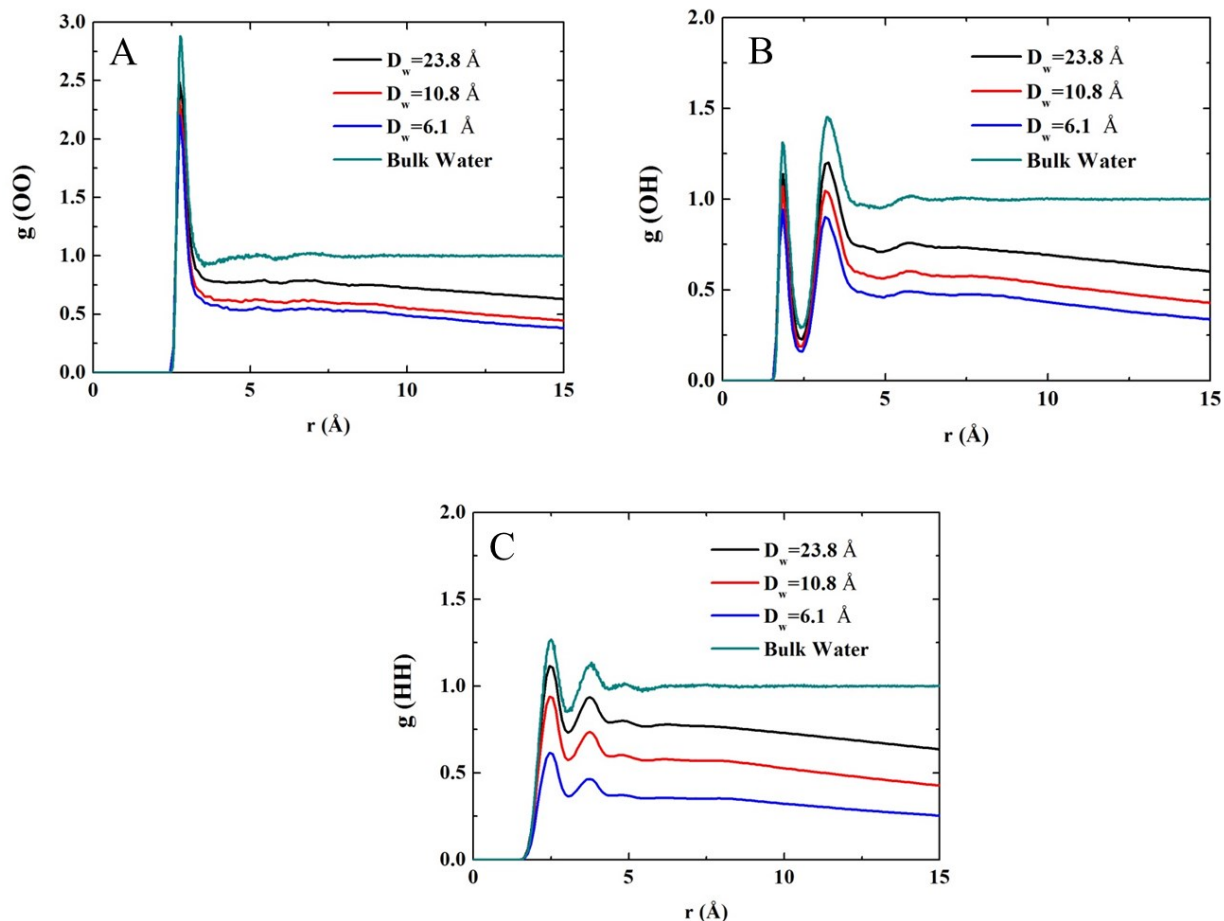
**Figure 3.4** Radius distribution functions of water at three different separations of lipid surfaces, $D_w$ = 23.8 Å (black line), $D_w$ = 10.8 Å (red line), $D_w$ = 6.1 Å (blue line), Bulk (green line) respectively.

In addition to the analysis of water structure, we also performed the mean squared displacement (MSD) calculation to determine the dynamic property of water as a function of lipid bilayer separation distance. The MSD shown in Fig. 3.5A is defined as the $<x^2+y^2> = 4D_c\,t$, where $D_c$ is the diffusion coefficient in x-y plane. The diffusivity of water molecules could be obtained by fitting the mean square displacement with simulation time at all separations between bilayers. As shown in Fig. 3.5B, the diffusion coefficient increased from $0.5 \times 10^{-5}$ cm$^2$/s with separation of 6.1 Å to $0.92 \times 10^{-5}$ cm$^2$/s with a separation of 8.8 Å, nearly two folds magnitude. The diffusivity continues to increase until it reaches $2.26 \times 10^{-5}$ cm$^2$/s when $D_w$ was 23.8 Å, which agreed well with the experiment two dimensional diffusion coefficient of the bulk water (2.3 $\times 10^{-5}$ cm$^2$/s at 298 K).[36] The distinct reduction of interfacial solvent mobility was in accord

with the implications of a number of past experiments.[37] A separate study on the permeation of water molecules through lipid membranes [38] pointed out the slowing down mobility of water molecules at the water membrane interfacial region was due to the partial charge distribution of lipid head groups, which might form hydration shell with water molecules.

The SISF was calculated with a $Q_0$ value of 2.25 Å$^{-1}$ and the results were shown in Fig. 5C. It was reported that the SISF of super-cooled water molecules on the SPC/E model [39] can be fit to the equation

$$F_S(Q_0, t) = [1 - f_{Q_0}] \exp[-\left(\frac{t}{\tau_{short}}\right)^2] + f_{Q_0} \exp[-\left(\frac{t}{\tau_\alpha}\right)^{\beta_\alpha}]$$

(3.11)

where $Q_0$ equals 2.25 Å$^{-1}$ at the peak of oxygen-oxygen structure factor, $\tau_{short}$ and $\tau_\alpha$ refer to the relaxation time of Gaussian term and α relaxation (also stretched exponential term) respectively. To describe the dynamics of the water molecules hydrating the lysozyme in the presence of trehalose [40], a third stretched exponential term was added to Eq. 3.11

$$F_S(Q_0, t) = [1 - f_{Q_0} - f_{Q_0}'] \exp[-\left(\frac{t}{\tau_{short}}\right)^2] + f_{Q_0} \exp[-\left(\frac{t}{\tau_\alpha}\right)^{\beta_\alpha}] + f_{Q_0}' \exp[-\left(\frac{t}{\tau_{long}}\right)^{\beta_{long}}]$$

(3.12)

Similarly, we adopted Eq. 3.12 to describe the dynamics of water molecules confined between lipid bilayers. At three different thickness of water layer, it was found that all the data fit quite well to Eq. 3.12 noted as the dashed lines in Fig. 3.5C. Compared the relaxation times extracted from the fitting curves, we found that dehydration of the lipid bilayers lead to elevated value of both $\tau_\alpha$ and $\tau_{long}$ seen in Fig. 3.5D. Consequently, the thinner the water layer, the slower dynamics of water molecules were obtained.

A                 B

C                 D
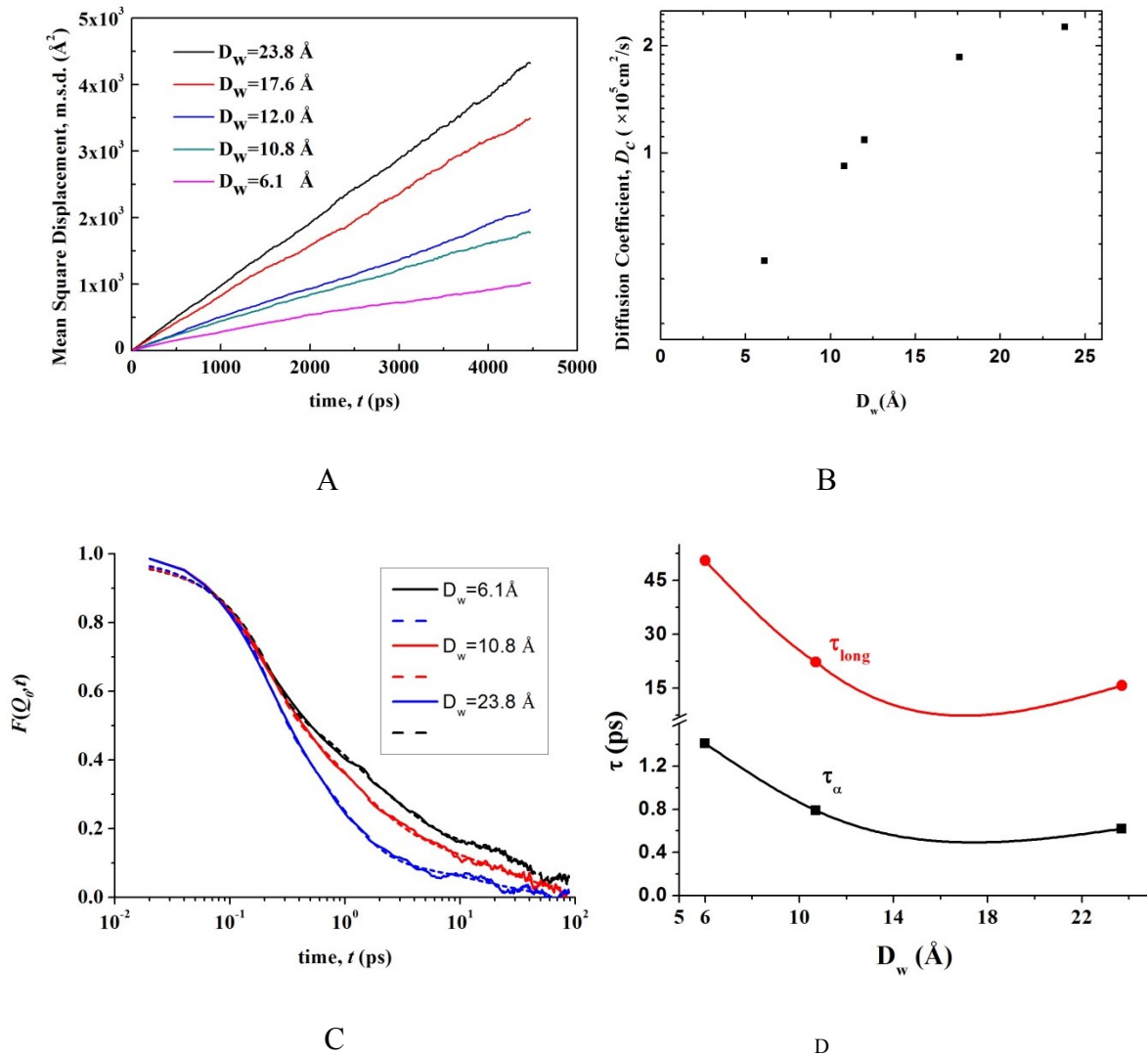
**Figure 3.5** The dynamics of water molecules between lipid bilayers. A: Mean square displacement (MSD) versus with simulation time. B: Diffusion coefficient of water versus water thickness between opposing lipid bilayers. C: The self- intermediate scattering function for the $Q_0$ value and the three different thicknesses of water between bilayers examined. The dashed lines are fits to Eq. 3.12. D: Water thickness dependence of the relaxation times.

### 3.4.5 Lipid bilayer thickness and area per molecule

During PMF calculation, we pulled the bottom bilayer towards the upper bilayer by mounting a spring in the COM of the bottom bilayer. With reduced number of water molecules between the bilayers, the thickness of bottom bilayer experienced two-stage variation as shown in Fig. 3.6A ~ D. First, the thickness of bilayer $D_{p-p}$ increases shown from Fig. 3.6 A to B (red

area reduced), which is corresponding to the attractive part in the simulated PMF result. In this stage, the variation of thickness and area per molecule was highly matched with the experimental result when the bilayer was moderately dehydrated.[31] Later on the thickness of bilayer gradually reduced with increasing area of red region as seen in Fig. 3.6B towards D. This stage was consistent with the PMF result that the repulsive force dominates over the attractive force. The area per molecule varied reversely compared with the thickness of the lipid $D_{p-p}$. Shown as the blue line in Fig. 3.6E, the area decreased as the bilayers were brought together from $D_w =$ 23.8 Å to $D_w = 17.6$ Å. After that, the area per lipid was gradually elevated to a final value of ~ 58 Å$^2$ with thickness of bilayer was generally decreased to a final value of ~ 3.85 nm. At this stage of dehydration, the reduced thickness could be verified with the phenomena of chain interdigitating as shown in Fig. 3.7B. For other simulations with method of umbrella sampling, the area per molecule increased with reduced thickness of water layer.[15] However, they failed to reveal attractive force and the regime when area per molecule was reduced with increased thickness of bilayer.
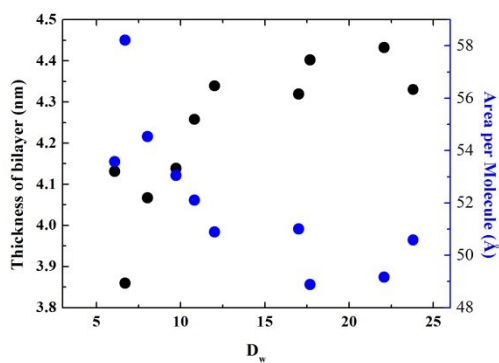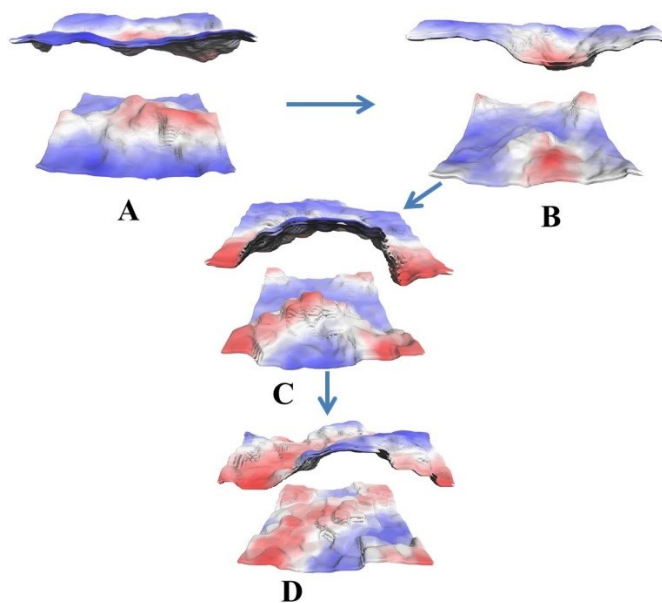
**Figure 3.6** The average thickness of bottom bilayer (phosphate-phosphate distance of the same bilayer) during the dehydration process with water thickness $D_w$ = 23.8 Å, 17.6 Å, 10.8 Å, 6.1 Å, from A ~ D respectively. From red to blue, the value of thickness was increased. E: The average thickness of bottom bilayer $D_{p-p}$ and area per lipid molecule varied with the thickness of water between bilayers.

### 3.4.6 Lipid chain packing during dehydration



**A**                                                                **B**
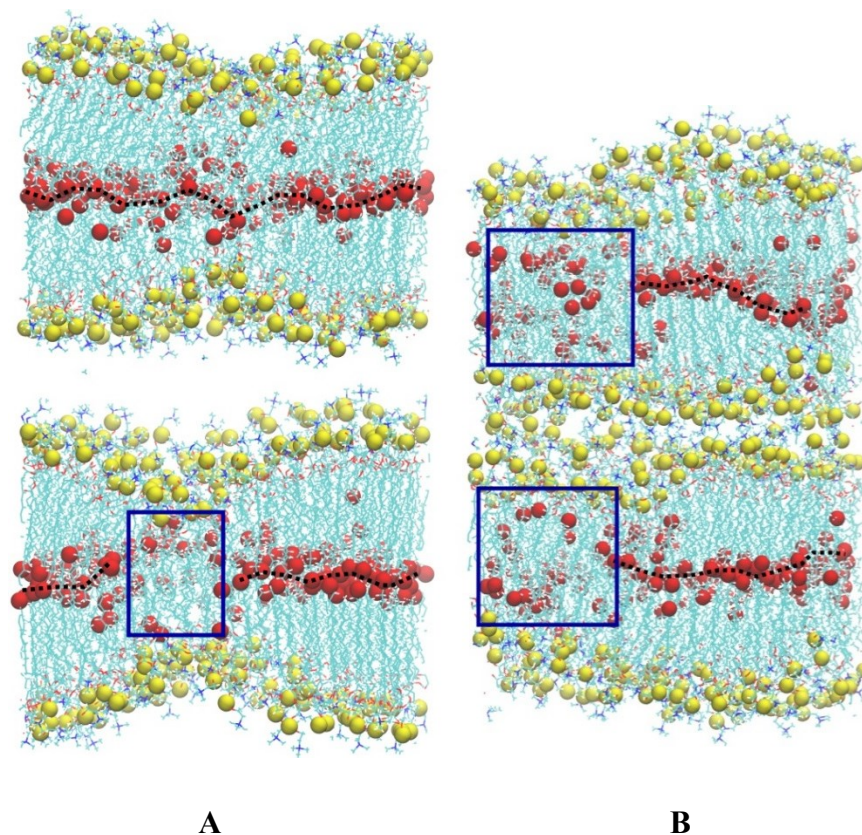
**Figure 3.7** The chain packing of bilayers changes during dehydration of the bilayers, where A: $D_w = 23.8$ Å, B: $D_w = 6.1$ Å. Yellow color means phosphate atoms in the head groups, red stands for the end carbon atoms of one lipid chains. Blue squares show the interdigitating region of lipid chains.

As we have mentioned before, the PMF between DPPC bilayers were calculated by pulling the bottom bilayer towards the upper bilayer through three stages distinguished by the spring constant of the "spring" applied on the COM of bottom bilayer. When $D_w = 23.8$ Å, ripple phase of lipid bilayers with characteristic of interdigitated area and thinner domains were observed shown as blue square in Fig. 3.7A. We could also locate partially the middle plane within bilayer with dashed black line. When the water was greatly reduced with $D_w = 6.1$ Å, the portion of ripple phase increased shown as larger blue squares in Fig. 3.7B. Also, the chains in upper and lower leaflet of the same bilayer interpenetrated with no distinguished middle plane observable. Ripple phase noted as $P_{\beta'}$ was also obtained by cooling the lecithin bilayers through MD simulations.[41] The formation of ripple phase were associated with the membrane dehydration

process,[42] increased pressure applied on lipid bilayers,[43] and the addition of alcohols and fatty acid.[44, 45] Here, in our case, the perturbation of lipid chains were possibly attributed to two reasons: first, it is originated from the dehydration process, which destroying the hydrogen bond network of lipid head group. This is why the chain interdigitating of PC is easier to occur comparing with DPPE, where DPPE head groups could form denser network of hydrogen bond.[43] Second, the chain interpenetration was induced by the strong pressure applied when bring the two lipid bilayers close together. From the simulated PMF, we could estimate a pressure as high as $\sim 10^7$ Pa applied on the opposing lipid bilayers.

### 3.4.7 Adhesion between lipid bilayers from lipid head groups

The adhesion between the lipid chains is closely related to biological processes such as membrane self-assembling [46] and fusion.[47] Fig. 3.8 shows the radius distribution functions between partially negatively charged phosphate atoms and positively charged nitrogen atoms in two approaching bilayer head groups at smaller distance $D_w$ = 6.1 Å and larger distance $D_w$ = 23.8 Å. When $D_w$ = 6.1 Å, the first peak of N-P distribution as shown blue line in Fig. 3.8 was greatly shifted to a smaller separation compared to the first peaks of P-P and N-N. This reconstruction of the lipid head group was due to the electrostatic energy minimization between positively charges N group and negatively charged P group, which was consistent with simulation results from thermodynamic extrapolation method.[14] For larger distance, i.e., $D_w$ = 23.8 Å, the surface was less constraint, confirmed in the inset of Fig. 3.8. Besides the van der Waals force and hydrophobic force we have mentioned, here the simulation showed that the interactions between N groups and P groups from opposing bilayers are another possible resource for the adhesion measured from the SFA experiment. The simulated N-P peak also supported the existence of hydration attraction between neutral phospholipid bilayers found from previous experiments.[48]
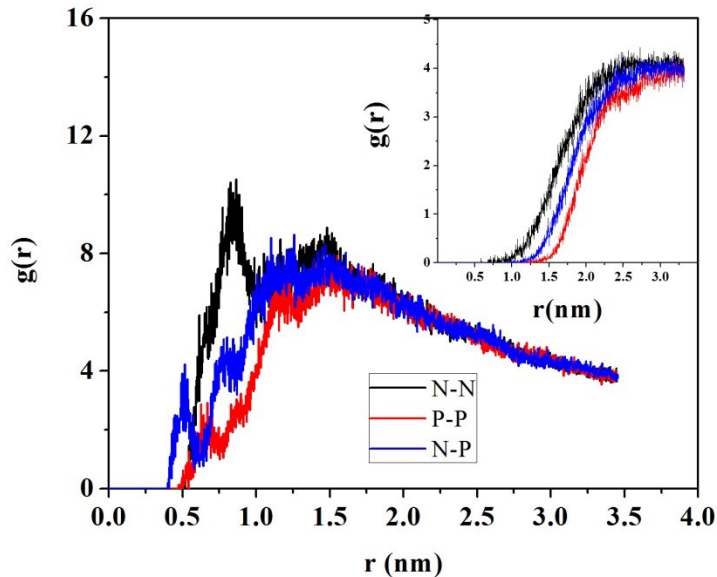
**Figure 3.8** Radius distribution functions between nitrogen (N) and phosphate (P) atoms at small distance $D_w = 6.1$ Å and (Inset) $D_w = 23.8$ Å in opposing lipid bilayers.

### 3.5 Conclusions

The interactions between DPPC bilayers in water were investigated using SFA force measurements an*d* simulated using umbrella sampling molecular dynamics methods with separation of bilayers ranging from ~ 27 Å to ~ 6 Å. Through umbrella sampling method of simulation, we confirmed the presence of an attractive force corresponding to the existence of an energy minimum, which is highly matched with results measured from SFA.[16] Also, it was found that the adhesion measured in our SFA experiment when separating the bilayers was assigned to three resources. Firstly, the adhesion originated from the attractive van der Walls force as suggested from previous reported results between DPPC lipid bilayers. In this sense, the existence of attractive part of measured force was remarkably consistent with the energy minimum found from the simulation results. Secondly, adhesive force might arise from the exposed hydrophobic chains. We found evidences from the AFM images of DPPC bilayers, lower area (defects) with smaller membrane thickness possibly contributing to the exposing of lipid chains. At last, the adhesion could also result from the nitrogen and phosphate groups, which is noticeable as the peak of N-P when the water thickness is ~ 0.6 nm as shown in Fig. 3.8.

The simulation also confirmed the existence of hydration repulsion followed by the energy minimum. During the dehydration process of lipid bilayers, it was found that the movement of water molecules was greatly restricted between highly compressed bilayers. In addition, the lipid chain thickness was first increased at moderate dehydration condition and later decreased with characteristic of chain interdigitating, which is possibly due to the dehydration and large pressure exhibited on the bilayers when water molecules were largely removed between bilayers. Overall, our simulations showed nice consistency with experimental results in the high sensitivity of locating both attractive and repulsive part of the energy-distance curve and provided molecular level and detailed information of lipid chain parking and water properties for bilayers interacting in water.

**Reference**

[1] H. Bachofen, U. Gerber, P. Gehr, M. Amrein, S. Schurch, Structures of pulmonary surfactant films adsorbed to an air-liquid interface in vitro, Bba-Biomembranes, 1720 (2005) 59-72.

[2] S. Schurch, R. Qanbar, H. Bachofen, F. Possmayer, The Surface-Associated Surfactant Reservoir in the Alveolar Lining, Biol Neonate, 67 (1995) 61-76.

[3] D. Follows, F. Tiberg, R.K. Thomas, M. Larsson, Multilayers at the surface of solutions of exogenous lung surfactant: Direct observation by neutron reflection, Bba-Biomembranes, 1768 (2007) 228-235.

[4] Lindqvis.B, An Introduction to Clay Colloid Chemistry for Clay Technologists Geologist and Soil Scientists, Sven Kem Tidskr, 77 (1965) 382.

[5] V.A. Parsegian, N. Fuller, R.P. Rand, Measured Work of Deformation and Repulsion of Lecithin Bilayers, P Natl Acad Sci USA, 76 (1979) 2750-2754.

[6] S.D. Shoemaker, T.K. Vanderlick, Intramembrane electrostatic interactions destabilize lipid vesicles, Biophys J, 83 (2002) 2007-2014.

[7] J.N. Israelachvili, R.M. Pashley, Double-Layer, Vanderwaals and Hydration Forces between Surfaces in Electrolyte-Solutions, H-S Z Physiol Chem, 362 (1981) 1178-1179.

[8] J. Marra, Controlled Deposition of Lipid Monolayers and Bilayers onto Mica and Direct Force Measurements between Galactolipid Bilayers in Aqueous-Solutions, J Colloid Interf Sci, 107 (1985) 446-458.

[9] R.M. Pashley, Hydration Forces between Mica Surfaces in Aqueous-Electrolyte Solutions, J Colloid Interf Sci, 80 (1981) 153-162.

[10] T. Hayashi, A.J. Pertsin, M. Grunze, Grand canonical Monte Carlo simulation of hydration forces between nonorienting and orienting structureless walls, J Chem Phys, 117 (2002) 6271-6280.

[11] A. Pertsin, D. Platonov, M. Grunze, Direct computer simulation of water-mediated force between supported phospholipid membranes, J Chem Phys, 122 (2005) 244708.

[12] A. Pertsin, M. Grunze, Computer simulations of water-mediated force between phospholipid membranes, Curr Opin Colloid In, 16 (2011) 534-541.

[13] M. Kanduc, E. Schneck, R.R. Netz, Hydration Interaction between Phospholipid Membranes: Insight into Different Measurement Ensembles from Atomistic Molecular Dynamics Simulations, Langmuir, 29 (2013) 9126-9137.

[14] E. Schneck, F. Sedlmeier, R.R. Netz, Hydration repulsion between biomembranes results from an interplay of dehydration and depolarization, P Natl Acad Sci USA, 109 (2012) 14405-14409.

[15] Y.G. Smirnova, S. Aeffner, H.J. Risselada, T. Salditt, S.J. Marrink, M. Muller, V. Knecht, Interbilayer repulsion forces between tension-free lipid bilayers from simulation, Soft Matter, 9 (2013) 10705-10718.

[16] J. Marra, J. Israelachvili, Direct Measurements of Forces between Phosphatidylcholine and Phosphatidylethanolamine Bilayers in Aqueous-Electrolyte Solutions, Biochemistry, 24 (1985) 4608-4618.

[17] S. Yu, P.G.R. Harding, N. Smith, F. Possmayer, Bovine Pulmonary Surfactant - Chemical-Composition and Physical-Properties, Lipids, 18 (1983) 522-529.

[18] H. Zhang, Q.H. Fan, Y.E. Wang, C.R. Neal, Y.Y. Zuo, Comparative study of clinical pulmonary surfactants using atomic force microscopy, Bba-Biomembranes, 1808 (2011) 1832-1842.

[19] T.L. Kuhl, D.E. Leckband, D.D. Lasic, J.N. Israelachvili, Modulation of Interaction Forces between Bilayers Exposing Short-Chained Ethylene-Oxide Headgroups, Biophys J, 66 (1994) 1479-1488.

[20] R. Orozco-Alcaraz, T.L. Kuhl, Interaction Forces between DPPC Bilayers on Glass, Langmuir, 29 (2013) 337-343.

[21] S. Kumar, D. Bouzida, R.H. Swendsen, P.A. Kollman, J.M. Rosenberg, The Weighted Histogram Analysis Method for Free-Energy Calculations on Biomolecules .1. The Method, J Comput Chem, 13 (1992) 1011-1021.

[22] W.L. Jorgensen, J. Chandrasekhar, J.D. Madura, R.W. Impey, M.L. Klein, Comparison of Simple Potential Functions for Simulating Liquid Water, J Chem Phys, 79 (1983) 926-935.

[23] D.J. Evans, B.L. Holian, The Nose-Hoover Thermostat, J Chem Phys, 83 (1985) 4069-4074.

[24] J.R. Ray, A. Rahman, Statistical Ensembles and Molecular-Dynamics Studies of Anisotropic Solids, J Chem Phys, 80 (1984) 4423-4428.

[25] M. Benz, T. Gutsmann, N.H. Chen, R. Tadmor, J. Israelachvili, Correlation of AFM and SFA measurements concerning the stability of supported lipid bilayers, Biophys J, 86 (2004) 870-879.

[26] Y.F. Dufrene, W.R. Barger, J.B.D. Green, G.U. Lee, Nanometer-scale surface properties of mixed phospholipid monolayers and bilayers, Langmuir, 13 (1997) 4779-4784.

[27] P. Bassereau, F. Pincet, Quantitative analysis of holes in supported bilayers providing the adsorption energy of surfactants on solid substrate, Langmuir, 13 (1997) 7003-7007.

[28] R.P. Rand, V.A. Parsegian, Hydration Forces between Phospholipid-Bilayers, Biochim Biophys Acta, 988 (1989) 351-376.

[29] C.A. Helm, J.N. Israelachvili, P.M. Mcguiggan, Molecular Mechanisms and Forces Involved in the Adhesion and Fusion of Amphiphilic Bilayers, Science, 246 (1989) 919-922.

[30] J. Kurniawan, N.N. Yin, G.Y. Liu, T.L. Kuhl, Interaction Forces between Ternary Lipid Bilayers Containing Cholesterol, Langmuir, 30 (2014) 4997-5004.

[31] L.J. Lis, M. Mcalister, N. Fuller, R.P. Rand, V.A. Parsegian, Interactions between Neutral Phospholipid-Bilayer Membranes, Biophys J, 37 (1982) 657-665.

[32] D.C. Rapaport, The art of molecular dynamics simulation, 2nd ed., Cambridge University Press, Cambridge ; New York, 2004.

[33] T. Head-Gordon, G. Hura, Water structure from scattering experiments and simulation, Chem Rev, 102 (2002) 2651-2669.

[34] W.L. Jorgensen, J.D. Madura, Temperature and Size Dependence for Monte-Carlo Simulations of Tip4p Water, Mol Phys, 56 (1985) 1381-1392.

[35] A. Luzar, D. Chandler, Structure and Hydrogen-Bond Dynamics of Water-Dimethyl Sulfoxide Mixtures by Computer-Simulations, J Chem Phys, 98 (1993) 8160-8173.

[36] P. Mark, L. Nilsson, Structure and dynamics of the TIP3P, SPC, and SPC/E water models at 298 K, J Phys Chem A, 105 (2001) 9954-9960.

[37] C.F. Polnaszek, R.G. Bryant, Self-Diffusion of Water at the Protein Surface - a Measurement, J Am Chem Soc, 106 (1984) 428-429.

[38] S.J. Marrink, H.J.C. Berendsen, Simulation of Water Transport through a Lipid-Membrane, J Phys Chem-Us, 98 (1994) 4155-4168.

[39] P. Gallo, F. Sciortino, P. Tartaglia, S.H. Chen, Slow dynamics of water molecules in supercooled states, Phys Rev Lett, 76 (1996) 2730-2733.

[40] D. Corradini, E.G. Strekalova, H.E. Stanley, P. Gallo, Microscopic mechanism of protein cryopreservation in an aqueous solution with trehalose, Sci Rep-Uk, 3 (2013) srep01218.

[41] A.H. de Vries, S. Yefimov, A.E. Mark, S.J. Marrink, Molecular structure of the lecithin ripple phase, P Natl Acad Sci USA, 102 (2005) 5392-5396.

[42] C.H. Hsieh, S.C. Sue, P.C. Lyu, W.G. Wu, Membrane packing geometry of diphytanoylphosphatidylcholine is highly sensitive to hydration: Phospholipid polymorphism induced by molecular rearrangement in the headgroup region, Biophys J, 73 (1997) 870-877.

[43] N. Tamai, M. Goto, H. Matsuki, S. Kaneshina, A mechanism of pressure-induced interdigitation of lipid bilayers, J Phys Conf Ser, 215 (2010).

[44] L. Lobbecke, G. Ceve, Effects of Short-Chain Alcohols on the Phase-Behavior and Interdigitation of Phosphatidylcholine Bilayer-Membranes, Bba-Biomembranes, 1237 (1995) 59-69.

[45] A.P. Ramos, P. Lague, G. Lamoureux, M. Lafleur, Effect of Saturated Very Long-Chain Fatty Acids on the Organization of Lipid Membranes: A Study Combining H-2 NMR Spectroscopy and Molecular Dynamics Simulations, J Phys Chem B, 120 (2016) 6951-6960.

[46] P.A. Monnard, D.W. Deamer, Membrane self-assembly processes: Steps toward the first cellular life, Anat Rec, 268 (2002) 196-207.

[47] C.A. Helm, J.N. Israelachvili, P.M. Mcguiggan, Role of Hydrophobic Forces in Bilayer Adhesion and Fusion, Biochemistry, 31 (1992) 1794-1805.

[48] R.P. Rand, N. Fuller, V.A. Parsegian, D.C. Rau, Variation in Hydration Forces between Neutral Phospholipid-Bilayers - Evidence for Hydration Attraction, Biochemistry, 27 (1988) 7711-7722.

# Chapter 4. The effects of pulmonary surfactant-associated protein B on the interfacial properties of phospholipid monolayer *

## 4.1 Introduction

The pulmonary surfactant is composed of predominately lipids with a small portion of proteins. In all surfactant lipids, phospholipids make up ~ 80-90%, and generally ~ 40% of the phospholipids are dipalmitoylphosphatidylcholine (DPPC).[1] The pulmonary surfactant film can reduce the surface tension of air-water interface to a value near zero and minimize the work of the lung during the inspiration and expiration cycles.[2] Four major pulmonary proteins, SP-A, B, C and D, play a critical role in interfacial activities and immune defense. Proteins SP-A and SP-D are collectins involved in lung defense functions, such as the clearance of bacteria, fungi and apoptotic cells and the reduction of allergic reactions.[3] Proteins SP-B and SP-C are hydrophobic proteins, which are mainly related to the structure and interfacial behaviors of surfactant.[4] Mature SP-B is a homodimeric protein and each monomer is composed of 79 amino acids with a molecular weight of 8.7 kDa.[5] In vivo, SP-B is critically required for lung functioning and survival, as it was found that the disruption of gene could cause respiratory failure in animals.[6] The deficiency of SP-B results in lethal respiratory distress syndrome [7] and relates to the congenital alveolar proteinosis [8] in humans. The neonatal respiratory distress syndrome (NRDS) results from a lack or failure in production of mature pulmonary surfactant.[9] The surfactant replacement therapy has been developed with promising results on NRDS.[10, 11] Surfactant extracted from animals was unsatisfactory since it can cause potential immunological responses and has significant associated reutilization costs. Hence, attention is turning to synthetic lipids as a possible resource of exogenous surfactant and genetically engineered proteins with similar interfacial activities as pulmonary proteins.

Understanding the roles of both the lipids and proteins was required to develop a successful substitute. Previous studies show that DPPC monolayer could develop the circular domains [12] and stripes phases,[13] where the line tension favors the round shapes and the long range electrostatic force favors long strip phases.[14] At certain circumstances, circular (or hexagonal) and strip phases coexist and phase transition can occur in the monolayer.[15, 16] SP-B was found to enhance a network formation in palmitic acid monolayer [17] and reduce the area of the liquid-condensed region in DPPC film.[18] In addition, SP-B induced reversible folding of lipid

monolayer by forming reservoirs at high surface pressure,[19] which challenges the "squeeze out" model.[20] When aggregates or multilayered structure were observed for surfactant monolayers in atomic force microscopy (AFM) studies,[21-23] a question was raised: Do the aggregates re-spread during monolayer expansion with flowing subphase? Though fluorescent images indicating small spots (aggregates) seemly disappeared on expansion, the resolution of those images was quite limited in showing the detailed structure of the monolayer.[17] Hence, morphology of the surfactant monolayer at low surface pressure after cyclic compression-expansion processes may provide important and detailed structural information in the evolution of surfactant film as well as the aggregates formed in those processes. However, the topography of surfactant monolayer at low surface pressure after cyclic isotherm test was not well characterized. Compared to experimental studies, simulations were able to provide complementary information about the structure and dynamic properties for pulmonary surfactant monolayers. An atomistic study found that peptide SP-B$_{1-25}$ partially disordered the palmitic acid (PA) monolayer by anchoring its residues into the monolayer-water interface.[24] At equilibrium, the SP-B$_{1-25}$ preferred a position of parallel to the lipid-water interface in the DPPC monolayer.[25] Coarse grained molecular dynamics (MD) simulations showed that SP-B initiated the formation of the bilayer reservoir connecting with the monolayer and folding of lipid monolayers.[26, 27] These simulations provided important information for lipid-protein interactions. However, the roles of protein on monolayer compression as well as the structural conversion of both SP-B and lipid molecules remains unclear.

In the current study, using microscopy we show that SP-B containing DPPC monolayers form a network with a highly detailed structure and through molecular dynamics simulations we provide possible explanations for lipid-protein interaction mechanisms. Experimental cyclic compression-expansion tests suggest monolayers with proteins developed a network of nano-sized domains and showed an enhanced re-spreading efficiency characterized by fewer aggregates observed in the monolayer after expansion from high surface pressures. Molecular dynamics studies indicated that mini-SP-B might act as nucleation sites by disordering packing of lipid chains upon monolayer compression for the formation of local nano-sized domains. Additionally, the five arginine (ARGs) residues of the peptide showed high but varied hydrogen bonding ability with water, protein and DPPC molecules, providing an interpretation of how the monolayer was retained at the air-water interface during respiratory process.

## 4.2 Experimental methods

The protein was recombinant human pulmonary surfactant-associated protein B derived from yeast, purchased from Mybiosource (San Diego, CA). The storage buffer of protein was phosphate buffered saline and 50% glycerol, and the concentration of protein was 0.75mg/ml. 1,2 Dipalmitoyl-sn-glycero-3-phosphocholine (DPPC) (melting point 41 °C) was purchased from Avanti Polar Lipids, Inc. (Alabaster, AL). Lipids were dissolved in chloroform: methanol (3:1) at a concentration of 1 mg/mL. 4% weight ratio of protein with appropriate amounts of DPPC was also dissolved in chloroform: methanol (3: 1). The water used was purified with a Milli-Q gradient water purification system with a resistivity of 18 MΩ·cm.

Surface pressure-area curves were obtained through a Langmuir Blodgett (LB) trough with a surface area of 98 cm$^2$. The mixture of lipid-protein solution was incubated at room temperature overnight before spreading. After the solution was spread on the water subphase at room temperature, the initial compression started after 10 min. In this work, our focus is to investigate the effects of multiple cyclic tests on model monolayers, where the films were compressed and expanded for cycles with surface pressures ranging from several mN/m (end of expansion) to 50 mN/m (end of compression).

The films were compressed at a rate of 10 mm/min until a surface pressure of 5 mN/m, 10 mN/m or 20 mN/m was reached. Then the films were transferred onto the mica by dipping the freshly cleaved mica in the subphase of Milli-Q water at room temperature at a rate of 3 mm/min. The transfer ratio, t.r., was calculated by the equation, t.r.=$A_{\text{monolayer-reduced}}/A_{\text{substrate}}$ ($A$ means area). The transfer ratio of the monolayers for the AFM studies was 0.95 (±0.03).

AFM studies were carried out using an MFP-3D AFM (Asylum Research Santa Barbara, CA). Bruker silicon nitride cantilevers with spring constant 3-5 N/m were used for imaging the mounted samples with tapping mode in air. For transmission electron microscopy studies, monolayers were first deposited on copper grid (coated with carbon film) and then stained with a heavy metal solution of uranium to enhance the contrast of the TEM observation. Later, the samples were put into a vacuum desiccator. The studies were finally done with a JEOL 2100 transmission electron microscope.

### 4.3 Simulation methods

The simulation systems consisted of a DPPC monolayer centered in a periodic simulation cell with a water layer underneath and vacuum above. Two monolayers were used: one is a DPPC monolayer with 64 lipids and the other is a DPPC monolayer with 62 lipids and 1 mini-SP-B (PDB entry 2DWF). The starting structure of the monolayer was built from the equilibrium bilayer [28] with a united atom model. The protein-DPPC monolayer system was set up with InflateGRO methodology [29] by expanding the distances between lipid molecules and removing those lipids overlapped with protein. Both α-helix in C and N terminals were placed parallel with the monolayer surface fitting the amphipathic helix model.[5] The center of mass for protein was superimposed at the same position as the lipid monolayer. Then the lipid monolayer was gradually shrunk followed by energy minimization (EM) steps while the protein was restrained at the same place. After 27 cycles of shrinking and EM, the monolayer with a protein system was built with a starting area per lipid of $\sim 65$ Å$^2$.

The MD simulations were carried out using GROMACS package of 4.6.1 with a temperature of $T = 298$ K. The force field, GROMOS96 53 A6, was extended with Berger lipid parameters (a united atom model). A Nose-Hoover thermostat [30] was used to maintain a constant temperature. Both the short-range cut-off distance for van der Waal and Coulombic energy calculations was 1.2 nm. For long-range electrostatic force, Particle Mesh Ewald (PME) was employed. After a 500 ps NVT equilibrium process, 40 ns of production simulations were carried out in the NVT ensemble. 3 parallel simulations were performed for all monolayers with and without protein mini-SP-B.

### 4.4 Results and discussion

#### 4.4.1 Effect of protein on the surface activity of the DPPC monolayers

Isotherm experiments were performed at a protein/lipid ratio of 4 wt%, which is close to the SP-B concentration in natural systems. In the isotherm experiments, the surface pressure Π is the difference between the surface tension of pure water at room temperature ($\sim 72.8$ mN/m) [31] and the measured surface tension γ, i.e., $\Pi = 72.8 - \gamma$. Thus, a high surface pressure means a high surface density of lipid and low surface tension. The experimental pressure-area isotherm of DPPC monolayers with SP-B (black solid line in Fig. 4.1 (a)) exhibited higher surface pressure with area per lipid of over 80 Å$^2$ to 50 Å$^2$. The DPPC monolayers (black dashed line in Fig. 4.1

(a)) showed a well-characterized isotherm with a phase transition plateau of 4-8 mN/m.[32, 33] A higher surface pressure indicates that the addition of protein to the monolayer resulted in higher surface activity. The isotherms for multiple compression-expansion cycles of both DPPC monolayers and DPPC monolayers with protein were shown in Fig. 4.1 (b). Similar effects of SP-B in increasing the surface activity of monolayers for all the cycles can be observed. For an area per lipid smaller than 50 $Å^2$, isotherms of DPPC with SP-B and pure lipid membranes are comparable until the end of compression. A crossover was observed at 48 $Å^2$ per lipid molecule between the pure lipid and lipid with protein. Similar crossover point was previously reported to occur at area per lipid about 42 $Å^2$ for the N-terminal part of SP-B [34] and 45 $Å^2$ for minced porcine SP-B mixed with DPPC monolayers.[18] During monolayer expansion (see Fig. 4.1 (b)), the isotherms of monolayers with SP-B proteins showed a pronounced hysteresis compared to the pure lipid monolayers because the monolayer with protein require longer time to reach equilibrium.

We also performed MD simulations to investigate pressure-area isotherms of DPPC monolayers with or without mini-SP-B (2DWF) using an NVT ensemble at 298K. For each monolayer, 40 ns simulations were performed with area per lipid molecule of 70 $Å^2$ to 45 $Å^2$ by rescaling the simulation box. The resulting isotherms are shown in Fig. 4.1 (b). To calculate the surface pressure, the surface tension of SPC water with a value of 52.5 mN/m was derived from molecular simulation of pure SPC water box at 298 K, which agreed well with the simulated surface tension (54.7 mN/m) of SPC water at 300K.[35] The surface pressure of a monolayer can be calculated based on the following equations:

$$\gamma_{system} = \gamma_{monolayer} + \gamma_{water} \tag{4.1}$$

$$\Pi_{monolayer} = \gamma_{water} - (\gamma_{system} - \gamma_{water}) \tag{4.2}$$

For large molecular area (A = 70-65 $Å^2$), the monolayer exhibits a liquid expanded (LE) phase. When the monolayer was compressed from 65 $Å^2$ to 50 $Å^2$, the simulated isotherm showed a higher surface pressure in the presence of protein, which captured the same trend as the experiment result within the same range of area per lipid. This was also consistent with reported experimental results for isotherms of lipid only and protein SP-B containing monolayers.[36] The slopes of the calculated plateau (A= 60-50 $Å^2$) were steeper compared to the slopes in the

experiment. This is possibly related to the finite size effect since smaller systems exhibited higher compressibility without undulation and higher symmetry with periodic boundary conditions in the simulation.[37] For more condensed film (A= 45-50 Å$^2$), the lipid chains of DPPC monolayers showed a more ordered state. Using the SPC water model,[38] simulated surface pressures at high surface lipid density were much larger than the experimental results, which was consistent with other simulations. The surface pressures at high lipid surface density were comparable to experimental results when the CG water (water surface tension: ~ 72 mN/m 298K) model was used.[39] However, the molecular detail of water molecules in the CG model was lost, which means that the model can't be used to study the interactions between water molecules and biological macromolecules.



(a)                                                                (b)
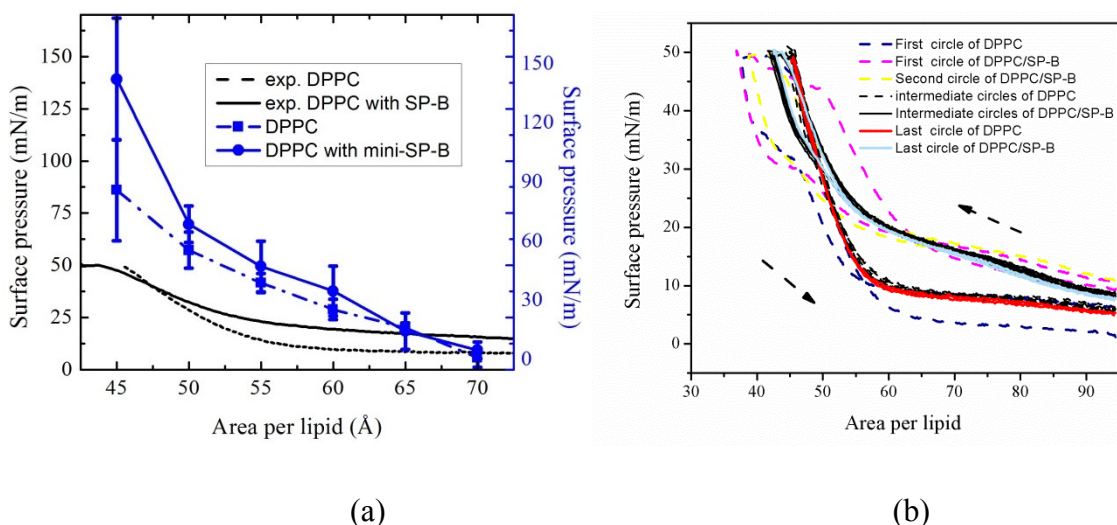
**Figure 4.1** Isotherms for DPPC monolayers. (a) Surface pressure-area isotherms for pure DPPC monolayers and DPPC monolayers mixed with protein SP-B. Representative plots of experimental results (noted as exp.) are presented, where the black dashed line represents DPPC monolayer, the black solid line represents DPPC monolayer with 4 wt% protein SP-B. Atomistic simulated isotherms are depicted, where the blue dashed line with solid squares represents the DPPC monolayer, and the blue solid line with solid circles represents the monolayer with mini-SP-B. Results of three independent simulations were shown as the mean ± standard error of the mean. (b) Multiple cyclic surface pressure-area isotherms for the model monolayers. Representative plots of 7 cyclic experimental results are presented for DPPC monolayers and DPPC monolayers with 4 wt% SP-B. The arrows indicate the direction of cyclic tests. For DPPC monolayers with protein, the isotherms showed little area offset starting the third cycle. The

isotherm of DPPC monolayers kept little area offset starting the second cycle. The isotherm results indicated that fracture of whole monolayers was never reached during the cyclic tests.

## 4.4.2 Effect of protein on the formation of aggregates and the morphology of monolayers.

The morphology of the DPPC monolayers was sensitive to the speed of compression. Round, bean shaped and multi-lobe shaped ordered domains were observed for DPPC monolayers for speed ranging from 0.2 to 8 Å$^2$/ molecule / min.[40] Before film preparation, we conducted cyclic compression-expansion tests at different compression rates and we chose a speed of 10 mm/min (~ 9.8 Å$^2$/ molecule / min).

The AFM images of monolayers after cyclical compression and expansion (surface pressure Π ranging from several mN/m to 50 mN/m) are shown in Fig. 4.2. At a surface pressure of 5 mN/m, the DPPC monolayers show a typical topography of parallel stripe phases [41] in which the high brighter phase is the liquid condensed (LC) phase and the low darker phase is the liquid expanded (LE) phase, as shown in Fig. 4.2 (a). The formation of long continuous LC stripe phases for lipid in the LE phase might originate from the quick absorption of lipids on the solid substrate when transferring the monolayer from the air-water interface.[42]  The width and direction of the stripes can be affected by the properties of monolayer, deposition speed and temperature of subphase.[43, 44] At the same surface pressure, we found that the width of stripes increased due to the presence of protein SP-B. In addition, when SP-B was added, network began to develop between the stripes, as shown in blue squares in Fig. 4.2 (c). However, many stripes with short lengths were found connecting with or between long continuous stripes in lipid only monolayers, which might be the results of the effect of line tension and electrostatic forces within monolayer, as well as viscous forces within both monolayer and the subphase under high compression-expansion speed.[45]

Aggregates (white spots in Fig. 4.2 (a), and Fig. 4.2 (f)) were detected for DPPC monolayers, which might originate from the irreversible folding of hydrophobic lipid chains after multiple compressions to a surface pressure of 50 mN/m. These aggregates due to folding of lipid chains in the monolayer were consistent with previous results.[46] Compared to the DPPC monolayers prepared at surface pressure of 10 mN/m after one-cycle compression-expansion test (Fig. 4.2 (f)), the aggregates were accumulated after 7 cycles and indicating the irreversibility of the

folding for pure lipid monolayers. SP-B containing monolayers showed a significant decrease in the number of aggregates (Fig. 4.2 (c), (d) and Fig. 4.2 (g)), which could be attributed to an enhanced re-spreading ability.

Why aggregates were accumulated in pure lipid monolayers but not those when SP-B was added? This could be understood through how the monolayers response to the high surface pressures. When Π was increased to 20 mN/m, the DPPC film displayed a coalescence of stripe phases with the bright lines as a consequence of the extrusion of edges from adjacent stripes on compression, as shown in Fig. 4.2 (b). These long extrusions gave strong signal that certain lipid molecules were folded under high surface pressures. When pressure was released, those accumulated aggregates were the results of irreversible folding of lipid chains. However, the monolayers with protein response to high surface pressures differently. Instead of tightly packed stripe phases as in the DPPC monolayer, the SP-B containing monolayer (Fig. 4.2 (d)) became a network with nano-sized domains, which can be seen clearly with higher magnification (Fig. 4.2 (e)). In addition, the AFM image of monolayers after one cycle of compression-expansion showed that the stripe phases of LC phases with more branched structure were developed for lipids with proteins monolayers (seen in Fig. 4.2 (g)). From AFM studies by Keating et al.,[21] both micro- and nano-sized LC phases were developed for naturally extracted surfactant (with protein) systems. In Fig. 4.2 (d), monolayers with SP-B formed a network with homogeneously distributed lipid molecules. The disappearance of a large area of the continuous LC phase may be the result of a multiple cyclic compression-expansion process and possibly be related to SP-B dependent lipid reorganization. The morphology shown from TEM results in Fig. 4.3 is consistent with the AFM images. In Fig. 4.3 (a), the DPPC monolayer displayed stripe phases. The monolayer with SP-B exhibited a network with nano-domains, as shown in Fig. 4.3 (b) and (c). The size of the domains in the membrane ranged from several nm to ~ 50 nm. The electrophysiological experiment showed that SP-B induced pores in lipid bilayers and changed the permeation of membranes.[47] However, the mechanisms for nano-domains formation here for monolayers and pore formation in bilayers might be different, which deserved additional study.

(a)    (b)    (c)

(d)    (e)

(f)    (g)
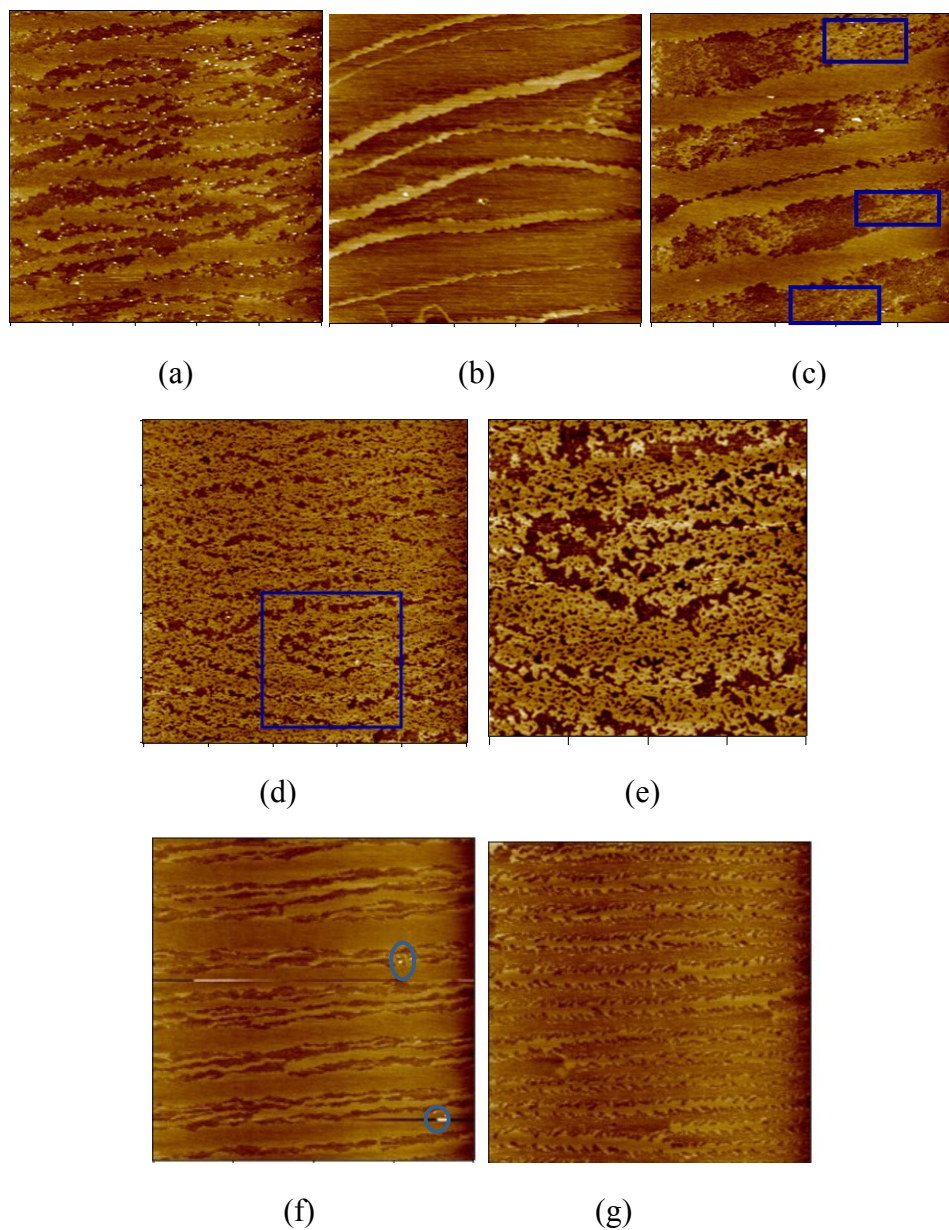
**Figure 4.2** Tapping mode images of model monolayers transferred from air-water interface onto a mica substrate after 7 cycles of compression-expansion (from (a) to (e)). The images from (a) ~ (d) are with width in the 5μm. (a) The DPPC monolayer at 5 mN/m.  (b) The DPPC monolayer at 20 mN/m. (c) The DPPC monolayer with 4% SP-B at 5mN/m. (d) The DPPC monolayer with 4% SP-B at 20 mN/m.  (e) High magnification image (2×2 μm) collected from the region highlighted by a blue box in (d). (f) and (g) (20×20 μm) are tapping mode images of model DPPC monolayer with and without protein transferred from air-water interface after one cycle of compression-expansion at surface pressure of 10 mN/m onto a mica substrate at 20 °C, respectively. Aggregates were found in lipid only monolayers noted as blue circles in (f) while protein

containing monolayer (g) showed highly branches structure of stripe phases. The branched structure highlighted the possible process for the monolayer to develop into a network after more compression-expansion cycles.



(a)                                        (b)



(c)
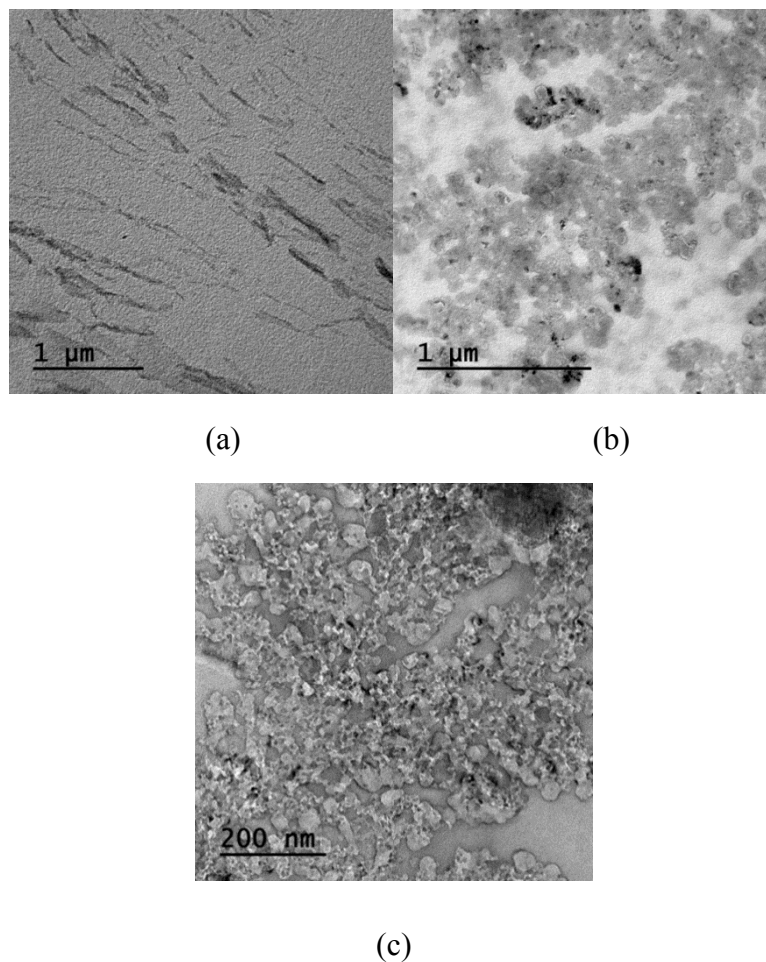
**Figure 4.3** TEM images of model monolayers prepared after 3 compression-expansion cycles at a surface pressure of 10 mN/m. (a) the DPPC monolayer. (b) and (c) DPPC with 4% SP-B monolayer.

### 4.4.3 The orientation and structure of protein SP-B in monolayer

Although the structure of full length SP-B remains unknown, structure analysis of the protein from experiments showed that both the N-terminal and C-terminal of the whole molecule contain a structure of α-helix.[48] In our MD simulation, a peptide (2DWF) with both the N-terminal and C-terminal of SP-B was employed to investigate the lipid protein interaction during the compression of the monolayer system. Fig. 4.4 shows the conformation change of SP-B in

the monolayer during monolayer compression. The starting orientation of peptide is that both helixes are parallel with the surface of the monolayer. Upon compressing, a migration of the whole peptide occurs when the area per lipid molecule was reduced from 65 Å² to 55 Å².
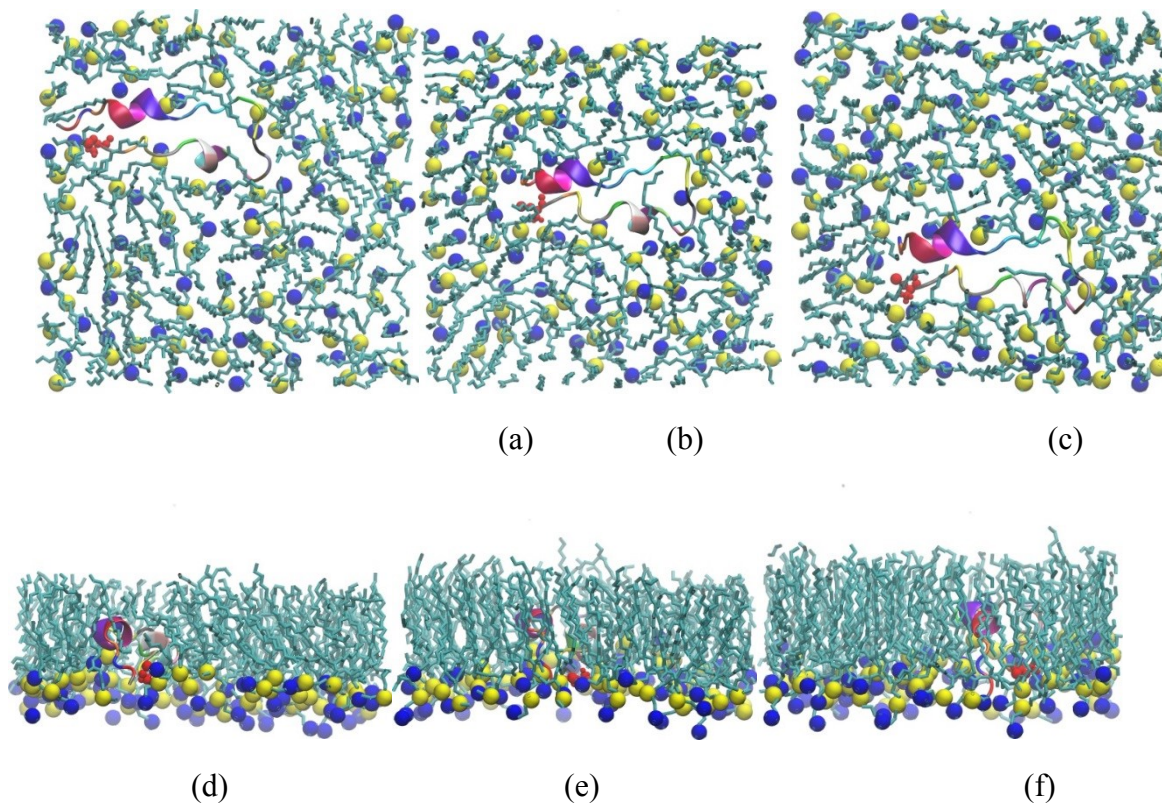


**Figure 4.4** Orientation and structure for mini-SP-B in DPPC monolayers at different area per lipid. Top view of monolayers: (a) 65 Å², (b) 60 Å², (c) 55 Å². Lateral view: (d) 65 Å², (e) 60 Å² (f) 55 Å². Each residue is colored differently with the starting residue CYS1 shown with a van der Waals model (red). Blue represents nitrogen and yellow represents phosphate atoms in DPPC monolayer. The figures are generated with VMD.

Generally, the C-terminal and N terminal helix behaved quite differently; while the C terminus helix remained stable, the N terminus helix was lost at the area per lipid molecule of 55 Å². The helix was also reported to have been partially lost upon compression for SP-B$_{1-25}$ in palmitic acid monolayers when the area per lipid was reduced by ~ 10 Å².[49] Moreover, simulations of the pulmonary model peptide in monolayers demonstrated an interconversion of α-helix to β-sheet with increasing surface pressure.[50] The loss of the helix resulted from the

breaking of intra hydrogen bonds between residues of the mini-SPB, which will be discussed in more detail later in a separate section.

### 4.4.4 The role of protein during the formation of network with nano-sized domains and inhibition of irreversible lipid aggregations.

The packing of lipid chains can be revealed using lipid tail order parameter. The lipid tail order parameter is expressed as:[51]

$$s = \frac{1}{2} < 3\cos^2\theta - 1 > \tag{4.3}$$

where $< 3cos^2\theta >$ denotes the time average of angular fluctuations of the i (i=x,y,z) coordinate axis with respect to the director axis z'. The z' is the normal on the monolayer surface, $\theta$ is the angle between carbon-deuterium (C-D) hydrogen bond to the normal of the monolayer surface. In our case with a united atom model of DPPC molecules, the C-D bond was reconstructed by taking the $C_{i-1}$-$C_{i+1}$ as the z axis, where the y axis is in the plane of $C_{i-1}$-$C_i$-$C_{i+1}$ and perpendicular to the x and z axes. The desired order parameter $S_{cd}$ was calculated from the equation $S_{cd} = 2/3$ $S_{xx} + 1/3$ $S_{yy}$, where the prefactors emerge from an assumption of tetrahedral geometry of the central carbon $C_i$ and equal the approximate of $\cos^2$ and $\sin^2$ of 109.5 degrees, the H-C-H angle. To calculate order parameter, the DPPC molecules were first divided into two groups: 1) lipids in pure DPPC monolayers (shown as black solid circles and black line in Fig. 4.5) and 2) lipids in the monolayer with protein. The second group contained two categories: lipids close to the protein (shown as red squares and red line in Fig. 4.5) were defined as those lipid molecules directly interacting with the protein based on the configurations after production run and all the remaining lipids in the lipid-protein monolayer were treated as lipids far from protein (shown as a red solid triangle and red line in Fig. 4.5. In general, lipid order decreases from the interface region towards the end of the chain. In Fig. 4.5 (a) to (d), when the area per lipid was between 70 Å$^2$ and 55 Å$^2$, the protein restricted the fluctuations of the lipid head-groups, which lead to an increase of order parameter for lipids both close to and far from protein. However, for the segments close to the end of the chain, the lipids close to the protein showed a disordered state compared to the lipids far from the protein. This indicates that the presence of protein might induce the tilting of chain ends by directly interacting with lipids nearby. The condensed packed monolayers (area per lipid= 50 Å$^2$ and 45 Å$^2$) as shown in Fig. 4.5 (c), (f) displayed a distinct

order from high to low, i.e., lipids far from protein, lipids in the DPPC monolayer and lipids close to protein. According to the density map of lipids, the DPPC monolayer formed a clear fold (red circles in Fig. 4.6 (a)), whereas SP-B containing monolayers (Fig. 4.6 (b)) showed no folding, as seen in Fig. 4.6 (c). Full length SP-B simulations demonstrated that the protein promoted lipid reorganization in bilayers through the loop region.[52] Here the loop region of mini-SP-B also exhibited close interactions with the monolayer, in which lipid chains adapted a groove-like domain on the hydrophobic protein surface. In other words, at high surface pressure, the presence of protein blocked the formation of aggregation by creating local domains with low lipid packing density. At the end of compression as shown in Fig. 4.6 (c), the C terminal helix of SP-B was perpendicular to the monolayer. As protein was inserted in the monolayer, the free volume of lipids far away from the protein was reduced, which led to the constrained movement and more ordered packing for lipids far from the protein. Overall, the difference of order parameter between two ends of the chains (carbon numbers 1 and 14) decreased when the area per lipid was reduced from 70 $\text{Å}^2$ to 55 $\text{Å}^2$, consistent with results for the DPPC monolayer simulation.[38]

The diffusion coefficient of lipids was further calculated to investigate the effects of protein on the dynamical properties of lipids as shown in Fig. 4.6 (d). It was found that the diffusion coefficient $D$ for DPPC monolayers decreased sequentially with a reduced area per lipid, showing the same trend as previous studies.[53] The calculated coefficient for lipid molecules in DPPC monolayers ranged from 1 to 4.98 $\times 10^{-7}$ $\text{cm}^2$/s, which was consistent with the reported experimental results for the lateral diffusion coefficient of fluorescent labeled lipid in phospholipid monolayers.[54] Generally, when the area changed from 70 $\text{Å}^2$ to 55 $\text{Å}^2$, the diffusivity of protein containing monolayers was smaller than the DPPC monolayer. While the diffusion coefficient of DPPC monolayers decreased with an increasing surface density of lipid chains, results for monolayers with SP-B remained relatively stable. The $D$ values for DPPC monolayers at area of 55 $\text{Å}^2$ (2.8 ($\pm 0.1$) $\times 10^{-7}$ $\text{cm}^2$/s) and 60 $\text{Å}^2$ (3.2 ($\pm 0.1$) $\times 10^{-7}$ $\text{cm}^2$/s) showed nice agreement with the earlier coarse grained simulations.[37] Upon further compressed to area per lipid of 50 $\text{Å}^2$ ~ 45 $\text{Å}^2$, the monolayers with and without protein showed comparable diffusivity. One explanation is that SP-B disordered the packing of lipids nearby by inducing a groom as seen in Fig. 4.6 (c), which created more room for the overall dynamical movement of lipid molecules.
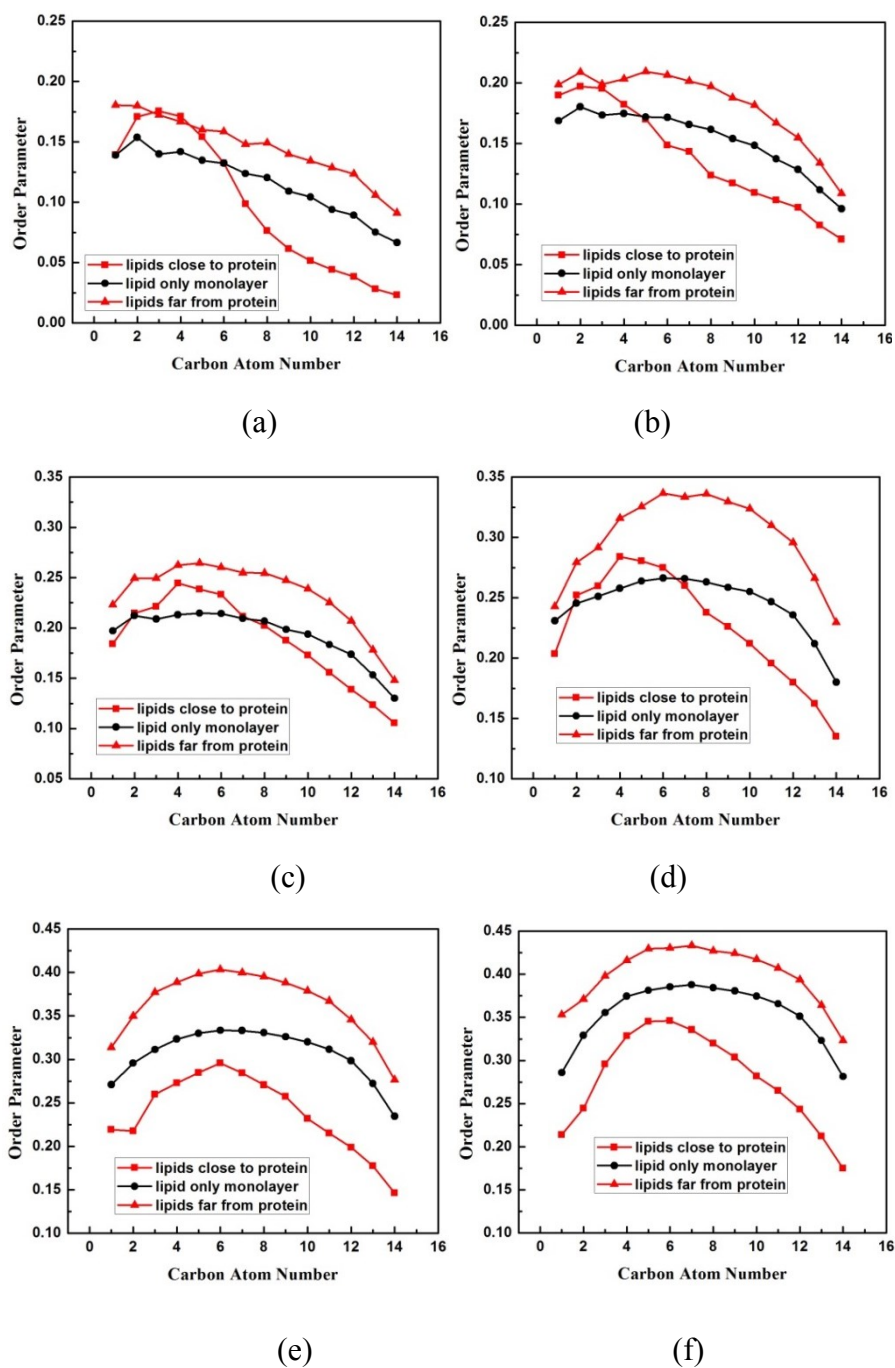
**Figure 4.5** The lipid tail order parameter in chain sn1 for DPPC molecules at the condition of lipids close to protein; lipids far from protein and lipid only monolayer with different area per lipid. (a) 70 Å$^2$, (b) 65 Å$^2$, (c) 60 Å$^2$, (d) 55Å$^2$, (e) 50 Å$^2$, (f) 45 Å$^2$.

(a)

(b)



(c)

(d)
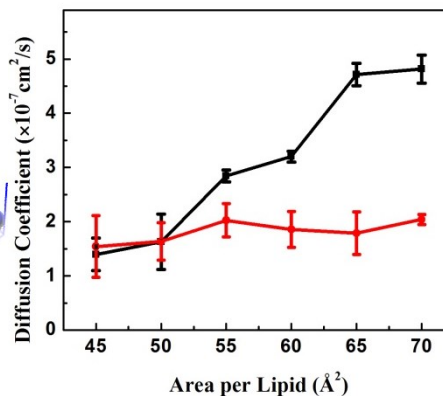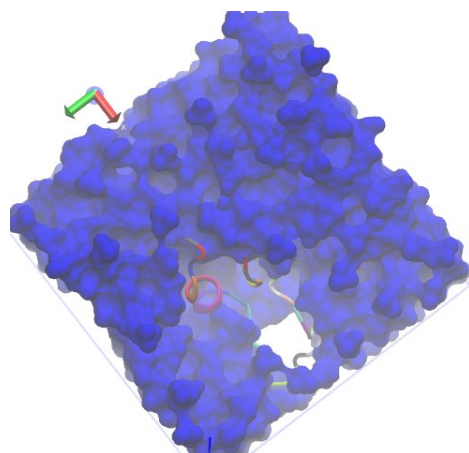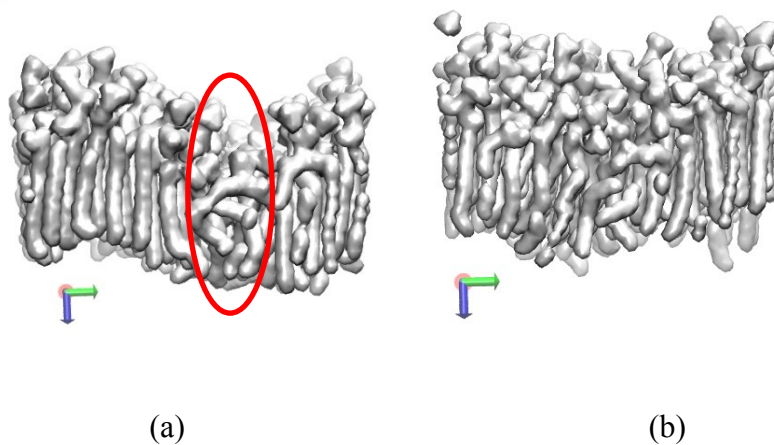
**Figure 4.6** Lateral view of density maps for lipid molecules when area per lipid equals 45 Å$^2$: (a) DPPC monolayer (b) protein containing monolayer. Lipids are shown as a silver solid surface. (c) Top view of protein containing monolayers with lipid drawn as a blue surface. The protein was colored by the residue name using VMD. (d) Diffusion coefficient as a function of area per lipid molecule for monolayers with or without protein. The black line with solid circles represents the DPPC monolayer, and the red line with solid circles represents the DPPC monolayer with SP-B.

The disordered lipid area due to the presence of mini-SP-B protein may act as a nucleation site for the formation of naon-sized domain during the cyclic compression observed in the experiments. In experiment, at the same surface pressure, the lipids with pure DPPC monolayer exhibit ordered phase while the lipids with protein diverged to disordered (those close to protein) and ordered domains. The formation of nano-domains is likely related to the presence of proteins as shown in the AFM images in Fig. 4.2 (d) and Fig. 4.2 (e). Forming these nano-domains not only facilitates a more homogenous distribution of lipid molecules, but also provides a larger surface area of the monolayer exposed to the air, which has significance in the enhancement of the pulmonary gas exchange at the air-water interface.

### 4.4.5 Monolayer interactions of SP-B at water-air interface.

Water molecules are actively involved in the surfactant film at the air-water interface, where the hydrophilic head groups of lipids are always immersed in the water layer and the hydrophobic chains orient towards the air. The structure and dynamics of water molecules are greatly affected by the surfactant-water interface.[55] Hence, hydrogen bonds analysis of lipid-water, lipid-protein and protein-water was quite helpful for understanding the complex monolayer systems. In Table 4.1, all the possible hydrogen bonds were summarized between each residue and protein, lipid or water when the area per lipid was 45 $\text{Å}^2$. All the residues were divided into three groups, depending on the number of hydrogen bonds i.e., 1) residues that could form one to three hydrogen bonds, TRP, LEU, ALA and GLY formed hydrogen bonds with protein and DPPC, and ILE, ALE and MET could form bonds with DPPC and water; 2) residues with intermediate ability of hydrogen bonding (hydrogen bond number from five to eight), LYS, GLN and ARG, could form bonds with protein, DPPC and water; and 3) residues like ARG5, ARG20, and ARG32 have a high probability of forming hydrogen bonds (each residue could have at least eight sites).

**Table 4.1** Hydrogen bonds distribution for all the residues of SP-B in DPPC monolayer when the area per lipid is 45 Å$^2$. Results were obtained through the program of Pymol.

| Residues | Proteins | DPPC | Water | Number of hydrogen bond |
|---|---|---|---|---|
| TRP2 | LEU/O31 | DPPC41/O16 | H | |
| LEU3, LEU7,LEU22, LEU25, LEU29, LEU31, | ARG5/H,GLN24/H LEU29/H,ARG28/H TRP2/H | DPPC40/O10 DPPC60/O10, | H,OW | |
| ALA6, | ARG28/H | DPPC40/O10 | | |
| ILE8,ILE11, ILE15, | | DPPC67/O9 | H,OW | |
| ALE13, | | DPPC46/O16 | H | |
| MET14, MET21, | | DPPC47/O9 | H,OW | |
| PRO16, PRO23, | ARG28/H,GLY18/H | | | |
| GLY18,GLY19, | PRO16/O, ARG20/H | DPPC96/O35, DPPC47/O10 | H | 1 ~ 3 |
| VAL26, VAL30, | VAL30/H, VAL26/O | | | |
| CYS27,CYS33 | | DPPC60/O9, DPPC41/O35 | H | |
| CYS1,CYS4 | | DPPC41/(O9,O16), DPPC49/O9 | H | |
| LYS9, LYS17, | GLN12/O, ARG20/H | DPPC44/O35, DPPC67/(O7,O9), DPPC72/(O9,O11) | OW | 5 ~ 8 |

| | | | |
|---|---|---|---|
| GLN12,GLN24, | LYS9/H, LYS17/H ARG28/H, | DPPC67/O9, DPPC60/(O10,O16) | OW |
| ARG10,ARG28, | ARG5/O,LEU25/O, PRO23/O, GLN24/O, ALA6/O | DPPC44/O9 | H,OW |
| SER34 | ARG32/O | | H,OW |
| ARG5,ARG20,ARG32 | LEU3/O, ARG28/H, GLY19/O, SER34/H, | DPPC36/(O9,O14,O35) DPPC37/(O9,O16)DPPC41/O14,DPPC47/O16, DPPC96/(O9,O11),DPPC42/(O7,O16),DPPC78/O16,DPPC79/O16 | H,OW | Above 8 |

**Table 4.2** Dynamics of hydrogen bonds between ARGs and DPPC were shown in (a) when area per lipid is 50 Å$^2$ and (b) 70 Å$^2$. The cut-off distance for hydrogen bond calculation was 3.5 Å. Results were calculated from the plug in of VMD.

| Donor | Acceptor | Occupancy | Donor | Acceptor | Occupancy |
|---|---|---|---|---|---|
| ARG32-Side | DPPC42 | 61.07% | ARG20-Main | DPPC68 | 89.13% |
| ARG10-Side | DPPC44 | 59.47% | ARG5-Main | DPPC44 | 64.91% |
| ARG5-Side | DPPC44 | 51.56% | ARG20-Side | DPPC96 | 63.39% |
| ARG20-Side | DPPC68 | 50.20% | ARG5-Side | DPPC44 | 62.83% |
| ARG20-Side | DPPC71 | 42.69% | ARG5-Side | DPPC40 | 60.99% |
| ARG20-Side | DPPC67 | 38.13% | ARG10-Side | DPPC44 | 60.19% |
| ARG10-Side | DPPC63 | 37.89% | ARG32-Side | DPPC42 | 52.92% |
| ARG32-Side | DPPC38 | 31.41% | ARG20-Side | DPPC68 | 49.40% |

| ARG5-Side | DPPC43 | 14.63% | ARG20-Side | DPPC57 | 37.01% |
|---|---|---|---|---|---|
| ARG32-Side | DPPC79 | 12.71% | ARG32-Side | DPPC79 | 35.09% |
| ARG32-Side | DPPC55 | 10.23% | ARG10-Side | DPPC46 | 9.83% |
| ARG10-Side | DPPC46 | 3.44% | ARG10-Side | DPPC43 | 8.95% |

(a)                                             (b)

Since both the structure and charge for α-helical N- and C- domains are key to SP-B function,[56] we further analyzed the hydrogen bonds formed for all five ARGs (positively charged) in detail at different area per lipid. The average number of hydrogen bonds formed within the last 10 ns of simulation is shown in Fig. 4.7 and the dynamics of hydrogen bond between ARGs and DPPC molecules is shown in Table 4.2 (a) and (b). Upon compressing the monolayer, ARG5 could form a higher number of hydrogen bond with DPPC and the protein than with water. For ARG10, the hydrogen bonds formed show an interconversion between DPPC and water while keeping the total number of hydrogen bonds almost the same. The number of hydrogen bonds formed by ARG20 for all three groups was kept stable for all the areas per lipid we considered, which may lead to the stable orientation of residue noted by the black arrows in Fig. 4.8. Here ARG20 is just like the ARG17 in SP-B$_{1-25}$, which was reported around the core region anchoring between the lipid monolayer and the peptide.[24] The ARG28 formed a relatively high number of hydrogen bonds within the protein on monolayer compression, and this was possibly the reason that the C- terminal helix was more stable compared to the N- terminal helix. In addition, as shown in Fig. 4.8 (a) ~ (c), the red arrows indicate how the ARG28 rotates from about 45 degrees to ~ 90 degrees to the x-y plane. The rotation of ARG28 was accompanied with the increased number of hydrogen bonds with water. ARG32 shows its high priority to form hydrogen bonds with DPPC (mainly with oxygen atoms in the head group) and a lesser ability for hydrogen bonding with water no matter whether the lipid monolayer was loose or tight, as seen in  Table 4.2 (a) and (b).

The significant ability of ARG10, ARG20 and ARG32 to form hydrogen bonds both with DPPC and water reveals the significance of the protein SP-B: By competing with DPPC to form a hydrogen bond with water while grasping DPPC by hydrogen bond formation with lipid head-

groups, the protein SP-B could keep the protein-lipid monolayer at the air-water surface, which could promote reducing surface tension and re-spreading the monolayer during the inhalation and exhalation of the respiratory process. Indeed, this observation is consistent with our experimental results of isotherm for monolayers with protein showing no loss of ability to reduce surface tension after 7 cycles of compress-expansion.

Further, protein SP-B may act as nucleation sites in the monolayer, which is consistent with the model that SP-B affected the phase transitions in the model monolayer.[57] In other words, at the same high surface pressure, the lipids in pure DPPC monolayer exist as mostly ordered phase while the lipids in monolayers with protein diverged to disordered (those close to protein) and ordered components. It explains how those nano-domains may develop we have observed according to the AFM images seen in Fig. 2 (d) and Fig. 2 (e). Forming these nano-domains not only facilitates a more homogenous distribution of lipid molecules, but also provides a larger surface area of the monolayer exposed to the air side, which has significance in the enhancement of the pulmonary gas exchange at the air-water interface.



(a)                                    (b)                                    (c)
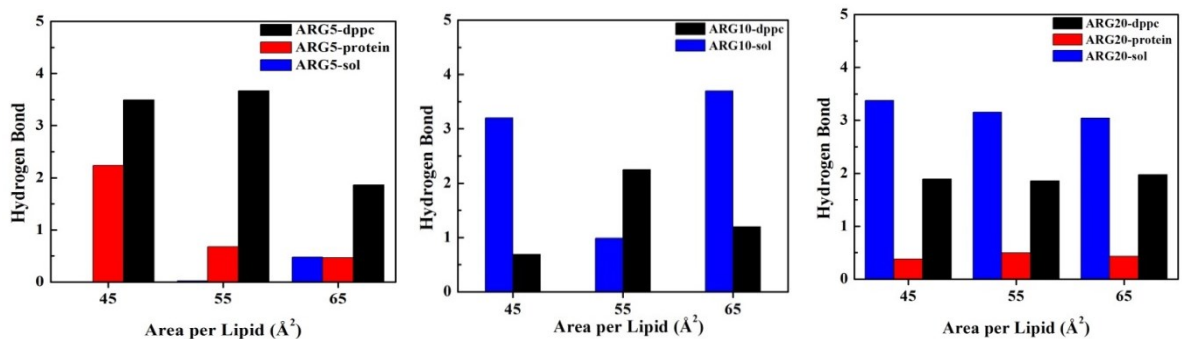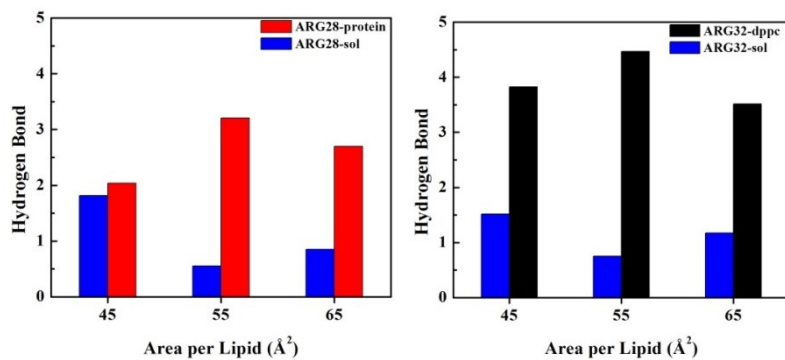
**Figure 4.7** The average hydrogen bonds for the last 10ns simulation among all ARGs, protein, DPPC and water when the area per lipid is 65 $Å^2$, 55 $Å^2$, and 45 $Å^2$. Black stands for the number of hydrogen bonds between the ARGs and DPPC molecules, red stands for ARGs and protein, and blue stands for ARGs and water.
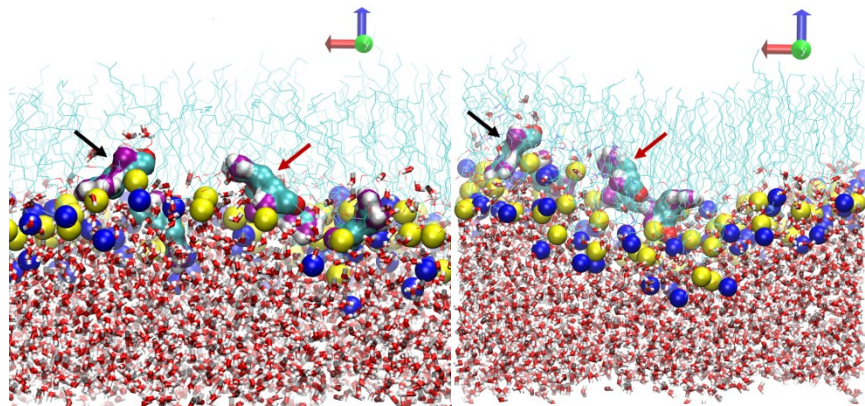


(a)　　　　　　　　　　　　　　(b)
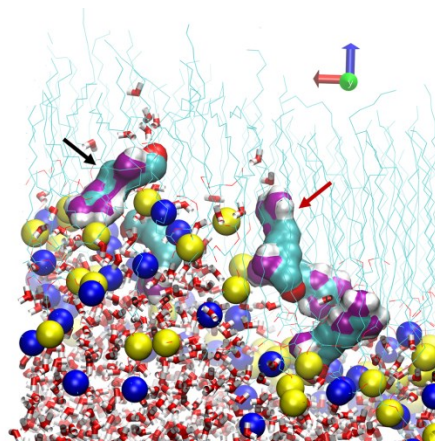


(c)

**Figure 4.8** The location of all five ARGs in monolayers when the area per lipid is (a) 65 $Å^2$, (b) 55 $Å^2$, and (c) 45 $Å^2$. The red arrows indicate the rotation of ARG28 from around 45 degrees to

normal to the x-y plane of the simulation box. Black arrows indicate that the ARG20 did not change its orientation towards the x-y plane upon compression. Purple and light blue stand for nitrogen and carbon atoms in ARG, blue stands for nitrogen in the DPPC choline group, yellow stands for phosphate in DPPC molecules, and red and white stand for oxygen and hydrogen atoms.

### 4.5 Conclusions

Our atomic force microscopy and electronic microscopy studies provides a molecular view on protein SP-B-mediated monolayer evolution after cyclic compression-expansion isotherm tests. When monolayers are prepared at low surface pressures after expansion from the high surface density, we show that the protein can efficiently inhibited the formation of aggregates in monolayers in the presence of SP-B. This effect can be explained by considering the high surface activity and high re-spreading efficiency of monolayers with protein. These observations were illustrated by our molecular simulations, i.e., the protein mini-SP-B containing monolayers affected the packing of monolayer by disordering lipid chains nearby shown in Fig. 4.6 (c), while lipid only monolayers showed a high trend of folding at high surface pressure as shown in Fig. 4.6 (a). Our data support the model of Lipp et al., in which protein induced buckled monolayers re-incorporated in the monolayer upon expansion and reduced the material loss.[58] We show that the SP-B can actively interact with the saturated lipids (DPPC) and inhibited the irreversible aggregations of lipid chains.

In addition, this work shows good support for the assumption that SP-B promoted the spreading of lipid molecules by forming a homogeneous network. The increased surface area by forming a network with nano-sized domains for monolayers in the presence of protein SP-B has significance for higher efficiency in air exchange during repeated respiratory processes.

Finally, hydrogen bonding analysis for those positively charged ARGs at varied locations of the protein mini-SP-B supported the hypothesis that the protein kept the monolayer systems retained at the air-water interface and reduced the surface tension by dynamically forming hydrogen bonds with DPPC head-groups, water and protein itself. Overall, our work provides an important guide for designing the experiments and simulations for pulmonary surfactant monolayer systems and finding qualified potential peptide substitutes with characteristics, such as network promotion and high hydrogen bonding ability.

**Reference**

[1] F. Possmayer, S.H. Yu, J.M. Weber, P.G.R. Harding, Pulmonary Surfactant, Can J Biochem Cell B, 62 (1984) 1121-1133.

[2] P. Gruenwald, Surface Tension as a Factor in the Resistance of Neonatal Lungs to Aeration, Am J Obstet Gynecol, 53 (1947) 996-1007.

[3] U. Kishore, A.L. Bernal, M.F. Kamran, S. Saxena, M. Singh, P.U. Sarma, T. Madan, T. Chakraborty, Surfactant proteins SP-A and SP-D in human health and disease, Arch Immunol Ther Ex, 53 (2005) 399-417.

[4] T.E. Weaver, J.J. Conkright, Functions of surfactant proteins B and C, Annu Rev Physiol, 63 (2001) 555-578.

[5] S.W. Glasser, T.R. Korfhagen, T. Weaver, T. Pilotmatias, J.L. Fox, J.A. Whitsett, Cdna and Deduced Amino-Acid-Sequence of Human Pulmonary Surfactant-Associated Proteolipid Spl(Phe), P Natl Acad Sci USA, 84 (1987) 4007-4011.

[6] J.C. Clark, S.E. Wert, C.J. Bachurski, M.T. Stahlman, B.R. Stripp, T.E. Weaver, J.A. Whitsett, Targeted Disruption of the Surfactant Protein-B Gene Disrupts Surfactant Homeostasis, Causing Respiratory-Failure in Newborn Mice, P Natl Acad Sci USA, 92 (1995) 7794-7798.

[7] L.M. Nogee, G. Garnier, H.C. Dietz, L. Singer, A.M. Murphy, D.E. Demello, H.R. Colten, A Mutation in the Surfactant Protein-B Gene Responsible for Fatal Neonatal Respiratory-Disease in Multiple Kindreds, J Clin Invest, 93 (1994) 1860-1863.

[8] D.E. Demello, L. Nogee, S. Heyman, H.F. Krous, D. Phelps, H.R. Colten, Inherited Surfactant Protein-B (Sp-B) Deficiency in Congenital Alveolar Proteinosis (Cap), Clin Res, 41 (1993) A271-A271.

[9] M.E. Avery, The Role of Surface Forces in Atelectasis of Prematurity and Hyaline Membrane Disease, Ama J Dis Child, 98 (1959) 560.

[10] E. Robillard, P. Dagenaisperusse, Guilbeau.A, E. Baril, Y. Alarie, Microaerosol Administration of Synthetic Beta-Gamma-Dipalmitoyl-L-Alpha-Lecithin in Respiratory Distress Syndrome - Preliminary Report, Can Med Assoc J, 90 (1964) 55.

[11] M.J. Kresch, W.H. Lin, R.S. Thrall, Surfactant replacement therapy, Thorax, 51 (1996) 1137-1154.

[12] H.M. Mcconnell, L.K. Tamm, R.M. Weis, Periodic Structures in Lipid Monolayer Phase-Transitions, Proceedings of the National Academy of Sciences of the United States of America-Physical Sciences, 81 (1984) 3249-3253.

[13] D.J. Keller, H.M. Mcconnell, V.T. Moy, Theory of Superstructures in Lipid Monolayer Phase-Transitions, J Phys Chem-Us, 90 (1986) 2311-2315.

[14] H.M. Mcconnell, V.T. Moy, Shapes of Finite Two-Dimensional Lipid Domains, J Phys Chem-Us, 92 (1988) 4520-4525.

[15] D.J. Keller, J.P. Korb, H.M. Mcconnell, Theory of Shape Transitions in Two-Dimensional Phospholipid Domains, J Phys Chem-Us, 91 (1987) 6417-6422.

[16] H.M. Mcconnell, Theory of Hexagonal and Stripe Phases in Monolayers, P Natl Acad Sci USA, 86 (1989) 3452-3455.

[17] M.M. Lipp, K.Y.C. Lee, J.A. Zasadzinski, A.J. Waring, Phase and morphology changes in lipid monolayers induced by SP-B protein and its amino-terminal peptide, Science, 273 (1996) 1196-1199.

[18] A. Cruz, L.A. Worthman, A.G. Serrano, C. Casals, K.M.W. Keough, J. Perez-Gil, Microstructure and dynamic surface properties of surfactant protein SP-B/dipalmitoylphosphatidylcholine interfacial films spread from lipid-protein bilayers, Eur Biophys J Biophy, 29 (2000) 204-213.

[19] J.Q. Ding, D.Y. Takamoto, A. von Nahmen, M.M. Lipp, K.Y.C. Lee, A.J. Waring, J.A. Zasadzinski, Effects of lung surfactant proteins, SP-B and SP-C, and palmitic acid on monolayer stability, Biophys J, 80 (2001) 2262-2272.

[20] P. Tchoreloff, A. Gulik, B. Denizot, J.E. Proust, F. Puisieux, A Structural Study of Interfacial Phospholipid and Lung Surfactant Layers by Transmission Electron-Microscopy after Blodgett Sampling - Influence of Surface Pressure and Temperature, Chem Phys Lipids, 59 (1991) 151-165.

[21] E. Keating, Y.Y. Zuo, S.M. Tadayyon, N.O. Petersen, F. Possmayer, R.A.W. Veldhuizen, A modified squeeze-out mechanism for generating high surface pressures with pulmonary surfactant, Bba-Biomembranes, 1818 (2012) 1225-1234.

[22] S. Krol, M. Ross, M. Sieber, S. Kunneke, H.J. Galla, A. Janshoff, Formation of three-dimensional protein-lipid aggregates in monolayer films induced by surfactant protein B, Biophys J, 79 (2000) 904-918.

[23] H. Zhang, Q.H. Fan, Y.E. Wang, C.R. Neal, Y.Y. Zuo, Comparative study of clinical pulmonary surfactants using atomic force microscopy, Bba-Biomembranes, 1808 (2011) 1832-1842.

[24] H. Lee, S.K. Kandasamy, R.G. Larson, Molecular dynamics simulations of the anchoring and tilting of the lung-surfactant peptide SP-B1-25 in palmitic acid monolayers, Biophys J, 89 (2005) 3807-3821.

[25] S.K. Kandasamy, R.G. Larson, Molecular dynamics study of the lung surfactant peptide SP-B1-25 with DPPC monolayers: Insights into interactions and peptide position and orientation, Biophys J, 88 (2005) 1577-1592.

[26] S. Baoukina, D.P. Tieleman, Lung Surfactant Protein SP-B Promotes Formation of Bilayer Reservoirs from Monolayer and Lipid Transfer between the Interface and Subphase, Biophys J, 100 (2011) 1678-1687.

[27] S.L. Duncan, R.G. Larson, Folding of lipid monolayers containing lung surfactant proteins SP-B1-25 and SP-C studied via coarse-grained molecular dynamics simulations, Bba-Biomembranes, 1798 (2010) 1632-1650.

[28] D.P. Tieleman, H.J.C. Berendsen, Molecular dynamics simulations of a fully hydrated dipalmitoyl phosphatidylcholine bilayer with different macroscopic boundary conditions and parameters, J Chem Phys, 105 (1996) 4871-4880.

[29] C. Kandt, W.L. Ash, D.P. Tieleman, Setting up and running molecular dynamics simulations of membrane proteins, Methods, 41 (2007) 475-488.

[30] D.J. Evans, B.L. Holian, The Nose-Hoover Thermostat, J Chem Phys, 83 (1985) 4069-4074.

[31] N.B. Vargaftik, B.N. Volkov, L.D. Voljak, International Tables of the Surface-Tension of Water, J Phys Chem Ref Data, 12 (1983) 817-820.

[32] C.W. Hollars, R.C. Dunn, Submicron structure in L-alpha-dipalmitoylphosphatidylcholine monolayers and bilayers probed with confocal, atomic force, and near-field microscopy, Biophys J, 75 (1998) 342-353.

[33] C.W. McConlogue, T.K. Vanderlick, A close look at domain formation in DPPC monolayers, Langmuir, 13 (1997) 7158-7164.

[34] S.L. Frey, L. Pocivavsek, A.J. Waring, F.J. Walther, J.M. Hernandez-Juviel, P. Ruchala, K.Y.C. Lee, Functional importance of the NH2-terminal insertion sequence of lung surfactant protein B, Am J Physiol-Lung C, 298 (2010) L335-L347.

[35] C. Vega, E. de Miguel, Surface tension of the most popular models of water by using the test-area simulation method, J Chem Phys, 126 (2007).

[36] P. Dhar, E. Eck, J.N. Israelachvili, D.W. Lee, Y.J. Min, A. Ramachandran, A.J. Waring, J.A. Zasadzinski, Lipid-Protein Interactions Alter Line Tensions and Domain Size Distributions in Lung Surfactant Monolayers, Biophys J, 102 (2012) 56-65.

[37] S. Baoukina, L. Monticelli, S.J. Marrink, D.P. Tieleman, Pressure-area isotherm of a lipid monolayer from molecular dynamics simulations, Langmuir, 23 (2007) 12617-12623.

[38] D. Rose, J. Rendell, D. Lee, K. Nag, V. Booth, Molecular dynamics simulations of lung surfactant lipid monolayers, Biophys Chem, 138 (2008) 67-77.

[39] W. Shinoda, R. DeVane, M.L. Klein, Coarse-grained molecular modeling of non-ionic surfactant self-assembly, Soft Matter, 4 (2008) 2454-2462.

[40] K.J. Klopfer, T.K. Vanderlick, Isotherms of dipalmitoylphosphatidylcholine (DPPC) monolayers: Features revealed and features obscured, J Colloid Interf Sci, 182 (1996) 220-229.

[41] X.D. Chen, S. Lenhert, M. Hirtz, N. Lu, H. Fuchs, L.F. Chi, Langmuir-Blodgett patterning: A bottom-up way to build mesostructures over large areas, Accounts Chem Res, 40 (2007) 393-401.

[42] H. Riegler, K. Spratte, Structural-Changes in Lipid Monolayers during the Langmuir-Blodgett Transfer Due to Substrate Monolayer Interactions, Thin Solid Films, 210 (1992) 9-12.

[43] M.H. Kopf, S.V. Gurevich, R. Friedrich, L.F. Chi, Pattern Formation in Monolayer Transfer Systems with Substrate-Mediated Condensation, Langmuir, 26 (2010) 10444-10447.

[44] H.D. Sikes, D.K. Schwartz, A temperature-dependent two-dimensional condensation transition during Langmuir-Blodgett deposition, Langmuir, 13 (1997) 4704-4709.

[45] R. DeKoker, H.M. McConnell, Stripe phase hydrodynamics in lipid monolayers, J Phys Chem-Us, 100 (1996) 7722-7728.

[46] H.E. Ries, H. Swift, Twisted Double-Layer Ribbons and the Mechanism for Monolayer Collapse, Langmuir, 3 (1987) 853-855.

[47] E. Parra, A. Alcaraz, A. Cruz, V.M. Aguilella, J. Perez-Gil, Hydrophobic Pulmonary Surfactant Proteins SP-B and SP-C Induce Pore Formation in Planar Lipid Membranes: Evidence for Proteolipid Pores, Biophys J, 104 (2013) 146-155.

[48] L.M. Gordon, S. Horvath, M.L. Longo, J.A.N. Zasadzinski, H.W. Taeusch, K. Faull, C. Leung, A.J. Waring, Conformation and molecular topography of the N-terminal segment of surfactant protein B in structure-promoting environments, Protein Sci, 5 (1996) 1662-1675.

[49] J.A. Freites, Y. Choi, D.J. Tobias, Molecular dynamics simulations of a pulmonary surfactant protein B peptide in a lipid monolayer, Biophys J, 84 (2003) 2169-2180.

[50] H. Nakahara, S. Lee, O. Shibata, Surface pressure induced structural transitions of an amphiphilic peptide in pulmonary surfactant systems by an in situ PM-IRRAS study, Bba-Biomembranes, 1828 (2013) 1205-1213.

[51] J. Seelig, Deuterium Magnetic-Resonance - Theory and Application to Lipid-Membranes, Q Rev Biophys, 10 (1977) 353-418.

[52] M.H. Khatami, I. Saika-Voivod, V. Booth, All-atom molecular dynamics simulations of lung surfactant protein B: Structural features of SP-B promote lipid reorganization, Bba-Biomembranes, 1858 (2016) 3082-3092.

[53] M.R. Buhaenko, J.W. Goodwin, R.M. Richardson, Surface Rheology of Spread Monolayers, Thin Solid Films, 159 (1988) 171-189.

[54] R. Peters, K. Beck, Translational Diffusion in Phospholipid Monolayers Measured by Fluorescence Microphotolysis, P Natl Acad Sci-Biol, 80 (1983) 7183-7187.

[55] A. Ghosh, R.K. Campen, M. Sovago, M. Bonn, Structure and dynamics of interfacial water in model lung surfactants, Faraday Discuss, 141 (2009) 145-159.

[56] A.J. Waring, F.J. Walther, L.M. Gordon, J.M. Hernandez-Juviel, T. Hong, M.A. Sherman, C. Alonso, T. Alig, A. Braun, D. Bacon, J.A. Zasadzinski, The role of charged amphipathic helices in the structure and function of surfactant protein B, J Pept Res, 66 (2005) 364-374.

[57] S.L. Duncan, I.S. Dalal, R.G. Larson, Molecular dynamics simulation of phase transitions in model lung surfactant monolayers, Bba-Biomembranes, 1808 (2011) 2450-2465.

[58] M.M. Lipp, K.Y.C. Lee, D.Y. Takamoto, J.A. Zasadzinski, A.J. Waring, Coexistence of buckled and flat monolayers, Phys Rev Lett, 81 (1998) 1650-1653.

# Chapter 5. Fusing and adhesion mediated by pulmonary surfactant-associated protein B in model lipid bilayers *

## 5.1 Introduction

Membrane fusing is an essential process involved in activities such as cell-to-cell communications,[1] fertilization [2] and viral infections.[3] For protein free lipid bilayers, the fusing might be resulted from the exposing of hydrophobic chains due to multiple lipid depletion,[4] fusing enhancing curvature depending on lipid composition,[5] and close inter-bilayer contact.[6] High pressures were needed for hemi-fusion of gel state lipid bilayers with saturated chains.[7] For protein-medicated membrane fusing, SNARE catalyzed the process through a zippering model accompanying a structure change from trans- to low energy cis-SNARE complex.[8] Other segments contributed to the fusion mechanism in addition to the fusion peptides.[9, 10]

Pulmonary surfactant, mainly composed of lipids and minor proteins, is produced by type II pneumocyte.[11] The protein and lipid molecules are first synthesized in endoplasmic reticulum and then transferred to the Golgi apparatus, where the routines of proteins and lipids diverge. The protein contained liposomes and lipids vesicles fuse and form a storage form of surfactant, lamellar bodies (LBs). The pulmonary surfactant-associated protein B, a hydrophobic protein with molecular weight of 8.7 kDa, is critical important for respiratory [12, 13] and also required to form tubular myelin, a three dimensional lattice-like structure re-arranged from LBs.[14] SP-B also plays a role in the lipid mixing during the vesicle fusing.[15]

Studies have found that surfactant film is a complex system of multilayered structure (tubular myelin) connecting with monolayer.[16, 17] To understand the transformation of structure intermediates in surfactant film functioning as well as surfactant recycling, it is important to measuring the interactions between membranes. Fluorescent measurements have successfully demonstrated the lipid mixing efficiency of SP-B [15] and molecular dynamics simulations showed a protein-mediated vesicle fusion.[18] However, as these studies were performed in the context of vesicles, the interplay of lipids and SP-B in membrane fusion could not be captured and characterized.

---

* The content of this chapter is under preparation for publication. 76

In this study, using surface force apparatus (SFA), we directly measured the interaction energy between protein-containing (DPPC) bilayers and DPPC/ (POPG) lipid bilayers and investigated protein-mediated membrane fusing. The detailed information about fusing of model lipid bilayers, including membrane conformation change and adhesion energy were in real time explored through measurements of forces versus distance.

## 5.2 Methods and materials

### 5.2.1 Materials

DPPC and POPG were purchased from Avanti Polar Lipids, Inc. (Alabaster, AL). Protein SP-B was synthesized as a full length peptide and purchased from the Biomatik corporation (Canada). Lipids and proteins were dissolved separately in chloroform: methanol (3:1)  at a concentration of 1 mg/mL. The water used was purified with a Milli-Q gradient water purification system with a resistivity of 18 MΩ·cm. All other solvents and materials were purchased from Fisher (Pittsburgh, PA).

### 5.2.2 Isotherm tests, construction of supported bilayers and atomic force microscopy imaging

Surface pressure-area curves were obtained through LB trough with a surface area of 98 cm$^2$. Before the isotherm test, the organic solution of lipids or lipids with appropriated concentration of protein was spread on 1mmol/L sodium chloride solution. After 10 minutes, the organic solvent totally evaporated and isotherm tests started.

The protein containing bilayers were prepared with the inner layer of DPPC by pulling a fresh cleave mica out of the subphase (DPPC monolayer covered) using the LB method. Then protein-lipid mixture was spread and protein containing bilayers were constructed by dipping down the substrate back into the electrolyte containing subphase. The pulling out rate is two mm/min and the dipping down rate is three mm/min, which the speed for outer layer deposition is a little bit higher to reduce desorption of the inner layers of lipid molecules. The protein free DPPC bilayers and DPPC:POPG (7:3) bilayers are prepared directly on mica substrate. All the bilayers are prepared at the surface pressure of 30 mN/m.

AFM studies were carried out using the spectral imaging facility with an MFP-3D AFM (Asylum Research Santa Barbara, CA). Bruker silicon nitride MSCT levers, $k \approx 3 \sim 5$ N/m, were used for imaging the mounted bilayers with tapping mode in water.

### 5.2.3 Surface force measurement

The force measurements were performed in a SFA 2000. The distance between surfaces (mounted on two cylindrical disks) was determined by introducing an optical technique, "fringes of equal chromatic order" (FECO), which uses multi-beam interference fringes. The optical technique could be achieved by coating the mica sheets with a semi reflective silver layer. The forces, attractive or repulsive, could be evaluated through the deformation of the spring (spring constant $k = 338$ mN/m) attached to the lower disk. In particular, the SFA chamber was first filled with 1mmol/L sodium chloride water solution which was saturated with DPPC molecules to prevent lipid desorption from mica-supported bilayer during the measurement process. Then the cylindrical disks (glued with mica) with lipid bilayers deposited were carefully transferred and mounted into SFA chamber under water. The experimental devices were placed in a temperature-controlled room and all the force measurements were performed at 20 °C.

### 5.2.4 Secondary structure determination of SP-B through circular dichroism (CD)

Circular dichroism spectra were recorded on JASCO J-715 CD spectrometer using a quartz cuvette of 0.1 cm path length. The spectra were collected in 40% acetonitrile water solution and the signal of blank solvent was subtracted. For each spectrum, 3 scans at a scanning speed of 100 nm /min were averaged.

### 5.3 Results and discussion

### 5.3.1 The effect of protein on the surface activity of Langmuir monolayers

The results of isotherm tests of the monolayer spreading on 1mmol/L sodium chloride water solution were shown in Fig. 5.1. The relationship between surface pressure $\Pi$ and surface tension is as following:

$$\Pi = \gamma_{water} - \gamma_{monolayer} ,$$ 
(5.1)

where $\gamma_{water}$ is the surface tensions of pure water and $\gamma_{monolayer}$ is the surface tension after the monolayer covered at the air-water interface. In other words, a higher surface pressure

corresponds to a lower surface tension of the subphase. Generally, the DPPC monolayer increases the surface pressure Π with reduced area per lipid. In the presence of 4% SP-B, the result was shifted significantly upward with higher surface pressure, which is agreed with the previous study using porcine SP-B.[19] The isotherm of DPPC monolayer exhibited a slope increase between the area per lipid from ~ 60 Å$^2$ to ~ 50 Å$^2$, indicating a drop in the compressibility of the film. When the surface pressure reached 50 mN/m, the isotherms DPPC monolayer with protein showed a plateau with higher area per lipid compared with the DPPC monolayer. The surface pressures increased continually to ~ 60 mN/m until collapse occurred for the monolayers.  Here the effects of protein on surface tension reduction generally agrees with the results reported in the literature [20] but with larger effects on the area per lipid in both low and high pressure regions. The DPPC:POPG (7:3) lipid monolayer showed higher ability of lowering surface tension in low surface pressure region since the lipids were of enhanced fluidity in the presence of POPG. The maximum surface pressure of DPPC:POPG (7:3) monolayer was quite smaller compared to the DPPC monolayer and protein containing DPPC monolayer  at the end of the membrane compression. The isotherm results of this mixed lipid components was also consistent with results of previous studies.[21]
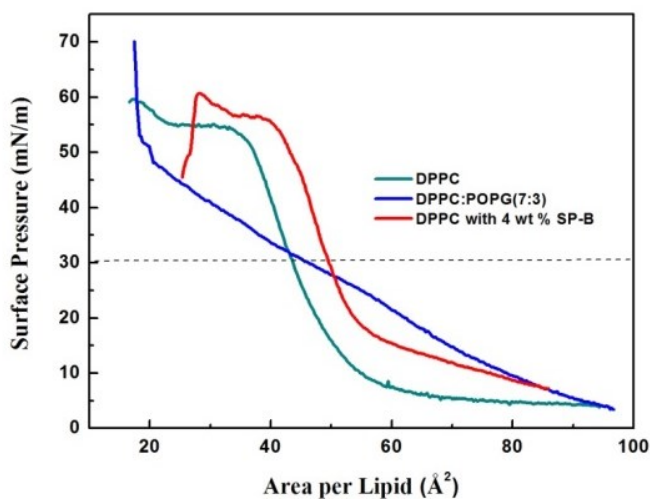


**Figure 5.1** Representative plots of isotherms for lipid monolayers at 20°C. Each solid line represents the results of DPPC monolayer (green), DPPC:POPG (7:3) (blue), DPPC with 4% SP-B (red). All the monolayers were spread on 1mmol/L sodium chloride solution. The black dashed line indicates the surface pressure at which the monolayers were transferred on substrate for later AFM and SFA studies.

### 5.3.2 The SP-B fluidizes the DPPC bilayers

The morphologies of supported model lipid bilayers were shown in Fig. 5.2. From the LB isotherm results, at a surface pressure of 30 mN/m, the bilayers with 4% protein displayed large area of solid phase patches (lighter color) surrounded by the liquid phase (darker color) Fig. 5.2 (a). With higher magnification (Fig.5.2 (b)), three major thicknesses could be distinguished in the height profile,$\Delta h_1$,$\Delta h_m$, and $\Delta h_B$, where $\Delta h_1$ represented the height difference of the liquid phase and solid phase, $\Delta h_m$ represented the thickness of the monolayer and $\Delta h_B$ meant the thickness of the bilayer. Hence, both the monolayer and bilayer defects were found in the membranes. Actually, the defects were commonly observed in solid supported bilayers.[22, 23] In the DPPC: POPG bilayers shown in Fig. 5.2 (c), a larger number of smaller separated solid patches were found, which meant the membrane was with higher fluidity compared to bilayer with second leaflet composed by DPPC mixed with 4% SP-B. The DPPC bilayers were shown as mostly solid phase with monolayer defects (monolayer-bilayer height difference around 3 nm), as seen in Fig. 5.2 (d). Overall, the fluidity of the bilayers can be ordered as DPPC:POPG > DPPC with SP-B > DPPC based on the  separated solid  patches or islands observed. The AFM imaging was carried out on different regions of the membranes prepared through the LB methods with similar topography. The characteristic structure of bilayers is stable in water within several hours of preparation.
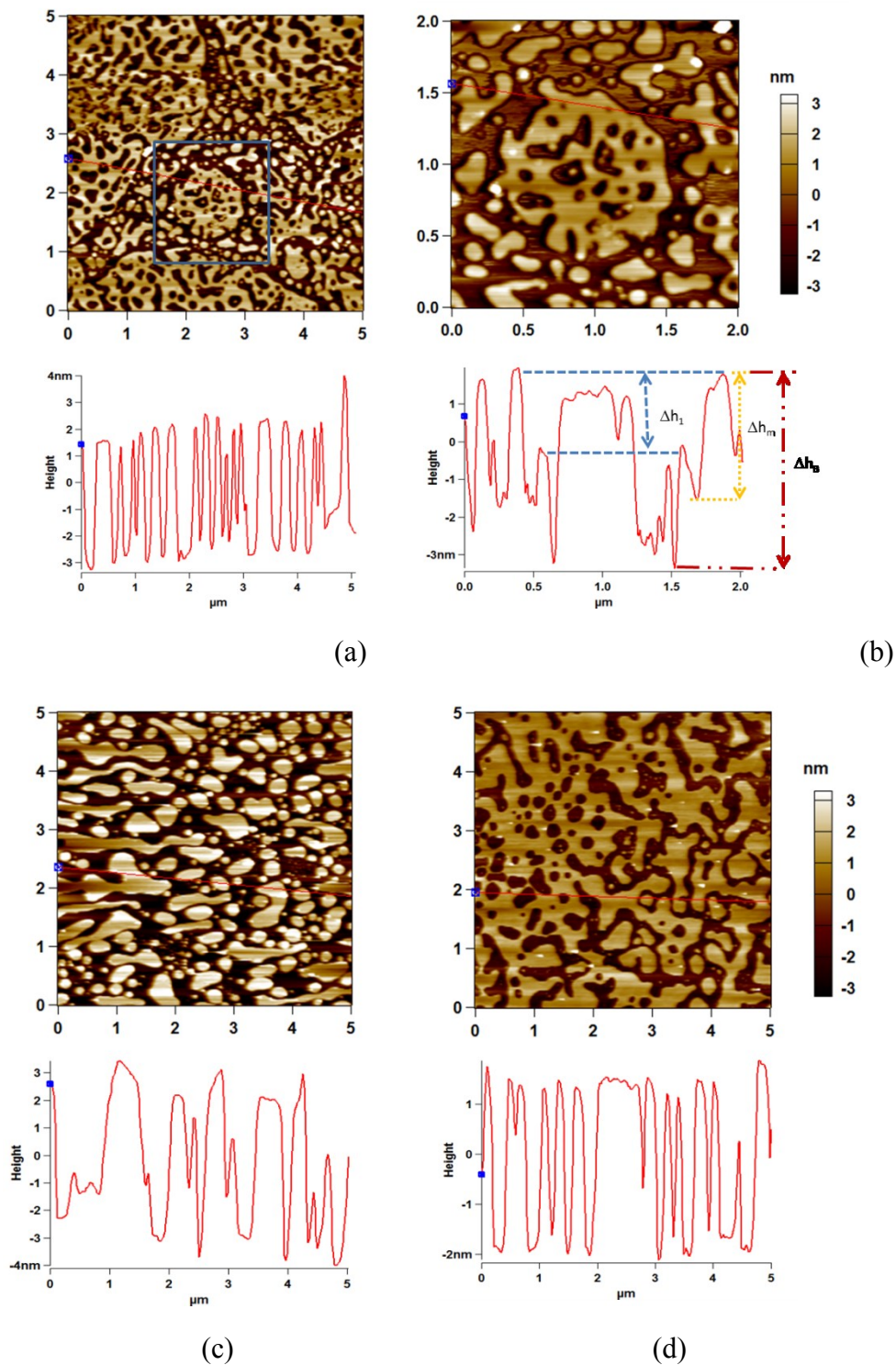
**Figure 5.2** Tapping mode images of model bilayers transferred from the air-water interface onto a mica substrate. (a) DPPC bilayers containing 4% SP-B. (b) High magnification of image collected from the region highlighted by blue square in (a). (c) DPPC:POPG (7:3) lipid

bilayers.(d) DPPC bilayers. The red bottom lines display the height profile of the red line region in each above image.

### 5.3.3 Protein induces fusing and larger adhesion in DPPC bilayers

Fig.5.3 (a) shows the measured force-distance profile between DPPC bilayers in the presence of SP-B. When the separation of the mica-mica was ~ 13 nm, the bilayers firstly experienced a moderate structure deformation due to possibly steric force (seen blue arrow in Fig. 5.3 (a)). At F/R ~ 13mN/m, hemi-fusion occurred characterized by a sudden change of distance between the two mica from ~ 12 nm (~thickness of two hydrated bilayers) to a single bilayer thickness of ~ 6 nm. A similar hemi-fusion was observed for the polymer-cushioned DMPC bilayer at F/R ~ 20 mN/m.[7] High adhesion energy was measured (~ 15 mJ/m$^2$) when the two surfaces were separated. The second run of the force measurement is represented by red solid circles in Fig. 5.3 (a). For this second run, we found that hemi-fusion happened again during the approach, and a lightly smaller adhesion was obtained. Hemi-fusion can be measured consecutively, which can be possibly explained: bilayer islands randomly formed on both surfaces after separation; with higher fluidity these islands might move to places different from the fusion site of first run (Fig. 5.6 (a)); when bringing the two surfaces together a second time, those bilayer islands might fuse in a manner similar to what they did during the first run. However, for force measurement between the DPPC bilayers, there was no fusion observed, as seen in Fig. 5.3 (b). It was found that fusing only happened for gel state DPPC bilayers when the lipids were depleted continually by the dilution of the buffer in the SFA chamber or by repeatedly compression the bilayers, where the hydrophobic force due to explosion of the lipid chains induced the fusion.[4] Though "jump out" happened, the adhesion energy was largely reduced to only ~ 0.2 mJ/m$^2$ compared to the condition of protein containing bilayers.

We also measured the interactions between DPPC bilayers with protein and bare mica Fig. 5.3 (c). The measured surface potential of DPPC vesicles in 1mmol/L sodium chloride solution was -56.7 mV.[24] Hence, the forces during approach were shown to exist because of electrostatic "double–layer" repulsion between charged surfaces, where both the surface of bilayer and mica were negatively charged. The adhesive force measured was larger than that can be accounted for by van der Waals forces acting alone, indicating that the adhesion also resulted from the electrostatic bridging force (ionic bonds between negatively charged mica and the

positively charged lysine or arginine of SP-B). Since the adhesion energy measured is the largest for protein mediated fusing of DPPC bilayers (~ 15 mJ/m$^2$) compared with the results of DPPC bilayer-bilayer interaction (0.2 mJ/m$^2$) and DPPC_SP-B bilayer-mica interaction(1 mJ/m$^2$),  we can propose that the adhesive energy in SP-B present bilayers may also originate from the interactions between the proteins and lipids.



(a)

(b)

(c)
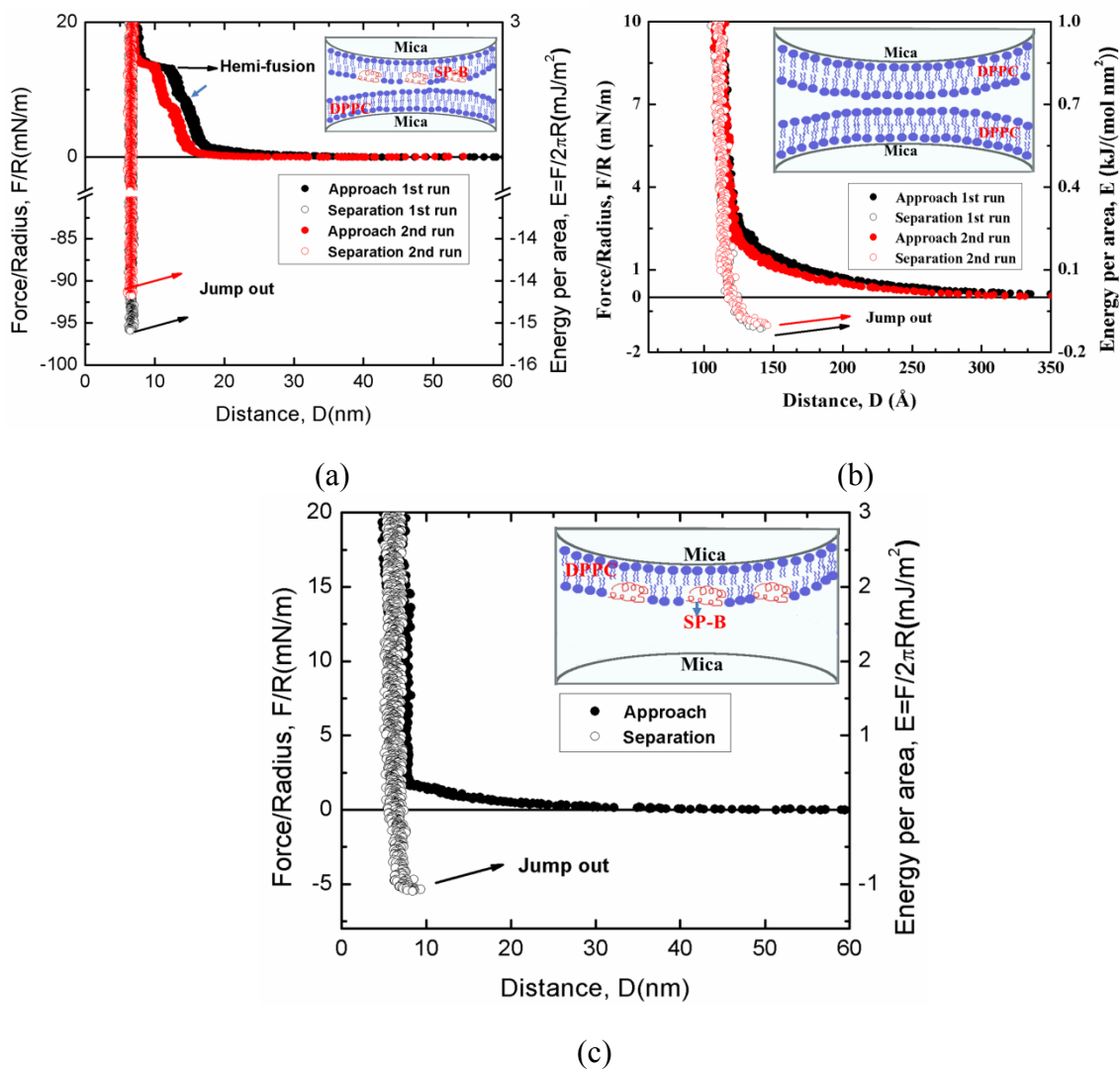
**Figure 5.3** Normalized force-distance profiles of DPPC bilayers. Force measured on approach and on separation between DPPC bilayers in the presence of 4% SP-B (in weight percent of lipids) (a), absence of protein (b) and DPPC bilayers, or between the bilayer with protein and mica (c). D = 0 corresponds to mica-mica contact. The right axis shows the corresponding interaction energy, E (D) = F (D) / 2πR, calculated according to Derjaguin approximation. Hemi-

fusion was indicated by black colored arrows. The red and black arrows during separation indicate "jump out" and maximum adhesion force measured in each curve.

### 5.3.4 The protein modifies the lipid organization during fusing of DPPC:POPG bilayer with DPPC bilayers

Fig. 5.4 shows the force-distance profiles when the outer leaflet of one bilayer was composed of a mixture of lipids DPPC:POPG (7:3). We found that DPPC bilayers fused with the DPPC/DPPC:POPG (7:3) bilayer in the presence or absence of protein SP-B. However, the processes may be different. While initiation of the fusion in the presence of SP-B could be clearly noted (black arrow in Fig. 5.4 (a)), the beginning of fusion was difficult to capture for lipid only bilayers. Further, the approach-separation pathways showed larger hysteresis when SP-B was present in the bilayer, indicating that protein-lipid reorganization might happen during these processes. When the contact time was increased, adhesion was not observed. As POPG molecules were negatively charged, it is possible that the DPPC/POPG bilayer was detached from negatively charged mica in a way that POPG located on one of the disk after separation (seen in Fig. 5.6(b)).
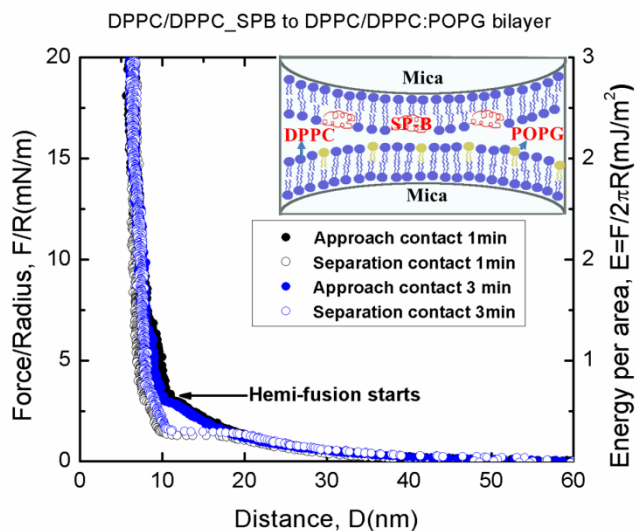
(a)
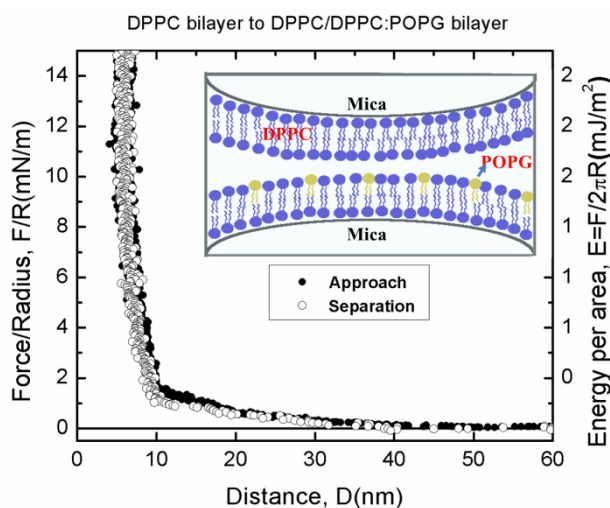


(b)

**Figure 5.4** Normalized force-distance profiles of model bilayers. Force measured on approach and on separation between DPPC bilayers in the presence of 4% SP-B (a), absence of protein (b) and DPPC/DPPC:POPG (7:3) bilayers. D = 0 corresponds to mica-mica contact. The right axis shows the corresponding interaction energy, $E(D) = F(D) / 2\pi R$, calculated according to the Derjaguin approximation.

**5.3.5 The secondary structure determination of synthesized SP-B**
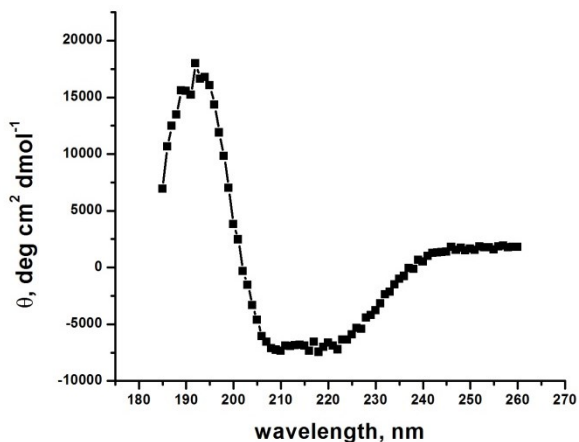


**Figure 5.5** The secondary structure of SP-B. Circular dichroism result of SP-B dissolved in 40 % acetonitrile water solution.

Fig. 5.5 gives more details about the secondary structure of synthesized SP-B from the circular dichroism result. The spectra yields 65 % α-helix and 2.5 % β-sheet based on the on-line tool of K2D2.[25]  The content of α-helix is a little higher than the FTIR results of porcine SP-B in lipid environment (~ 43% to 52 % of α-helix depending on the lipid-protein molar ratio).[26] Hence we propose that one possible source of the high adhesion energy measured between protein-mediated DPPC bilayers was the hydrophobic interactions between the α-helix and lipid chains.

Fusing                    After separation

(a)



Fusing                    After separation
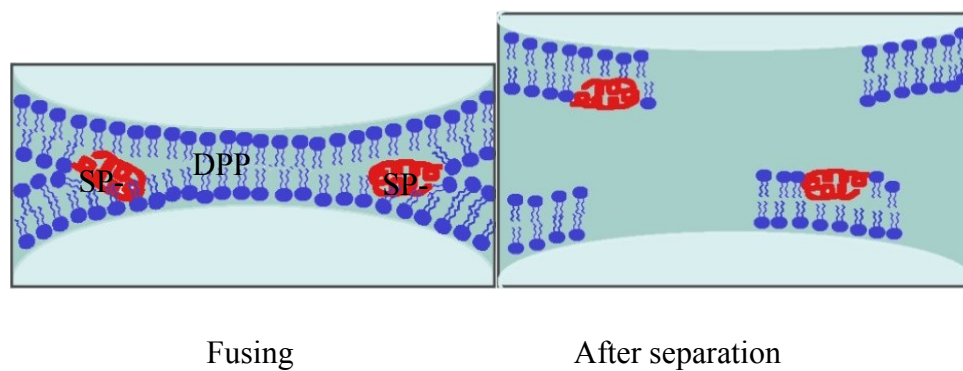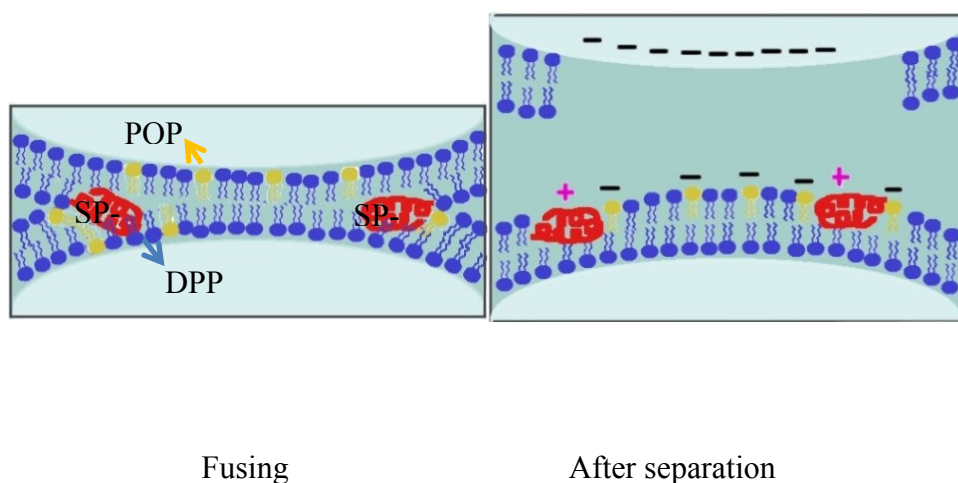
(b)

**Figure 5.6** Effects of SP-B on the fusion of DPPC bilayers and DPPC/DPPC:POPG bilayers. (a) Possible model of SP-B mediated fusion of DPPC bilayers. (b) Possible model of fusion and membrane organization after separation for DPPC:POPG (7:3) bilayers in the presence of SP-B. The first leaflet of all the bilayers was the DPPC monolayer. The black lines means the POPG and mica are negatively charged. Purple crossings represent the positive charges of SP-B (without meaning of number of charge).

### 5.4 Conclusion

The SP-B induces liquid phase and small islands in DPPC bilayers. The protein mediated hemi-fusion of DPPC bilayers and larger adhesion energy as high as ~ 15 mJ/m$^2$ was measured.

Though defects were commonly found on lipid only DPPC bilayers, they failed to induce fusion and significant adhesion energy. After fused DPPC bilayers in the presence of SP-B were separated, a second fusion occurred between the islands of bilayers on each mica surface which were formed, as shown in Fig. 5.6 (a).

The DPPC:POPG bilayer fused with DPPC bilayers in the absence of SP-B. SP-B actually modified the fusing process possibly by interacting with the negatively charged POPG molecules. The hysteresis was observed for the approach and separation of the force-distance profiles in the presence of SP-B, indicating the reorganization of lipid molecules. The adhesion has not been measured in mixed lipid bilayer systems, which can be explained from two aspects: first, the positively charged residues of SP-B closely interacted with the negatively charged POPG molecules with the hydrophobic part buried by lipid chains; second, the negatively charged POPG molecules were easily separated with the negatively charged mica surface (Fig. 5.6 (b)).

**Reference**

[1] D. Zenisek, J.A. Steyer, W. Almers, Transport, capture and exocytosis of single synaptic vesicles at active zones, Nature, 406 (2000) 849-854.

[2] P. Primakoff, D.G. Myles, Penetration, adhesion, and fusion in mammalian sperm-egg interaction, Science, 296 (2002) 2183-2185.

[3] S.A. Connolly, J.O. Jackson, T.S. Jardetzky, R. Longnecker, Fusing structure and function: a structural view of the herpesvirus entry machinery, Nat Rev Microbiol, 9 (2011) 369-381.

[4] C.A. Helm, J.N. Israelachvili, P.M. Mcguiggan, Molecular Mechanisms and Forces Involved in the Adhesion and Fusion of Amphiphilic Bilayers, Science, 246 (1989) 919-922.

[5] L.V. Chernomordik, M.M. Kozlov, Protein-lipid interplay in fusion and fission of biological membranes, Annu Rev Biochem, 72 (2003) 175-207.

[6] L. Yang, H.W. Huang, A rhombohedral phase of lipid containing a membrane fusion intermediate structure, Biophys J, 84 (2003) 1808-1817.

[7] J.Y. Wong, C.K. Park, M. Seitz, J. Israelachvili, Polymer-cushioned bilayers. II. An investigation of interaction forces and fusion using the surface forces apparatus, Biophys J, 77 (1999) 1458-1468.

[8] T.C. Sudhof, J.E. Rothman, Membrane Fusion: Grappling with SNARE and SM Proteins, Science, 323 (2009) 474-477.

[9] S.G. Peisajovich, O. Samuel, Y. Shai, Paramyxovirus F1 protein has two fusion peptides: Implications for the mechanism of membrane fusion, J Mol Biol, 296 (2000) 1353-1365.

[10] M. Rabenstein, Y.K. Shin, A Peptide from the Heptad Repeat of Human-Immunodeficiency-Virus Gp41 Shows Both Membrane-Binding and Coiled-Coil Formation, Biochemistry-Us, 34 (1995) 13390-13397.

[11] G. Chevalier, A.J. Collet, In-Vivo Incorporation of Choline-H-3, Leucine-H-3 and Galactose-H-3 in Alveolar Type-Ii Pneumocytes in Relation to Surfactant Synthesis - Quantitative Autoradiographic Study in Mouse in Electron-Microscopy, Anat Rec, 172 (1972) 289.

[12] J.C. Clark, S.E. Wert, C.J. Bachurski, M.T. Stahlman, B.R. Stripp, T.E. Weaver, J.A. Whitsett, Targeted Disruption of the Surfactant Protein-B Gene Disrupts Surfactant Homeostasis, Causing Respiratory-Failure in Newborn Mice, P Natl Acad Sci USA, 92 (1995) 7794-7798.

[13] J.M. Klein, M.W. Thompson, J.M. Snyder, T.N. George, J.A. Whitsett, E.F. Bell, P.B. McCray, L.M. Nogee, Transient surfactant protein B deficiency in a term infant with severe respiratory failure, J Pediatr-Us, 132 (1998) 244-248.

[14] Y. Suzuki, Y. Fujita, K. Kogishi, Reconstitution of Tubular Myelin from Synthetic Lipids and Proteins Associated with Pig Pulmonary Surfactant, Am Rev Respir Dis, 140 (1989) 75-81.

[15] F.R. Poulain, S. Nir, S. Hawgood, Kinetics of phospholipid membrane fusion induced by surfactant apoproteins A and B, Bba-Biomembranes, 1278 (1996) 169-175.

[16] H. Bachofen, U. Gerber, P. Gehr, M. Amrein, S. Schurch, Structures of pulmonary surfactant films adsorbed to an air-liquid interface in vitro, Bba-Biomembranes, 1720 (2005) 59-72.

[17] D. Follows, F. Tiberg, R.K. Thomas, M. Larsson, Multilayers at the surface of solutions of exogenous lung surfactant: Direct observation by neutron reflection, Bba-Biomembranes, 1768 (2007) 228-235.

[18] S. Baoukina, D.P. Tieleman, Direct Simulation of Protein-Mediated Vesicle Fusion: Lung Surfactant Protein B, Biophys J, 99 (2010) 2134-2142.

[19] S. Krol, M. Ross, M. Sieber, S. Kunneke, H.J. Galla, A. Janshoff, Formation of three-dimensional protein-lipid aggregates in monolayer films induced by surfactant protein B, Biophys J, 79 (2000) 904-918.

[20] F. Bringezu, J.Q. Ding, G. Brezesinski, A.J. Waring, J.A. Zasadzinski, Influence of pulmonary surfactant protein B on model lung surfactant monolayers, Langmuir, 18 (2002) 2319-2325.

[21] J.W. Ma, S. Koppenol, H.U. Yu, G. Zografi, Effects of a cationic and hydrophobic peptide, KL4, on model lung surfactant lipid monolayers, Biophys J, 74 (1998) 1899-1907.

[22] P. Bassereau, F. Pincet, Quantitative analysis of holes in supported bilayers providing the adsorption energy of surfactants on solid substrate, Langmuir, 13 (1997) 7003-7007.

[23] Z.F. Shao, J. Mou, D.M. Czajkowsky, J. Yang, J.Y. Yuan, Biological atomic force microscopy: What is achieved and what is needed, Adv Phys, 45 (1996) 1-86.

[24] E. Chibowski, A. Szczes, Zeta potential and surface charge of DPPC and DOPC liposomes in the presence of PLC enzyme, Adsorption, 22 (2016) 755-765.

[25] C. Perez-Iratxeta, M.A. Andrade-Navarro, K2D2: estimation of protein secondary structure from circular dichroism spectra, Bmc Struct Biol, 8 (2008).

[26] G. Vandenbussche, A. Clercx, M. Clercx, T. Curstedt, J. Johansson, H. Jornvall, J.M. Ruysschaert, Secondary Structure and Orientation of the Surfactant Protein Sp-B in a Lipid Environment - a Fourier-Transform Infrared-Spectroscopy Study, Biochemistry, 31 (1992) 9169-9176.

# Chapter 6. Conclusions and future directions

## 6.1 Conclusions and implications of the work

In this thesis, we established a combined high-resolution method to study the DPPC bilayer-bilayer interaction and the effects of protein SP-B on model monolayer and bilayers using surface force apparatus (SFA) and molecular dynamics (MD) simulations. The structure and dynamics of DPPC and water molecules during the bilayer-bilayer interaction (Min et al.., under preparation) have been characterized, and the effects of recombinant pulmonary surfactant-associated protein B (SP-B) on the multiple compression-expansion of the DPPC monolayer (Min et al., submitted to Scientific Reports) and SP-B-mediated fusion and adhesion in model lipid bilayers (Min et al. under preparation) have been illustrated. The network structure in DPPC monolayer after a multiple cyclic isotherm test and the fusing of the DPPC bilayers induced by SP-B were key structural factors affecting the surfactant monolayer spreading and multilayer unfolding during surfactant secretion. Overall, our results should enhance understanding of lipid-lipid and lipid-protein interactions in surfactant membrane systems.

1. Lipid bilayer-bilayer interaction

The storage format of pulmonary surfactant, LBs and "precursor" tubular myelin are both multilayer structures. The characterization of equilibrium distance or energy minimum between the lipid layers provided important information about the unfolding of the multilayered structure into the active surfactant film (mainly monolayer). We have recovered the free energy profile between two interacting DPPC bilayers for water thickness reduced from ~ 3 nm to ~ 0.6 nm through umbrella sampling MD simulations.

By pulling one bilayer towards the other through non-equilibrium simulation, we learned that the actual membrane structure change might occur during the surface force measurement in an SFA experiment. Then, through equilibrium simulations, the structure and dynamics of water molecules confined between the opposing lipid bilayers were analyzed. Our simulation also made it possible to do analysis about the relaxation of water molecules confined between lipid bilayers. The interdigitating of lipid chains was captured and possibly due to the fact that the bilayers were dehydrated and under high pressures.

2. Protein-lipid interaction in model surfactant monolayer

As the active surfactant film during respiratory is reutilized under physiological condition, it is quite necessary to put the model surfactant lipid and protein mixture under multiple isotherm test. Our results showed a structure revolution from a more rigid solid phase to a network with nano-sized domains for DPPC monolayer in the presence of SP-B. By forming these tiny domains, the surface area of surfactant film was greatly increased. The gas exchange at the air-water interface would benefit from this area increase. The significantly reduced aggregates were observed for monolayers with protein expanded from high surface pressures from the AFM imaging, which highly support the hypothesis that SP-B promotes monolayer re-spreading.

Given the quite short time needed for finishing a respiratory cycle in vivo, it is possible that the formation of surfactant film with high spreading efficiency was accompanied by the phase change of lipid molecules and the structural transformation of proteins. It is suggested that instead of forming lipid folds for lipid-only monolayer the SP-B created voids on monolayer compression. The protein SP-B may provide nucleation sites by disordering the lipid packing on monolayer compression, which explains how the network with nano-domains of monolayer in presence of protein was developed.

3. Protein mediated fusing in model lipid bilayers

The gel state of DPPC bilayers were difficult to fuse even with a certain number of defects and under high pressure. In our work presented here, it was found that SP-B mediated the fusing of two DPPC bilayers by creating smaller solid phase islands with liquid-expanded phase. The surface force apparatus was a powerful tool for not only investigating fusing but also for verifying the resources of adhesion measured when separating the two surfaces.

The detection of protein dependent modification in fusing process of POPG containing bilayers revealed a lipid reorganization process mediated by protein SP-B, indicating the possible mechanisms related to the formation of LBs during pulmonary surfactant secretion.

## 6.2 Future directions

Although some questions have been answered by the work presented in this thesis, still there is a long way to go before general key structural components of lipid membranes and proteins in active surfactant films can be resolved. It is quite necessary to combine multiple methods to

investigate the problem. Model simplification in computer simulation, in-vivo assays of the recombinant or synthesized peptides of surfactant proteins and molecular labeling of protein for in-situ tests of protein-lipid interactions may bring new insights to pulmonary surfactant research.

**6.2.1 Umbrella sampling MD simulation of the free energy profile between SP-B and model lipid bilayers**

By changing the composition of lipid bilayers and pulling the SP-B towards or away from the lipid bilayers, we can obtain the free energy profiles between SP-B and each lipid component of pulmonary surfactant.



(a)                              (b)



(c)
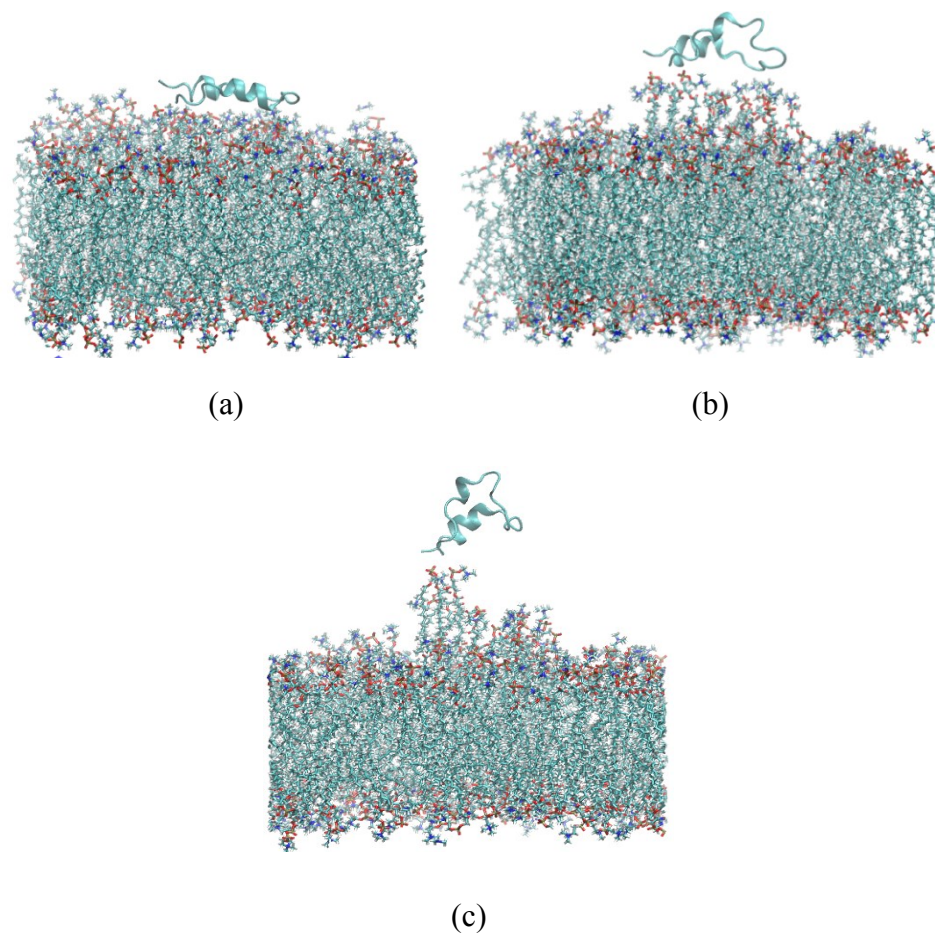
**Figure 6.1** Configuration change when pulling the mini-SP-B away from the model lipid bilayer (a) Starting configuration, (b) and (c) intermediate and final states of the mini-SP-B and bilayers were displayed during the pulling process.

Given our observation of adhesion mediated by SP-B during SFA force measurement, it would be interesting to probe the effects of the initial configuration of SP-B that change of the membrane structure from the simulation. The pulling process may change the water molecules which hydrate both the head groups of membranes and the proteins. Evidences for the role of these water molecules for maintaining or modifying the 3-D structure of protein can be provided through equilibrium simulations when the separation between lipid and protein varies. The preliminary results when pulling the SP-B away from the DPPC:POPG bilayer showed a transit membrane unfolding as a result of protein-lipid interaction, as seen in Fig. 6.1. Compared with the initial relatively flatten membrane surface in Fig. 6.1 (a), some lipid molecules were pulled partially out the membrane in Fig. 6.1 (b) and repacked in the membrane Fig. 6.1 (c). Also, changing the pulling direction of the protein will likely illustrate the pathway of monolayer-multilayer transformation and recover the corresponding free energy profiles.

### 6.2.2 Structure-function related mutations in protein SP-B

Two important facts about the protein SP-B are: it is highly hydrophobic with large percentage of α helix and it is positively charged. The protein SP-B belongs to saposin-like family and the full length is supposed to contain five α helixes.[1] Each helix may have varied ability in affecting membrane fusing, lysis and surface activity. The first N-terminal helix is enough to induce lysis of vesicles. However, the first and second helixes were both required for the fusing of vesicles.[2] By mutating those residues with high possibility of folding the peptide into helical structure, we could test the role of helix structure in the membrane spreading at the air-water interface. Similarly, if the loss of helix affected the fusion and adhesion of lipid bilayers could also be verified.

The positively charged residues might interact with negatively charged lipids and in this way the protein plays a role in lipid mixing and reorganization. By substituting these charged residues into neutral amino acids, we may get information how the charge may affect the membrane conformation and stability in active surfactant film. Changing those charged residues may also affect the formation of α helix. As a result, we could verify if the charges affect the properties directly or through affecting the secondary structure of the protein.

Tryptophan oxidation would do modification to the structure of surfactant protein-B under respiratory distress condition.[3] Substitution the proline to α-helix promoting residue would

connect the first two N- terminal helixes into one long helix, which affect the fusogenic ability of SP-B.[2] Changing any proline in the N terminal of peptide also can change surface activity.[4] Hence, mutations on these key amino acids are also necessary to resolve the structural change of protein involving in surface activity of surfactant film, monolayer-multilayer transformation and material reutilization.

**Reference**

[1] B. Olmeda, B. Garcia-Alvarez, J. Perez-Gil, Structure-function correlations of pulmonary surfactant protein SP-B and the saposin-like family of proteins, Eur Biophys J Biophy, 42 (2013) 209-222.

[2] M.A. Ryan, X.Y. Qi, A.G. Serrano, M. Ikegami, J. Perez-Gil, J. Johansson, T.E. Weaver, Mapping and analysis of the lytic and fusogenic domains of surfactant protein B, Biochemistry, 44 (2005) 861-872.

[3] M. Sarker, J. Rose, J. Bartlett, M. Browne, V. Booth, Modifications to Surfactant Protein B Structure and Lipid Interactions Under Ards Conditions: Consequences of Tryptophan Oxidation, Biophys J, 98 (2010) 280a-281a.

[4] A.G. Serrano, M. Ryan, T.E. Weaver, J. Perez-Gil, Critical structure-function determinants within the N-terminal region of pulmonary surfactant protein SP-B, Biophys J, 90 (2006) 238-249.

## Bibliography

[1] V. Condo, S. Cipriani, M. Colnaghi, R. Bellu, R. Zanini, C. Bulfoni, F. Parazzini, F. Mosca, Neonatal respiratory distress syndrome: are risk factors the same in preterm and term infants?, J Matern-Fetal Neo M, 30 (2017) 1267-1272.

[2] R.H. Notter, D.L. Shapiro, Lung Surfactant in an Era of Replacement Therapy, Pediatrics, 68 (1981) 781-789.

[3] B. Robertson, Lung Surfactant for Replacement Therapy, Clin Physiol, 3 (1983) 97-110.

[4] W. Seeger, A. Gunther, H.D. Walmrath, F. Griminger, H.G. Lasch, Alveolar Surfactant and Adult Respiratory-Distress Syndrome - Pathogenetic Role and Therapeutic Prospects, Clin Investigator, 71 (1993) 177-190.

[5] M. Filoche, C.F. Tai, J.B. Grotberg, Three-dimensional model of surfactant replacement therapy, P Natl Acad Sci USA, 112 (2015) 9287-9292.

[6] K. von neergaard, Neue Auffassungen uber einen Grundbegriff der Atemmechanik. Die Retraktionskraft der Lunge, abhangig von der Ober-flachenspannung in den Alveolen, Z.Gesamte. Exp. Med., 66 (1929) 373-394.

[7] J.A. Clements, Surface Tension of Lung Extracts, P Soc Exp Biol Med, 95 (1957) 170-172.

[8] K.L. Hartshorn, E.C. Crouch, M.R. White, P. Eggleton, A.I. Tauber, D. Chang, K. Sastry, Evidence for a Protective Role of Pulmonary Surfactant Protein-D (Sp-D) against Influenza-a Viruses, J Clin Invest, 94 (1994) 311-319.

[9] A.M. LeVine, J.A. Whitsett, J.A. Gwozdz, T.R. Richardson, J.H. Fisher, M.S. Burhans, T.R. Korfhagen, Distinct effects of surfactant protein A or D deficiency during bacterial infection on the lung, J Immunol, 165 (2000) 3934-3940.

[10] R.J. King, Pulmonary Surfactant, J Appl Physiol, 53 (1982) 1-8.

[11] S.A. Rooney, The Surfactant System and Lung Phospholipid Biochemistry, Am Rev Respir Dis, 131 (1985) 439-460.

[12] R.J.a.M. King, M.C., Interactions of lthe lipid and protein components of pulmonary surfactant: role of phophatidylglycerol and calcium, Biochim Biophys Acta, 647 (1981) 159-168.

[13] M.W. Hawco, Davis, P. J., and Keough, K. M. W., Lipid fluidity in lung surfactant: monolayers of saturated and unsaturated lections, J Appl Physiol, (1981) 509.

[14] M.J. Lau, K.M.W. Keough, Lipid-Composition of Lung and Lung Lavage Fluid from Map Turtles (Malaclemys-Geographica) Maintained at Different Environmental Temperatures, Canadian Journal of Biochemistry, 59 (1981) 208-219.

[15] M. Hallman, L. Gluck, Phosphatidylglycerol in Lung Surfactant .3. Possible Modifier of Surfactant Function, J Lipid Res, 17 (1976) 257-262.

[16] H.P. Haagsman, S. Hawgood, T. Sargeant, D. Buckley, R.T. White, K. Drickamer, B.J. Benson, The major lung surfactant protein, SP 28-36, is a calcium-dependent, carbohydrate-binding protein, J Biol Chem, 262 (1987) 13877.

[17] B.J. Benson, S. Hawgood, Structural and functional aspects of protein: phospholipid interactions in surfactant, European Journal of Respiratory Diseases Supplement, 142 (1985) 29-36.

[18] A.J. Tenner, S.L. Robinson, J. Borchelt, J.R. Wright, Human pulmonary surfactant protein (SP-A), a protein structurally homologous to C1q, can enhance FcR- and CR1-mediated phagocytosis, J Biol Chem, 264 (1989) 13923-13928.

[19] E. Wintergerst, H. Manzkeinke, H. Plattner, J. Schlepperschäfer, The interaction of a lung surfactant protein (SP-A) with macrophages is mannose dependent, European Journal of Cell Biology, 50 (1989) 291.

[20] S. Hawgood, ., B.J. Benson, J. Schilling, ., D. Damm, ., J.A. Clements, R.T. White, Nucleotide and amino acid sequences of pulmonary surfactant protein SP 18 and evidence for cooperation between SP 18 and SP 28-36 in surfactant lipid adsorption, P Natl Acad Sci USA, 84 (1987) 66.

[21] J. PerezGil, A. Cruz, I. Plasencia, C. Casals, Interaction of pulmonary surfactant proteins SP-B and SP-C with bilayers of DPPC, studied by fluorescence spectroscopy, Biophys J, 70 (1996) .

[22] A. Takahashi, A.J. Waring, J. Amirkhanian, B. Fan, H.W. Taeusch, Structure-Function-Relationships of Bovine Pulmonary Surfactant Proteins - Sp-B and Sp-C, Biochim Biophys Acta, 1044 (1990) 43-49.

[23] W.R. Rice, V.K. Sarin, J.L. Fox, J. Baatz, S. Wert, J.A. Whitsett, Surfactant peptides stimulate uptake of phosphatidylcholine by isolated cells, Biochim Biophys Acta, 1006 (1989) 237.

[24] F. Rausch, M. Schicht, F. Paulsen, I. Ngueya, L. Brauer, W. Brandt, "SP-G", a Putative New Surfactant Protein - Tissue Localization and 3D Structure, Plos One, 7 (2012) e47789.

[25] M. Schicht, F. Rausch, S. Finotto, M. Mathews, A. Mattil, M. Schubert, B. Koch, M. Traxdorf, C. Bohr, D. Worlitzsch, W. Brandt, F. Garreis, S. Sel, F. Paulsen, L. Brauer, SFTA3, a novel protein of the lung: three-dimensional structure, characterisation and immune activation, Eur Respir J, 44 (2014) 447-456.

[26] G. Chevalier, A.J. Collet, In-Vivo Incorporation of Choline-H-3, Leucine-H-3 and Galactose-H-3 in Alveolar Type-Ii Pneumocytes in Relation to Surfactant Synthesis - Quantitative Autoradiographic Study in Mouse by Electron-Microscopy, Anat Rec, 174 (1972) 289.

[27] M. Hallman, B.L. Epstein, L. Gluck, Analysis of Labeling and Clearance of Lung Surfactant Phospholipids in Rabbit - Evidence of Bidirectional Surfactant Flux between Lamellar Bodies and Alveolar-Lavage, J Clin Invest, 68 (1981) 742-751.

[28] H. Jacobs, A. Jobe, M. Ikegami, S. Jones, Surfactant Phosphatidylcholine Source, Fluxes, and Turnover Times in 3-Day-Old, 10-Day-Old, and Adult-Rabbits, J Biol Chem, 257 (1982) 1805-1810.

[29] S.L. Young, S.A. Kremers, J.S. Apple, J.D. Crapo, G.W. Brumley, Rat Lung Surfactant Kinetics - Biochemical and Morphometric Correlation, J Appl Physiol, 51 (1981) 248-253.

[30] G. Enhorning, D. Chamberlain, C. Contreras, R. Burgoyne, B. Robertson, Isoxsuprine-induced release of pulmonary surfactant in the rabbit fetus, American Journal of Obstetrics & Gynecology, 129 (1977) 197-202.

[31] J.P. Fabisiak, E.S. Vesell, D.E. Rannels, Interactions of beta adrenergic antagonists with isolated rat alveolar type II pneumocytes. I. Analysis, characterization and regulation of specific beta adrenergic receptors, Journal of Pharmacology & Experimental Therapeutics, 241 (1987) 722-727.

[32] E.E. Lawson, R.L. Birdwell, P.S. Huang, T.H. Jr, Augmentation of pulmonary surfactant secretion by lung expansion at birth, Pediatr Res, 13 (1979) 611-614.

[33] A.B. Fisher, A. Chander, J. Reicherter, Uptake and degradation of natural surfactant by isolated rat granular pneumocytes, Am J Physiol, 253 (1987) 792-796.

[34] K. Oguchi, M. Ikegami, H. Jacobs, A. Jobe, Clearance of Large Amounts of Natural Surfactants and Liposomes of Dipalmitoylphosphatidylcholine from the Lungs of Rabbits, Exp Lung Res, 9 (1985) 221.

[35] L.M. Nogee, D.E. Demello, L.P. Dehner, H.R. Colten, Brief Report - Deficiency of Pulmonary Surfactant Protein-B in Congenital Alveolar Proteinosis, New Engl J Med, 328 (1993) 406-410.

[36] L.M. Nogee, G. Garnier, H.C. Dietz, L. Singer, A.M. Murphy, D.E. Demello, H.R. Colten, A Mutation in the Surfactant Protein-B Gene Responsible for Fatal Neonatal Respiratory-Disease in Multiple Kindreds, J Clin Invest, 93 (1994) 1860-1863.

[37] R.S. Munford, P.O. Sheppard, P.J. Ohara, Saposin-Like Proteins (Saplip) Carry out Diverse Functions on a Common Backbone Structure, J Lipid Res, 36 (1995) 1653-1663.

[38] S. Hawgood, M. Derrick, F. Poulain, Structure and properties of surfactant protein B, Bba-Mol Basis Dis, 1408 (1998) 150-160.

[39] V. Booth, A.J. Waring, F.J. Walther, K.M.W. Keough, NMR structures of the C-terminal segment of surfactant protein B in detergent micelles and hexafluoro-2-propanol, Biochemistry, 43 (2004) 15187-15194.

[40] J.W. Kurutz, K.Y.C. Lee, NMR structure of lung surfactant peptide SP-B11-25, Biochemistry, 41 (2002) 9627-9636.

[41] M.M. Lipp, K.Y.C. Lee, A. Waring, J.A. Zasadzinski, Fluorescence, polarized fluorescence, and Brewster angle microscopy of palmitic acid and lung surfactant protein B monolayers, Biophys J, 72 (1997) 2783-2804.

[42] M.M. Lipp, K.Y.C. Lee, J.A. Zasadzinski, A.J. Waring, Phase and morphology changes in lipid monolayers induced by SP-B protein and its amino-terminal peptide, Science, 273 (1996) 1196-1199.

[43] J.Q. Ding, D.Y. Takamoto, A. von Nahmen, M.M. Lipp, K.Y.C. Lee, A.J. Waring, J.A. Zasadzinski, Effects of lung surfactant proteins, SP-B and SP-C, and palmitic acid on monolayer stability, Biophys J, 80 (2001) 2262-2272.

[44] R.V. Diemel, M.M.E. Snel, A.J. Waring, F.J. Walther, L.M.G. van Golde, G. Putz, H.P. Haagsman, J.J. Batenburg, Multilayer formation upon compression of surfactant monolayers depends on protein concentration as well as lipid composition - An atomic force microscopy study, J Biol Chem, 277 (2002) 21179-21188.

[45] Y.Y. Zuo, E. Keating, L. Zhao, S.M. Tadayyon, R.A.W. Veldhuizen, N.O. Petersen, F. Possmayer, Atomic force microscopy studies of functional and dysfunctional pulmonary surfactant films. I. Micro- and nanostructures of functional pulmonary surfactant films and the effect of SP-A, Biophys J, 94 (2008) 3549-3564.

[46] K.Y.C. Lee, J. Majewski, T.L. Kuhl, P.B. Howes, K. Kjaer, M.M. Lipp, A.J. Waring, J.A. Zasadzinski, G.S. Smith, Synchrotron X-ray study of lung surfactant-specific protein SP-B in lipid monolayers, Biophys J, 81 (2001) 572-585.

[47] J.A. Freites, Y. Choi, D.J. Tobias, Molecular dynamics simulations of a pulmonary surfactant protein B peptide in a lipid monolayer, Biophys J, 84 (2003) 2169-2180.

[48] M.H. Khatami, I. Saika-Voivod, V. Booth, All-atom molecular dynamics simulations of lung surfactant protein B: Structural features of SP-B promote lipid reorganization, Bba-Biomembranes, 1858 (2016) 3082-3092.

[49] S. Baoukina, D.P. Tieleman, Lung Surfactant Protein SP-B Promotes Formation of Bilayer Reservoirs from Monolayer and Lipid Transfer between the Interface and Subphase, Biophys J, 100 (2011) 1678-1687.

[50] S.L. Duncan, I.S. Dalal, R.G. Larson, Molecular dynamics simulation of phase transitions in model lung surfactant monolayers, Bba-Biomembranes, 1808 (2011) 2450-2465.

[51] S. Baoukina, D.P. Tieleman, Direct Simulation of Protein-Mediated Vesicle Fusion: Lung Surfactant Protein B, Biophys J, 99 (2010) 2134-2142.

[52] J. Egberts, H. Sloot, A. Mazure, Minimal Surface-Tension, Squeeze-out and Transition-Temperatures of Binary-Mixtures of Dipalmitoylphosphatidylcholine and Unsaturated Phospholipids, Biochim Biophys Acta, 1002 (1989) 109-113.

[53] J.N. Hildebran, J. Goerke, J.A. Clements, Pulmonary Surface-Film Stability and Composition, J Appl Physiol, 47 (1979) 604-611.

[54] K.M.W. Keough, E. Farrell, M. Cox, G. Harrell, H.W. Taeusch, Physical, Chemical, and Physiological-Characteristics of Isolates of Pulmonary Surfactant from Adult-Rabbits, Can J Physiol Pharm, 63 (1985) 1043-1051.

[55] B. Pastranarios, C.R. Flach, J.W. Brauner, A.J. Mautone, R. Mendelsohn, A Direct Test of the Squeeze-out Hypothesis of Lung Surfactant Function - External Reflection Ft-Ir at the Air/Water Interface, Biochemistry-Us, 33 (1994) 5121-5127.

[56] J.P.J.G. Vanliempd, A.A.H. Boonman, R.A. Demel, P.M.C. Gieles, T.C.M. Gorree, Nonselective Squeeze-out of Dioleoylphosphatidylcholine and Dioleoylphosphatidylglycerol from Binary Mixed Monolayers with Dipalmitoylphosphatidylcholine, Biochim Biophys Acta, 897 (1987) 495-501.

[57] N. Mathialagan, F. Possmayer, Low-Molecular-Weight Hydrophobic Proteins from Bovine Pulmonary Surfactant, Biochim Biophys Acta, 1045 (1990) 121-127.

[58] B. Piknova, W.R. Schief, V. Vogel, B.M. Discher, S.B. Hall, Discrepancy between phase behavior of lung surfactant phospholipids and the classical model of surfactant function, Biophys J, 81 (2001) 2172-2180.

[59] J.M. Crane, G. Putz, S.B. Hall, Persistence of phase coexistence in disaturated phosphatidylcholine monolayers at high surface pressures, Biophys J, 77 (1999) 3134-3143.

[60] J.M. Crane, S.B. Hall, Rapid compression transforms interfacial monolayers of pulmonary surfactant, Biophys J, 80 (2001) 1863-1872.

[61] S.H. Yu, F. Possmayer, Lipid compositional analysis of pulmonary surfactant monolayers and monolayer-associated reservoirs, J Lipid Res, 44 (2003) 621-629.

[62] E. Keating, Y.Y. Zuo, S.M. Tadayyon, N.O. Petersen, F. Possmayer, R.A.W. Veldhuizen, A modified squeeze-out mechanism for generating high surface pressures with pulmonary surfactant, Bba-Biomembranes, 1818 (2012) 1225-1234.

[63] J.Q. Ding, I. Doudevski, H.E. Warriner, T. Alig, J.A. Zasadzinski, Nanostructure changes in lung surfactant monolayers induced by interactions between palmitoyloleoylphosphatidylglycerol and surfactant protein B, Langmuir, 19 (2003) 1539-1550.

[64] D.J. Keller, H.M. Mcconnell, V.T. Moy, Theory of Superstructures in Lipid Monolayer Phase-Transitions, J Phys Chem-Us, 90 (1986) 2311-2315.

[65] C.W. McConlogue, T.K. Vanderlick, A close look at domain formation in DPPC monolayers, Langmuir, 13 (1997) 7158-7164.

[66] D.W. Lee, Y.J. Min, P. Dhar, A. Ramachandran, J.N. Israelachvili, J.A. Zasadzinski, Relating domain size distribution to line tension and molecular dipole density in model cytoplasmic myelin lipid monolayers, P Natl Acad Sci USA, 108 (2011) 9425-9430.

[67] L.J. Lis, M. Mcalister, N. Fuller, R.P. Rand, V.A. Parsegian, Interactions between Neutral Phospholipid-Bilayer Membranes, Biophys J, 37 (1982) 657-665.

[68] J. Marra, Direct Measurements of Attractive Vanderwaals and Adhesion Forces between Uncharged Lipid Bilayers in Aqueous-Solutions, J Colloid Interf Sci, 109 (1986) 11-20.

[69] J. Marra, J. Israelachvili, Direct Measurements of Forces between Phosphatidylcholine and Phosphatidylethanolamine Bilayers in Aqueous-Electrolyte Solutions, Biochemistry, 24 (1985) 4608-4618.

[70] L. Perera, U. Essmann, M.L. Berkowitz, Role of water in the hydration force acting between lipid bilayers, Langmuir, 12 (1996) 2625-2629.

[71] K. Hristova, S.H. White, Determination of the hydrocarbon core structure of fluid dioleoylphosphocholine (DOPC) bilayers by x-ray diffraction using specific bromination of the double-bonds: Effect of hydration, Biophys J, 74 (1998) 2419-2433.

[72] F. Volke, A. Pampel, Membrane Hydration and Structure on a Subnanometer Scale as Seen by High-Resolution Solid-State Nuclear-Magnetic-Resonance - Popc and Popc/C(12)Eo(4) Model Membranes, Biophys J, 68 (1995) 1960-1965.

[73] E.A. Disalvo, F. Lairion, F. Martini, E. Tymczyszyn, M. Frias, H. Almaleck, G.J. Gordillo, Structural and functional properties of hydration and confined water in membrane interfaces, Bba-Biomembranes, 1778 (2008) 2655-2670.

[74] R.J. Mashl, H.L. Scott, S. Subramaniam, E. Jakobsson, Molecular simulation of dioleoylphosphatidylcholine lipid bilayers at differing levels of hydration, Biophys J, 81 (2001) 3005-3015.

[75] S.Y. Bhide, M.L. Berkowitz, Structure and dynamics of water at the interface with phospholipid bilayers, J Chem Phys, 123 (2005) 244702-1-16.

[76] Z.C. Zhang, M.L. Berkowitz, Orientational Dynamics of Water in Phospholipid Bilayers with Different Hydration Levels, J Phys Chem B, 113 (2009) 7676-7680.

[77] C.A. Helm, J.N. Israelachvili, P.M. Mcguiggan, Molecular Mechanisms and Forces Involved in the Adhesion and Fusion of Amphiphilic Bilayers, Science, 246 (1989) 919-922.

[78] M.T. Stahlman, M.P. Gray, M.W. Falconieri, J.A. Whitsett, T.E. Weaver, Lamellar body formation in normal and surfactant protein B-deficient fetal mice, Lab Invest, 80 (2000) 395-403.

[79] K.B. Blodgett, Films built by depositing successive monomolecular layers on a solid surface, J Am Chem Soc, 57 (1935) 1007-1022.

[80] F.A. Askew, J.F. Danielli, Measurements of the pressures due to monolayers at oil-water interfaces., T Faraday Soc, 36 (1940) 0785-0793.

[81] F. Bringezu, J.Q. Ding, G. Brezesinski, J.A. Zasadzinski, Changes in model lung surfactant monolayers induced by palmitic acid, Langmuir, 17 (2001) 4641-4648.

[82] B.M. Discher, K.M. Maloney, D.W. Grainger, C.A. Sousa, S.B. Hall, Neutral lipids induce critical behavior in interfacial monolayers of pulmonary surfactant, Am J Resp Crit Care, 159 (1999) A896-A896.

[83] S.Y. Park, R.E. Hannemann, E.I. Franses, Dynamic tension and adsorption behavior of aqueous lung surfactants, Colloid Surface B, 15 (1999) 325-338.

[84] M. Amrein, A. vonNahmen, M. Sieber, A scanning force and fluorescence light microscopy study of the structure and function of a model pulmonary surfactant, Eur Biophys J Biophy, 26 (1997) 349-357.

[85] M. Fujihira, K. Nishiyama, H. Yamada, Photoelectrochemical Responses of Optically Transparent Electrodes Modified with Langmuir-Blodgett-Films Consisting of Surfactant Derivatives of Electron-Donor, Acceptor and Sensitizer Molecules, Thin Solid Films, 132 (1985) 77-82.

[86] J.N. Israelachvili, D. Tabor, Measurement of Van-Der-Waals Dispersion Forces in Range 1.4 to 130 Nm, Nature-Phys Sci, 236 (1972) 106.

[87] D. Tabor, Winterto.Rh, Direct Measurement of Normal and Retarded Van Der Waals Forces, Proc R Soc Lon Ser-A, 312 (1969) 435.

[88] J. Israelachvili, Y. Min, M. Akbulut, A. Alig, G. Carver, W. Greene, K. Kristiansen, E. Meyer, N. Pesika, K. Rosenberg, H. Zeng, Recent advances in the surface forces apparatus (SFA) technique, Rep Prog Phys, 73 (2010) 036601.

[89] H.J.C. Berendsen, J.P.M. Postma, W.F. Vangunsteren, A. Dinola, J.R. Haak, Molecular-Dynamics with Coupling to an External Bath, J Chem Phys, 81 (1984) 3684-3690.

[90] S. Nose, A Molecular-Dynamics Method for Simulations in the Canonical Ensemble, Mol Phys, 52 (1984) 255-268.

[91] S. Baoukina, L. Monticelli, S.J. Marrink, D.P. Tieleman, Pressure-area isotherm of a lipid monolayer from molecular dynamics simulations, Langmuir, 23 (2007) 12617-12623.

[92] A.J. Kox, J.P.J. Michels, F.W. Wiegel, Simulation of a Lipid Monolayer Using Molecular-Dynamics, Nature, 287 (1980) 317-319.

[93] S. Baoukina, E. Mendez-Villuendas, D.P. Tieleman, Molecular View of Phase Coexistence in Lipid Monolayers, J Am Chem Soc, 134 (2012) 17543-17553.

[94] V. Knecht, M. Muller, M. Bonn, S.J. Marrink, A.E. Mark, Simulation studies of pore and domain formation in a phospholipid monolayer, J Chem Phys, 122 (2005) 024704-1-9.

[95] O. Berger, O. Edholm, F. Jahnig, Molecular dynamics simulations of a fluid bilayer of dipalmitoylphosphatidylcholine at full hydration, constant pressure, and constant temperature, Biophys J, 72 (1997) 2002-2013.

[96] P.B. Moore, C.F. Lopez, M.L. Klein, Dynamical properties of a hydrated lipid bilayer from a multinanosecond molecular dynamics simulation, Biophys J, 81 (2001) 2484-2494.

[97] D.P. Tieleman, H. Leontiadou, A.E. Mark, S.J. Marrink, Simulation of pore formation in lipid bilayers by mechanical stress and electric fields, J Am Chem Soc, 125 (2003) 6382-6383.

[98] S. Leekumjorn, A.K. Sum, Molecular studies of the gel to liquid-crystalline phase transition for fully hydrated DPPC and DPPE bilayers, Bba-Biomembranes, 1768 (2007) 354-365.

[99] S.J. Marrink, M. Berkowitz, H.J.C. Berendsen, Molecular-Dynamics Simulation of a Membrane Water Interface - the Ordering of Water and Its Relation to the Hydration Force, Langmuir, 9 (1993) 3122-3131.

[100] S. Tristram-Nagle, H.I. Petrache, J.F. Nagle, Structure and interactions of fully hydrated dioleoylphosphatidylcholine bilayers, Biophys J, 75 (1998) 917-925.

[101] H. Bachofen, U. Gerber, P. Gehr, M. Amrein, S. Schurch, Structures of pulmonary surfactant films adsorbed to an air-liquid interface in vitro, Bba-Biomembranes, 1720 (2005) 59-72.

[102] S. Schurch, R. Qanbar, H. Bachofen, F. Possmayer, The Surface-Associated Surfactant Reservoir in the Alveolar Lining, Biol Neonate, 67 (1995) 61-76.

[103] D. Follows, F. Tiberg, R.K. Thomas, M. Larsson, Multilayers at the surface of solutions of exogenous lung surfactant: Direct observation by neutron reflection, Bba-Biomembranes, 1768 (2007) 228-235.

[104] Lindqvis.B, An Introduction to Clay Colloid Chemistry for Clay Technologists Geologist and Soil Scientists, Sven Kem Tidskr, 77 (1965) 382.

[105] V.A. Parsegian, N. Fuller, R.P. Rand, Measured Work of Deformation and Repulsion of Lecithin Bilayers, P Natl Acad Sci USA, 76 (1979) 2750-2754.

[106] S.D. Shoemaker, T.K. Vanderlick, Intramembrane electrostatic interactions destabilize lipid vesicles, Biophys J, 83 (2002) 2007-2014.

[107] J.N. Israelachvili, R.M. Pashley, Double-Layer, Vanderwaals and Hydration Forces between Surfaces in Electrolyte-Solutions, H-S Z Physiol Chem, 362 (1981) 1178-1179.

[108] J. Marra, Controlled Deposition of Lipid Monolayers and Bilayers onto Mica and Direct Force Measurements between Galactolipid Bilayers in Aqueous-Solutions, J Colloid Interf Sci, 107 (1985) 446-458.

[109] R.M. Pashley, Hydration Forces between Mica Surfaces in Aqueous-Electrolyte Solutions, J Colloid Interf Sci, 80 (1981) 153-162.

[110] T. Hayashi, A.J. Pertsin, M. Grunze, Grand canonical Monte Carlo simulation of hydration forces between nonorienting and orienting structureless walls, J Chem Phys, 117 (2002) 6271-6280.

[111] A. Pertsin, D. Platonov, M. Grunze, Direct computer simulation of water-mediated force between supported phospholipid membranes, J Chem Phys, 122 (2005).

[112] A. Pertsin, M. Grunze, Computer simulations of water-mediated force between phospholipid membranes, Curr Opin Colloid In, 16 (2011) 534-541.

[113] M. Kanduc, E. Schneck, R.R. Netz, Hydration Interaction between Phospholipid Membranes: Insight into Different Measurement Ensembles from Atomistic Molecular Dynamics Simulations, Langmuir, 29 (2013) 9126-9137.

[114] E. Schneck, F. Sedlmeier, R.R. Netz, Hydration repulsion between biomembranes results from an interplay of dehydration and depolarization, P Natl Acad Sci USA, 109 (2012) 14405-14409.

[115] Y.G. Smirnova, S. Aeffner, H.J. Risselada, T. Salditt, S.J. Marrink, M. Muller, V. Knecht, Interbilayer repulsion forces between tension-free lipid bilayers from simulation, Soft Matter, 9 (2013) 10705-10718.

[116] S. Yu, P.G.R. Harding, N. Smith, F. Possmayer, Bovine Pulmonary Surfactant - Chemical-Composition and Physical-Properties, Lipids, 18 (1983) 522-529.

[117] H. Zhang, Q.H. Fan, Y.E. Wang, C.R. Neal, Y.Y. Zuo, Comparative study of clinical pulmonary surfactants using atomic force microscopy, Bba-Biomembranes, 1808 (2011) 1832-1842.

[118] T.L. Kuhl, D.E. Leckband, D.D. Lasic, J.N. Israelachvili, Modulation of Interaction Forces between Bilayers Exposing Short-Chained Ethylene-Oxide Headgroups, Biophys J, 66 (1994) 1479-1488.

[119] R. Orozco-Alcaraz, T.L. Kuhl, Interaction Forces between DPPC Bilayers on Glass, Langmuir, 29 (2013) 337-343.

[120] S. Kumar, D. Bouzida, R.H. Swendsen, P.A. Kollman, J.M. Rosenberg, The Weighted Histogram Analysis Method for Free-Energy Calculations on Biomolecules .1. The Method, J Comput Chem, 13 (1992) 1011-1021.

[121] W.L. Jorgensen, J. Chandrasekhar, J.D. Madura, R.W. Impey, M.L. Klein, Comparison of Simple Potential Functions for Simulating Liquid Water, J Chem Phys, 79 (1983) 926-935.

[122] D.J. Evans, B.L. Holian, The Nose-Hoover Thermostat, J Chem Phys, 83 (1985) 4069-4074.

[123] J.R. Ray, A. Rahman, Statistical Ensembles and Molecular-Dynamics Studies of Anisotropic Solids, J Chem Phys, 80 (1984) 4423-4428.

[124] M. Benz, T. Gutsmann, N.H. Chen, R. Tadmor, J. Israelachvili, Correlation of AFM and SFA measurements concerning the stability of supported lipid bilayers, Biophys J, 86 (2004) 870-879.

[125] Y.F. Dufrene, W.R. Barger, J.B.D. Green, G.U. Lee, Nanometer-scale surface properties of mixed phospholipid monolayers and bilayers, Langmuir, 13 (1997) 4779-4784.

[126] P. Bassereau, F. Pincet, Quantitative analysis of holes in supported bilayers providing the adsorption energy of surfactants on solid substrate, Langmuir, 13 (1997) 7003-7007.

[127] R.P. Rand, V.A. Parsegian, Hydration Forces between Phospholipid-Bilayers, Biochim Biophys Acta, 988 (1989) 351-376.

[128] J. Kurniawan, N.N. Yin, G.Y. Liu, T.L. Kuhl, Interaction Forces between Ternary Lipid Bilayers Containing Cholesterol, Langmuir, 30 (2014) 4997-5004.

[129] D.C. Rapaport, The art of molecular dynamics simulation, 2nd ed., Cambridge University Press, Cambridge ; New York, 2004.

[130] T. Head-Gordon, G. Hura, Water structure from scattering experiments and simulation, Chem Rev, 102 (2002) 2651-2669.

[131] W.L. Jorgensen, J.D. Madura, Temperature and Size Dependence for Monte-Carlo Simulations of Tip4p Water, Mol Phys, 56 (1985) 1381-1392.

[132] A. Luzar, D. Chandler, Structure and Hydrogen-Bond Dynamics of Water-Dimethyl Sulfoxide Mixtures by Computer-Simulations, J Chem Phys, 98 (1993) 8160-8173.

[133] P. Mark, L. Nilsson, Structure and dynamics of the TIP3P, SPC, and SPC/E water models at 298 K, J Phys Chem A, 105 (2001) 9954-9960.

[134] C.F. Polnaszek, R.G. Bryant, Self-Diffusion of Water at the Protein Surface - a Measurement, J Am Chem Soc, 106 (1984) 428-429.

[135] S.J. Marrink, H.J.C. Berendsen, Simulation of Water Transport through a Lipid-Membrane, J Phys Chem-Us, 98 (1994) 4155-4168.

[136] P. Gallo, F. Sciortino, P. Tartaglia, S.H. Chen, Slow dynamics of water molecules in supercooled states, Phys Rev Lett, 76 (1996) 2730-2733.

[137] D. Corradini, E.G. Strekalova, H.E. Stanley, P. Gallo, Microscopic mechanism of protein cryopreservation in an aqueous solution with trehalose, Sci Rep-Uk, 3 (2013) srep01218.

[138] A.H. de Vries, S. Yefimov, A.E. Mark, S.J. Marrink, Molecular structure of the lecithin ripple phase, P Natl Acad Sci USA, 102 (2005) 5392-5396.

[139] C.H. Hsieh, S.C. Sue, P.C. Lyu, W.G. Wu, Membrane packing geometry of diphytanoylphosphatidylcholine is highly sensitive to hydration: Phospholipid polymorphism induced by molecular rearrangement in the headgroup region, Biophys J, 73 (1997) 870-877re.

[140] N. Tamai, M. Goto, H. Matsuki, S. Kaneshina, A mechanism of pressure-induced interdigitation of lipid bilayers, J Phys Conf Ser, 215 (2010).

[141] L. Lobbecke, G. Ceve, Effects of Short-Chain Alcohols on the Phase-Behavior and Interdigitation of Phosphatidylcholine Bilayer-Membranes, Bba-Biomembranes, 1237 (1995) 59-69.

[142] A.P. Ramos, P. Lague, G. Lamoureux, M. Lafleur, Effect of Saturated Very Long-Chain Fatty Acids on the Organization of Lipid Membranes: A Study Combining H-2 NMR Spectroscopy and Molecular Dynamics Simulations, J Phys Chem B, 120 (2016) 6951-6960.

[143] P.A. Monnard, D.W. Deamer, Membrane self-assembly processes: Steps toward the first cellular life, Anat Rec, 268 (2002) 196-207.

[144] C.A. Helm, J.N. Israelachvili, P.M. Mcguiggan, Role of Hydrophobic Forces in Bilayer Adhesion and Fusion, Biochemistry, 31 (1992) 1794-1805.

[145] R.P. Rand, N. Fuller, V.A. Parsegian, D.C. Rau, Variation in Hydration Forces between Neutral Phospholipid-Bilayers - Evidence for Hydration Attraction, Biochemistry, 27 (1988) 7711-7722.

[146] F. Possmayer, S.H. Yu, J.M. Weber, P.G.R. Harding, Pulmonary Surfactant, Can J Biochem Cell B, 62 (1984) 1121-1133.

[147] P. Gruenwald, Surface Tension as a Factor in the Resistance of Neonatal Lungs to Aeration, Am J Obstet Gynecol, 53 (1947) 996-1007.

[148] U. Kishore, A.L. Bernal, M.F. Kamran, S. Saxena, M. Singh, P.U. Sarma, T. Madan, T. Chakraborty, Surfactant proteins SP-A and SP-D in human health and disease, Arch Immunol Ther Ex, 53 (2005) 399-417.

[149] T.E. Weaver, J.J. Conkright, Functions of surfactant proteins B and C, Annu Rev Physiol, 63 (2001) 555-578.

[150] S.W. Glasser, T.R. Korfhagen, T. Weaver, T. Pilotmatias, J.L. Fox, J.A. Whitsett, Cdna and Deduced Amino-Acid-Sequence of Human Pulmonary Surfactant-Associated Proteolipid Spl(Phe), P Natl Acad Sci USA, 84 (1987) 4007-4011.

[151] J.C. Clark, S.E. Wert, C.J. Bachurski, M.T. Stahlman, B.R. Stripp, T.E. Weaver, J.A. Whitsett, Targeted Disruption of the Surfactant Protein-B Gene Disrupts Surfactant Homeostasis, Causing Respiratory-Failure in Newborn Mice, P Natl Acad Sci USA, 92 (1995) 7794-7798.

[152] D.E. Demello, L. Nogee, S. Heyman, H.F. Krous, D. Phelps, H.R. Colten, Inherited Surfactant Protein-B (Sp-B) Deficiency in Congenital Alveolar Proteinosis (Cap), Clin Res, 41 (1993) A271-A271.

[153] M.E. Avery, The Role of Surface Forces in Atelectasis of Prematurity and Hyaline Membrane Disease, Ama J Dis Child, 98 (1959) 560.

[154] E. Robillard, P. Dagenaisperusse, Guilbeau.A, E. Baril, Y. Alarie, Microaerosol Administration of Synthetic Beta-Gamma-Dipalmitoyl-L-Alpha-Lecithin in Respiratory Distress Syndrome - Preliminary Report, Can Med Assoc J, 90 (1964) 55.

[155] M.J. Kresch, W.H. Lin, R.S. Thrall, Surfactant replacement therapy, Thorax, 51 (1996) 1137-1154.

[156] H.M. Mcconnell, L.K. Tamm, R.M. Weis, Periodic Structures in Lipid Monolayer Phase-Transitions, Proceedings of the National Academy of Sciences of the United States of America-Physical Sciences, 81 (1984) 3249-3253.

[157] H.M. Mcconnell, V.T. Moy, Shapes of Finite Two-Dimensional Lipid Domains, J Phys Chem-Us, 92 (1988) 4520-4525.

[158] D.J. Keller, J.P. Korb, H.M. Mcconnell, Theory of Shape Transitions in Two-Dimensional Phospholipid Domains, J Phys Chem-Us, 91 (1987) 6417-6422.

[159] H.M. Mcconnell, Theory of Hexagonal and Stripe Phases in Monolayers, P Natl Acad Sci USA, 86 (1989) 3452-3455.

[160] A. Cruz, L.A. Worthman, A.G. Serrano, C. Casals, K.M.W. Keough, J. Perez-Gil, Microstructure and dynamic surface properties of surfactant protein SP-B/dipalmitoylphosphatidylcholine interfacial films spread from lipid-protein bilayers, Eur Biophys J Biophy, 29 (2000) 204-213.

[161] P. Tchoreloff, A. Gulik, B. Denizot, J.E. Proust, F. Puisieux, A Structural Study of Interfacial Phospholipid and Lung Surfactant Layers by Transmission Electron-Microscopy after Blodgett Sampling - Influence of Surface Pressure and Temperature, Chem Phys Lipids, 59 (1991) 151-165.

[162] S. Krol, M. Ross, M. Sieber, S. Kunneke, H.J. Galla, A. Janshoff, Formation of three-dimensional protein-lipid aggregates in monolayer films induced by surfactant protein B, Biophys J, 79 (2000) 904-918.

[163] H. Lee, S.K. Kandasamy, R.G. Larson, Molecular dynamics simulations of the anchoring and tilting of the lung-surfactant peptide SP-B1-25 in palmitic acid monolayers, Biophys J, 89 (2005) 3807-3821.

[164] S.K. Kandasamy, R.G. Larson, Molecular dynamics study of the lung surfactant peptide SP-B1-25 with DPPC monolayers: Insights into interactions and peptide position and orientation, Biophys J, 88 (2005) 1577-1592.

[165] S.L. Duncan, R.G. Larson, Folding of lipid monolayers containing lung surfactant proteins SP-B1-25 and SP-C studied via coarse-grained molecular dynamics simulations, Bba-Biomembranes, 1798 (2010) 1632-1650.

[166] D.P. Tieleman, H.J.C. Berendsen, Molecular dynamics simulations of a fully hydrated dipalmitoyl phosphatidylcholine bilayer with different macroscopic boundary conditions and parameters, J Chem Phys, 105 (1996) 4871-4880.

[167] C. Kandt, W.L. Ash, D.P. Tieleman, Setting up and running molecular dynamics simulations of membrane proteins, Methods, 41 (2007) 475-488.

[168] N.B. Vargaftik, B.N. Volkov, L.D. Voljak, International Tables of the Surface-Tension of Water, J Phys Chem Ref Data, 12 (1983) 817-820.

[169] C.W. Hollars, R.C. Dunn, Submicron structure in L-alpha-dipalmitoylphosphatidylcholine monolayers and bilayers probed with confocal, atomic force, and near-field microscopy, Biophys J, 75 (1998) 342-353.

[170] S.L. Frey, L. Pocivavsek, A.J. Waring, F.J. Walther, J.M. Hernandez-Juviel, P. Ruchala, K.Y.C. Lee, Functional importance of the NH2-terminal insertion sequence of lung surfactant protein B, Am J Physiol-Lung C, 298 (2010) L335-L347.

[171] C. Vega, E. de Miguel, Surface tension of the most popular models of water by using the test-area simulation method, J Chem Phys, 126 (2007).

[172] P. Dhar, E. Eck, J.N. Israelachvili, D.W. Lee, Y.J. Min, A. Ramachandran, A.J. Waring, J.A. Zasadzinski, Lipid-Protein Interactions Alter Line Tensions and Domain Size Distributions in Lung Surfactant Monolayers, Biophys J, 102 (2012) 56-65.

[173] D. Rose, J. Rendell, D. Lee, K. Nag, V. Booth, Molecular dynamics simulations of lung surfactant lipid monolayers, Biophys Chem, 138 (2008) 67-77.

[174] W. Shinoda, R. DeVane, M.L. Klein, Coarse-grained molecular modeling of non-ionic surfactant self-assembly, Soft Matter, 4 (2008) 2454-2462.

[175] K.J. Klopfer, T.K. Vanderlick, Isotherms of dipalmitoylphosphatidylcholine (DPPC) monolayers: Features revealed and features obscured, J Colloid Interf Sci, 182 (1996) 220-229.

[176] X.D. Chen, S. Lenhert, M. Hirtz, N. Lu, H. Fuchs, L.F. Chi, Langmuir-Blodgett patterning: A bottom-up way to build mesostructures over large areas, Accounts Chem Res, 40 (2007) 393-401.

[177] H. Riegler, K. Spratte, Structural-Changes in Lipid Monolayers during the Langmuir-Blodgett Transfer Due to Substrate Monolayer Interactions, Thin Solid Films, 210 (1992) 9-12.

[178] M.H. Kopf, S.V. Gurevich, R. Friedrich, L.F. Chi, Pattern Formation in Monolayer Transfer Systems with Substrate-Mediated Condensation, Langmuir, 26 (2010) 10444-10447.

[179] H.D. Sikes, D.K. Schwartz, A temperature-dependent two-dimensional condensation transition during Langmuir-Blodgett deposition, Langmuir, 13 (1997) 4704-4709.

[180] R. DeKoker, H.M. McConnell, Stripe phase hydrodynamics in lipid monolayers, J Phys Chem-Us, 100 (1996) 7722-7728.

[181] H.E. Ries, H. Swift, Twisted Double-Layer Ribbons and the Mechanism for Monolayer Collapse, Langmuir, 3 (1987) 853-855.

[182] E. Parra, A. Alcaraz, A. Cruz, V.M. Aguilella, J. Perez-Gil, Hydrophobic Pulmonary Surfactant Proteins SP-B and SP-C Induce Pore Formation in Planar Lipid Membranes: Evidence for Proteolipid Pores, Biophys J, 104 (2013) 146-155.

[183] L.M. Gordon, S. Horvath, M.L. Longo, J.A.N. Zasadzinski, H.W. Taeusch, K. Faull, C. Leung, A.J. Waring, Conformation and molecular topography of the N-terminal segment of surfactant protein B in structure-promoting environments, Protein Sci, 5 (1996) 1662-1675.

[184] H. Nakahara, S. Lee, O. Shibata, Surface pressure induced structural transitions of an amphiphilic peptide in pulmonary surfactant systems by an in situ PM-IRRAS study, Bba-Biomembranes, 1828 (2013) 1205-1213.

[185] J. Seelig, Deuterium Magnetic-Resonance - Theory and Application to Lipid-Membranes, Q Rev Biophys, 10 (1977) 353-418.

[186] M.R. Buhaenko, J.W. Goodwin, R.M. Richardson, Surface Rheology of Spread Monolayers, Thin Solid Films, 159 (1988) 171-189.

[187] R. Peters, K. Beck, Translational Diffusion in Phospholipid Monolayers Measured by Fluorescence Microphotolysis, P Natl Acad Sci-Biol, 80 (1983) 7183-7187.

[188] A. Ghosh, R.K. Campen, M. Sovago, M. Bonn, Structure and dynamics of interfacial water in model lung surfactants, Faraday Discuss, 141 (2009) 145-159.

[189] A.J. Waring, F.J. Walther, L.M. Gordon, J.M. Hernandez-Juviel, T. Hong, M.A. Sherman, C. Alonso, T. Alig, A. Braun, D. Bacon, J.A. Zasadzinski, The role of charged amphipathic helices in the structure and function of surfactant protein B, J Pept Res, 66 (2005) 364-374.

[190] M.M. Lipp, K.Y.C. Lee, D.Y. Takamoto, J.A. Zasadzinski, A.J. Waring, Coexistence of buckled and flat monolayers, Phys Rev Lett, 81 (1998) 1650-1653.

[191] D. Zenisek, J.A. Steyer, W. Almers, Transport, capture and exocytosis of single synaptic vesicles at active zones, Nature, 406 (2000) 849-854.

[192] P. Primakoff, D.G. Myles, Penetration, adhesion, and fusion in mammalian sperm-egg interaction, Science, 296 (2002) 2183-2185.

[193] S.A. Connolly, J.O. Jackson, T.S. Jardetzky, R. Longnecker, Fusing structure and function: a structural view of the herpesvirus entry machinery, Nat Rev Microbiol, 9 (2011) 369-381.

[194] L.V. Chernomordik, M.M. Kozlov, Protein-lipid interplay in fusion and fission of biological membranes, Annu Rev Biochem, 72 (2003) 175-207.

[195] L. Yang, H.W. Huang, A rhombohedral phase of lipid containing a membrane fusion intermediate structure, Biophys J, 84 (2003) 1808-1817.

[196] J.Y. Wong, C.K. Park, M. Seitz, J. Israelachvili, Polymer-cushioned bilayers. II. An investigation of interaction forces and fusion using the surface forces apparatus, Biophys J, 77 (1999) 1458-1468.

[197] T.C. Sudhof, J.E. Rothman, Membrane Fusion: Grappling with SNARE and SM Proteins, Science, 323 (2009) 474-477.

[198] S.G. Peisajovich, O. Samuel, Y. Shai, Paramyxovirus F1 protein has two fusion peptides: Implications for the mechanism of membrane fusion, J Mol Biol, 296 (2000) 1353-1365.

[199] M. Rabenstein, Y.K. Shin, A Peptide from the Heptad Repeat of Human-Immunodeficiency-Virus Gp41 Shows Both Membrane-Binding and Coiled-Coil Formation, Biochemistry-Us, 34 (1995) 13390-13397.

[200] G. Chevalier, A.J. Collet, In-Vivo Incorporation of Choline-H-3, Leucine-H-3 and Galactose-H-3 in Alveolar Type-Ii Pneumocytes in Relation to Surfactant Synthesis - Quantitative Autoradiographic Study in Mouse in Electron-Microscopy, Anat Rec, 172 (1972) 289.

[201] J.M. Klein, M.W. Thompson, J.M. Snyder, T.N. George, J.A. Whitsett, E.F. Bell, P.B. McCray, L.M. Nogee, Transient surfactant protein B deficiency in a term infant with severe respiratory failure, J Pediatr-Us, 132 (1998) 244-248.

[202] Y. Suzuki, Y. Fujita, K. Kogishi, Reconstitution of Tubular Myelin from Synthetic Lipids and Proteins Associated with Pig Pulmonary Surfactant, Am Rev Respir Dis, 140 (1989) 75-81.

[203] F.R. Poulain, S. Nir, S. Hawgood, Kinetics of phospholipid membrane fusion induced by surfactant apoproteins A and B, Bba-Biomembranes, 1278 (1996) 169-175.

[204] F. Bringezu, J.Q. Ding, G. Brezesinski, A.J. Waring, J.A. Zasadzinski, Influence of pulmonary surfactant protein B on model lung surfactant monolayers, Langmuir, 18 (2002) 2319-2325.

[205] J.W. Ma, S. Koppenol, H.U. Yu, G. Zografi, Effects of a cationic and hydrophobic peptide, KL4, on model lung surfactant lipid monolayers, Biophys J, 74 (1998) 1899-1907.

[206] Z.F. Shao, J. Mou, D.M. Czajkowsky, J. Yang, J.Y. Yuan, Biological atomic force microscopy: What is achieved and what is needed, Adv Phys, 45 (1996) 1-86.

[207] E. Chibowski, A. Szczes, Zeta potential and surface charge of DPPC and DOPC liposomes in the presence of PLC enzyme, Adsorption, 22 (2016) 755-765.

[208] C. Perez-Iratxeta, M.A. Andrade-Navarro, K2D2: estimation of protein secondary structure from circular dichroism spectra, Bmc Struct Biol, 8 (2008).

[209] G. Vandenbussche, A. Clercx, M. Clercx, T. Curstedt, J. Johansson, H. Jornvall, J.M. Ruysschaert, Secondary Structure and Orientation of the Surfactant Protein Sp-B in a Lipid Environment - a Fourier-Transform Infrared-Spectroscopy Study, Biochemistry, 31 (1992) 9169-9176.

[210] B. Olmeda, B. Garcia-Alvarez, J. Perez-Gil, Structure-function correlations of pulmonary surfactant protein SP-B and the saposin-like family of proteins, Eur Biophys J Biophy, 42 (2013) 209-222.

[211] M.A. Ryan, X.Y. Qi, A.G. Serrano, M. Ikegami, J. Perez-Gil, J. Johansson, T.E. Weaver, Mapping and analysis of the lytic and fusogenic domains of surfactant protein B, Biochemistry, 44 (2005) 861-872.

[212] M. Sarker, J. Rose, J. Bartlett, M. Browne, V. Booth, Modifications to Surfactant Protein B Structure and Lipid Interactions Under Ards Conditions: Consequences of Tryptophan Oxidation, Biophys J, 98 (2010) 280a-281a.

[213] A.G. Serrano, M. Ryan, T.E. Weaver, J. Perez-Gil, Critical structure-function determinants within the N-terminal region of pulmonary surfactant protein SP-B, Biophys J, 90 (2006) 238-249.